UNIVERSITY OF CALIFORNIA
RIVERSIDE

AND

SAN DIEGO STATE UNIVERSITY

Macroevolution and Diversification of Snakes at Multiple Taxonomic Levels

A Dissertation submitted in partial satisfaction
of the requirements for the degree of

Doctor of Philosophy

in

Evolutionary Biology

by

Sean Michael Harrington

March 2018

Dissertation Committee:
Dr. Tod Reeder, Co-Chairperson
Dr. David Reznick, Co-Chairperson
Dr. Timothy Higham
Dr. Kevin Burns

The Dissertation of Sean Michael Harrington is approved:

_____

_____

_____
Committee Co-Chairperson

_____
Committee Co-Chairperson

University of California, Riverside
San Diego State University

ACKNOWLEDGEMENTS

I thank my dissertation adviser, Tod Reeder, and the other members of my dissertation committee, Kevin Burns, Timothy Higham, and David Reznick. I thank all of my labmates that have helped me through this dissertation, especially Andrew Gottscho, John Andermann, Dean Leavitt, Alex Sumarli, and Sam Fellows. I also thank the many SDSU graduate students, my friends, and family that have supported me. For chapter one, I thank Richard Etheridge, Brad Hollingsworth, Laura Williams, the San Diego Natural History Museum and members of the Reeder laboratory for discussions that improved this manuscript. I thank Matt Brandley, Jim McGuire, Alex Pyron, Jeff Streicher and one anonymous reviewer for helpful comments on drafts of this manuscript. This project was supported by a US National Science Foundation-AToL grant to Tod W. Reeder (EF 0334967). For Chapter two, I thank Tony Gamble and Aaron Bauer for providing us with the tree and data from Gamble et al. (2012). I thank Rich FitzJohn for help with BiSSE analyses. I thank Jeremy Beaulieu for extensive help with HiSSE analyses, advice that improved our methodology, and comments on a draft of this manuscript. I thank Alex Pyron for comments on an earlier draft of this manuscript that improved this study. I thank members of the Reeder lab, especially Dean Leavitt, John Andermann and Andrew Gottscho, for discussions and comments that improved this manuscript. I also thank David Marjanović and one anonymous reviewer for comments that have improved this manuscript. For chapter three, I thank Andrew Gottscho, John Andermann, and Dean Leavitt for laboratory and analytical assistance. The 2003 binational expedition, including Oscar Flores-Villela, Dustin Wood, Jorge H. Valdez Villavicencio, Anny Peralta Garcia,

Cynthia Jauregui, Tom Myers, and Robert Hill, to the Agua Verde-Punta Mechudo conservation corridor contributed to the collection of specimens used in this study. I thank Jordan Satler for analytical advice. This work was supported by a UCR Newell Award to SMH and start-up funds from UCR to Timothy Higham. I thank my coauthors of each chapter, Tod Reeder on all three chapters, and Bradford Hollingsworth and Timothy Higham on chapter three.

ABSTRACT OF THE DISSERTATION

Macroevolution and Diversification of Snakes at Multiple Taxonomic Levels

by

Sean Michael Harrington

Doctor of Philosophy, Graduate Program in Evolutionary Biology
University of California, Riverside and San Diego State University, March 2018
Dr. Tod Reeder, Co-Chairperson
Dr. David Reznick, Co-Chairperson

In my dissertation, I explore macroevolutionary trait evolution and diversification of snakes at multiple taxonomic levels. In my first chapter, I use a combined morphological and molecular dataset for the higher clades of snakes and several important fossil lineages to infer the phylogenetic placement of fossil taxa and simultaneously use them to calibrate the phylogeny. I then use this time tree to reconstruct the early evolution of large gape size (followed by multiple losses) and multiple independent instances of limb reduction early in snake history. In my second chapter, I reanalyze the datasets of reproductive mode (i.e., oviparity and viviparity) in squamate reptiles and toepads in geckos to examine the influence that each trait has on rates of speciation and extinction, reconstruct the histories of these traits, and explore the differences between the Hidden State Speciation and Extinction (HiSSE) and Binary State Speciation and Extinction (BiSSE) models. I show that diversification rates have varied considerably across Squamata, with particularly high rates of diversification shown within snakes, and that use of HiSSE models provides less support for reversals

from viviparity to oviparity within snakes or other squamates, or for multiple evolutions of toepads in geckos than was obtained previously using the BiSSE model. In my final chapter, I use restriction site associated DNA sequence data to show that the Red Diamond Rattlesnake, *Crotalus ruber,* is made up of distinct northern and southern populations. Model selection analyses show that these populations were historically genetically isolated, but have since come into secondary contact and are now exchanging genes at relatively high levels. Both divergence and secondary contact are estimated to have occurred during the Pleistocene, suggesting a role for climatic cycling in driving these events and possibly producing similar genetic structure in other taxa. I have provided insight into how traits have evolved across the major clades of snakes, as well as lower-level processes that influence the divergence of local lineages that may or may not eventually become species and contribute to the global snake diversity.

TABLE OF CONTENTS

LIST OF FIGURES

LIST OF TABLES

INTRODUCTION

Snakes (Serpentes) are a highly diverse radiation of squamate reptiles composed of approximately 3,500 species. Many of the higher phylogenetic relationships of snakes and other squamates have recently been resolved with strong support using extensive sampling of nuclear loci, but several important systematic questions remain. These include the phylogenetic placement of key fossil taxa, how rates of speciation and extinction vary across clades and are influenced by traits, and what processes influence lineage divergence and fusion at phylogeographic scales, among many others.

In my first chapter, I combine published morphological and molecular datasets to infer the phylogenetic placement of several key snake fossils, including the oldest known snake fossils and fossil snakes that possessed external limbs, unlike all living snakes. I use a Bayesian tip-dating approach to simultaneously infer the phylogenetic placement of these fossils and use them to time-calibrate the tree and infer the divergence dates among the major lineages of snakes. With this dated phylogeny, I then use Bayesian ancestral state reconstruction to investigate the evolution of gape size and limblessness. All modern snakes lack well-developed external limbs (although some clades retain remnants of hind limbs internally or as spurs), and the most speciose groups are snakes characterized by large gapes that allow them to swallow prey that can be considerably larger than a snake's own head. Inferring the evolutionary history of these traits is complicated by the existence of fossil taxa that possess an amalgamation of seemingly ancestral (e.g., retention of well-developed limbs) and derived (e.g., ability to consume

large prey) traits. By including such fossils in reconstructions of gape size and limblessness, I am able explore the origins and losses of these important traits.

In my second chapter, I explore joint models of trait evolution, speciation, and extinction in snakes and other squamate reptiles. These models can be used to determine if a trait is correlated with increased or decreased rates of speciation and/or extinction, and can also be used to reconstruct the ancestral state of a given character while accounting for different rates of clade diversification, which can otherwise bias such reconstructions. The first joint model of these processes was the Binary State Speciation and Extinction, or BiSSE, model. The BiSSE model does not accommodate shifts in diversification that are unrelated to the trait being considered, and has been recently shown to be prone to misinterpretation when the assumptions of the model are poorly met. I explored the utility of the Hidden State Speciation and Extinction (HiSSE) model for inferring the effects of toepads and viviparity on rates of speciation and extinction in geckos and squamates, respectively. This method can accommodate differences in rates of diversification that are not related to the trait being considered, and I demonstrate the differences between inferences obtained using BiSSE and HiSSE models on these two datasets, with special focus on the implications of these results for the evolution of viviparity and speciation rates in snakes.

In my final chapter, I explore the phylogeographic history of the Red Diamond Rattlesnake, *Crotalus ruber*. *Crotalus ruber* is distributed across the Baja California Peninsula into southern California. Many squamate species have been studied in Baja California using molecular genetic methods, and phylogenetic or phylogeographic breaks

have been identified in most species studied. Despite the presence of two historically recognized subspecies within *C. ruber* that differ in color pattern and scalation, genetic divergence among populations of *C. ruber* has not been rigorously explored. I use a restriction site associated DNA sequencing (RADseq) approach to determine if genetically differentiated populations exist that correspond to major genetic breaks identified in other taxa along the Baja California Peninsula. After identifying populations, I use a model selection approach to determine if populations have diverged in the face of ongoing gene flow, in the absence of gene flow, or if populations were historically isolated with gene flow resuming in the more recent past.

These chapters provide novel insight into the evolution of key traits thought to be successful to snakes as a lineage, the interaction between the evolution of viviparity and speciation and extinction rates across snakes, and the processes that drive population divergence on a recent scale.

Chapter 1: Phylogenetic Inference and Divergence Dating of Snakes Using Molecules, Morphology, and Fossils: New Insights on Convergent Evolution of Feeding Morphology and Limb Reduction

Bayesian divergence time analyses were used to simultaneously infer the phylogenetic relationships and date the major clades of snakes including several important fossils that have not previously been included in divergence dating analyses as terminal taxa. We also explored the effect of using fossilized birth-death and uniform tree priors for divergence dating with terminal calibrations. Non-clock and relaxed clock analyses of the combined morphology and molecular dataset supported previous molecular phylogenetic hypotheses for the major clades of snakes, including the paraphyly of the traditionally recognized Scolecophidia and Macrostomata. Tip-dating analyses using either a uniform tree prior or fossilized birth-death prior that assumes that all fossils are tips and that extant lineages are randomly sampled resulted in older ages than those inferred using a fossilized birth-death prior assuming diversified sampling of extant lineages and those estimated by previous studies. We used Bayesian ancestral state reconstruction methods to map the evolution of the ability to consume large prey and the loss of limbs onto our inferred time-calibrated phylogeny. We found strong support for early evolution of the ability to consume large prey, indicating multiple independent losses of this ability. We also found strong support for retention of external hind limbs until relatively late in snake evolution, indicating multiple independent losses of hind limbs.

The fossil record of snakes (Serpentes) contains many important species that have the potential to illuminate many aspects of the early evolution of the clade, including the timing of origin of Serpentes, patterns of limb loss, and the evolution of the ability to swallow prey items considerably larger than an individual's own head. The snake fossil record has recently been expanded to include the oldest currently known stem snake fossils (Caldwell *et al.*, 2015), older than previously known specimens by more than 50 My, and the first snake fossil ever identified to possess forelimbs in addition to hind limbs, *Tetrapodophis* (Martill *et al.*, 2015). Prior to the discovery of *Tetrapodophis,* snake fossils with hind limbs were known (including Simoliophiidae, a marine group that has been of uncertain phylogenetic placement), but none were known to possess forelimbs.

Phylogenetic hypotheses for the placement of many fossil taxa have been historically unstable (Tchernov *et al.*, 2000; Scanlon & Lee, 2000; Rieppel *et al.*, 2002; Apesteguía & Zaher, 2006; Lee *et al.*, 2007; Conrad, 2008; Wilson *et al.*, 2010; Gauthier *et al.*, 2012; Zaher & Scanferla, 2012; Palci *et al.*, 2013; Palci, Caldwell & Nydam, 2013; Scanferla *et al.*, 2013). Additionally, phylogenetic analyses incorporating snake fossils are often performed using morphological data only. Some major clades (e.g., Scolecophidia, Macrostomata) traditionally recognized based on morphology are now strongly supported as paraphyletic, and the phylogenetic positions of many other extant taxa have shifted in recent large-scale multilocus molecular phylogenetic studies (Vidal & Hedges, 2002; Vidal *et al.*, 2007; Wiens *et al.*, 2012; Streicher & Wiens, 2016). The uncertain placement of fossil taxa leads to difficulties when using traditional divergence

dating methods that rely on node calibration, and studies using different calibrating fossils to calibrate nodes have recovered very different ages for the major clades of snakes (e.g., Burbrink & Pyron, 2008; Sanders & Lee, 2008; Wiens *et al.*, 2006; Vidal *et al.*, 2009; Scanlon & Lee, 2011; Pyron & Burbrink, 2012). Scanlon & Lee (2011) suggested that many of the calibrations used in some previous studies (e.g., Noonan & Chippindale, 2006; Vidal *et al.*, 2009) were of uncertain placement, and therefore should not be used, highlighting the importance of phylogenetic uncertainty in dating the major clades of snakes.

Bayesian tip-dating approaches allow for the uncertainty in phylogenetic placement of fossil taxa to be accounted for by simultaneously inferring the placement of fossil taxa and using them to calibrate the phylogeny (Pyron, 2011; Ronquist *et al.*, 2012a). Previously, Hsiang *et al.* (2015) used a tip-dating approach to estimate divergence dates for snakes on fixed topologies derived from non-clock analyses of a combined morphological and molecular dataset. However, the Hsiang *et al.* (2015) study was published before Caldwell *et al.* (2015) and Martill *et al.* (2015), and therefore did not include the important fossils described in these studies. Additionally, by fixing the topologies in their divergence dating analyses, Hsiang *et al.* (2015) did not fully account for the effect that topological uncertainty might have on inferred divergence dates.

In this study, we use a combined approach incorporating morphological and molecular data and terminal fossil taxa for estimating divergence dates among the major clades of snakes. By jointly inferring phylogeny and divergence dates, we are able to

include numerous important fossil snake lineages, including recently discovered fossils that include the oldest known stem snakes and the only known snake fossil to possess forelimbs. We additionally evaluate and compare the use of different tree priors in the tip-dating analyses. Our combined data phylogenetic analyses including fossils confirm the general findings of recent multilocus molecular phylogenetic studies of snakes (e.g., Vidal & Hedges, 2002; Vidal *et al.*, 2007; Wiens *et al.*, 2012) and fail to support the monophyly of the traditionally recognized clade Macrostomata. Macrostomata has long been identified based on characteristics of the skull and jaws that allow for large gapes and the consumption of whole prey that are often considerably larger than a snake's own head (Cundall & Greene, 2000). The paraphyly of Macrostomata as traditionally defined raises questions about whether these characters associated with gape size evolved independently multiple times or evolved once and were lost in subsequent lineages (Rieppel *et al.*, 2003; Rieppel, 2012). We also find that a group of extinct marine snakes with well-developed hind limbs (Simoliophiidae) is nested within Serpentes (extant snakes), a clade in which no extant species possesses more than rudimentary remnants of hind limbs. We use Serpentes to refer to crown snakes and Ophidia to refer to the clade composed of Serpentes + related fossil taxa identified as snakes, following Lee & Caldwell (2000), Conrad (2008), and Zaher & Scanferla (2012). This raises the question of whether hind limbs were lost once in the common ancestor of all snakes and regained in the simoliophiids or were maintained in the early lineages of the snake radiation and independently lost in Typhlopoidea + Leptotyphlopidae, Anomalepididae, and

Alethinophidia (Rieppel *et al.*, 2003; Zaher, Apesteguía & Scanferla, 2009; Palci *et al.*, 2013a).

To further investigate the evolution of these traits in snakes, we used Bayesian ancestral state reconstruction methods to evaluate the evolution of a generalized "macrostomatan phenotype" (i.e., ability to swallow prey of large diameter relative to a snake's head) and the limb-reduced phenotype on our inferred phylogeny of major extant and extinct lineages of snakes based on morphological and molecular data. The inclusion of fossil taxa is important because fossils increase the accuracy of comparative analyses in general (Finarelli & Flynn, 2006; Slater *et al.*, 2012; Slater 2013) and are critical for these analyses because fossil taxa exhibit character states that are not known in extant snakes (fully-developed limbs) or in particular groups of extant snakes (i.e., the presence of the macrostomatan phenotype by taxa outside of Alethinophidia).

METHODS

Phylogenetic Inference

We combined published molecular data (44 nuclear loci) from Wiens *et al.* (2012) with morphological data obtained from Hsiang *et al.* (2015), and Martill *et al.* (2015). The Martill *et al*. (2015) matrix includes data for the oldest known stem snake fossils from Caldwell et al. (2015). When combining morphological character matrices, we excluded characters from the Martill *et al.* (2015) matrix that are duplicates (or nearly so) of those from Hsiang et al. (2015) and retained the relevant character from the Hsiang *et al.* (2015) matrix. We further excluded characters from the combined matrix that were

not variable across the taxa that we included. Recent molecular studies strongly support Anguimorpha and Iguania as the closest extant outgroups to snakes (e.g., Wiens *et al.*, 2012; Reeder *et al.*, 2015), and representatives from these groups were included to root the snake phylogeny, including several fossils from these clades to provide reasonable dates for the outgroup taxa in divergence dating analyses. The genus *Rena* is represented by different species in the molecular and morphological datasets (*Rena humilis* and *R. dulcis,* respectively), as is the genus *Chamaeleo* (*Chamaeleo calyptratus* and *C. laevigatus,* respectively). In each case, we combined these molecular and morphological data into a single taxon representing the genus.

Our phylogenetic inference analyses were performed under non-clock and relaxed clock models as implemented in MrBayes v3.2.6 (Ronquist *et al.*, 2012b). The partitioning scheme for the molecular data was determined using PartitionFinder under the Bayesian information criterion using a greedy search (Lanfear *et al.*, 2012). For each molecular partition, we used the nst = mixed option in MrBayes to marginalize across all subset models of the GTR model using reversible-jump MCMC and accommodated rate heterogeneity among sites under a Γ distribution (Huelsenbeck *et al.*, 2004; Ronquist *et al.*, 2012b). Morphological data were analyzed using the *Mk* model (Lewis 2001) with character rate heterogeneity accommodated under a Γ distribution and the coding bias set to variable. All analyses were run on the CIPRES Science Gateway (Miller *et al.*, 2010). We ran our non-clock analyses for 20 M generations sampling every 5000 generations. We ran all clock analyses for 50 M generations sampling every 5000 generations. Convergence was assessed in Tracer v1.6 (Rambaut *et al.*, 2014) visually and by

examining ESS values of parameters, and the first 25% of each analysis was discarded as burn-in. For divergence dating analyses of the combined morphology and molecular dataset including fossils, we ran a total of six independent MrBayes analyses using 4 chains each and combined the results of all six runs into a single consensus tree for each set of analyses. For DNA-only relaxed clock analyses we performed two replicate runs of four chains each.

Divergence Dating

Relaxed clock analyses were performed using either uniform or fossilized birth-death (FBD) tree priors. To determine an appropriate clock rate prior, we ran a strict clock analysis with a fixed topology determined by the results of initial non-clock phylogenetic analyses. We implemented a lognormal clock rate prior with the mean set to the tree height determined by the strict clock analysis divided by the mean age calibration of the root node of the tree, and set the standard deviation so that the upper 95% estimate of tree height divided by the mean age calibration of the root is one standard deviation from the mean of the normal distribution, following the recommendations of Ronquist *et al.* (2012a). All relaxed clock analyses were run using the independent gamma rates (IGR) clock model (Ronquist *et al.*, 2012a). The IGR clock model is a continuous uncorrelated model in which branch rates are drawn independently from a gamma distribution with a mean equal to the branch length and a variance proportional to branch length (Lepage *et al.*, 2007). To set an appropriate prior on the increase in variance of the IGR clock, we used the R script provided by Ronquist *et al.* (2012a), which regresses the

variance of non-clock branch lengths against strict clock branch lengths to estimate a rate for the exponential prior distribution.

We calibrated the ages of the root node for all analyses, as required by MrBayes. We calibrated the root node with an offset lognormal distribution with the minimum and soft upper bounds (168.9 Ma and 209 Ma, respectively) based on the fossil iguanian *Bharatagama* in the Fossil Calibration Database (Ksepka *et al.*, 2015) and the mean arbitrarily set to 188.9 Ma. To ensure proper rooting of the phylogeny, we fixed the monophyly of the outgroup (Anguimorpha + Iguania) and the ingroup (Ophidia). Preliminary analyses resulted in some recent nodes being inferred as younger than known minima for these clades based on fossils not included in our analyses. Therefore, in all subsequent analyses, we calibrated a set of nodes in addition to the tip calibrations that are included in the analyses. These node calibrations are described in supplemental Table S1 available on the Dryad Digital Repository (http://datadryad.org/resource/doi:10.5061/dryad.cm603). The addition of these calibrations required fixing the monophyly of the calibrated nodes, however, these nodes were well-supported in our non-clock and preliminary clock analysis, and therefore fixing the monophyly of these nodes does not diminish the ability to fully account for uncertainty in dates that is induced by topological uncertainty. Terminal fossils were all assigned uniform distributions, with the upper and lower bounds reflecting the minimum and maximum estimated ages of the oldest geologic stratum from which each fossil species has been found.

We ran relaxed clock analyses using either a uniform tree prior or a FBD prior, and with the exception of the preliminary analysis without any internal node calibrations mentioned above (run with the uniform tree prior and not presented here), we ran all analyses including the node calibrations mentioned above. For the combined dataset with fossils as tips, we ran one analysis with the uniform tree prior with the added calibrations, one analysis using the FBD prior with sampling of extant lineages assumed to be random and all fossils treated as terminals (i.e., not permitted to be sampled ancestors; we refer to this as the FBD random fossil tip prior/model), and two analyses with the FBD prior assuming diversified sampling of extant lineages (we refer to this as the diversified FBD prior/model; these priors as implemented in MrBayes are described in Zhang *et al.*, 2015). Speciation, extinction, and fossil recovery rates are all parameters of the fossilized birth-death model (Heath *et al.*, 2014), and so adequate modeling of the sampling of extant taxa is important for proper estimation of dates. The diversified model assumes that extant higher taxa have been completely sampled before some cutoff point in the phylogeny and that after this cutoff, only a single representative of each higher clade has been sampled. In MrBayes, this cutoff is constrained to be younger than the most recent fossil included in the phylogeny (Zhang et al. 2015). As a result, preliminary analyses with all fossils included resulted in very young dates for several of the more recent splits in the tree, and we therefore removed the youngest fossils (*Wonambi, Yurlunggur,* and *Armandisaurus*) from all analyses presented here that utilized the diversified sampling model. For comparison, we also performed two analyses using only DNA data and excluding all fossil taxa. These analyses were calibrated only by the node calibrations

that were included in our analyses of the full dataset and were performed using either the diversified or random sampling, fossils as tips FBD tree priors.

We performed a set of analyses in which relationships were constrained to match those recovered by a recent phylogeny based on genomic data from ultraconserved elements (Streicher & Wiens, 2016). This involved fixing the monophyly of the clade containing Boidae, Calabariidae, Pythonidae, Loxocemidae, Xenopeltidae, Bolyeriidae, and Uropeltidae + Cylindrophiidae, as well as constraining Bolyeriidae to be a member of the clade that contains Pythonidae, Loxocemidae, and Xenopeltidae. These analyses were performed using both the diversified FBD prior and the random sampling, fossils as tips FBD prior, and we refer to these as the constrained analyses. We additionally repeated these two constrained analyses removing all morphology data, but retaining the terminal fossils to determine if the inclusion of terminal fossils under the fossilized birth-death process can be informative for divergence dating even in the absence of morphological data. For these analyses, we constrained the monophyly of additional clades to localize the terminal fossils to the part of the tree indicated by our previous analyses. These analyses approximate the original formulation of the fossilized birth-death model for divergence dating (Heath *et al.*, 2014).

The stem snakes *Eophis, Parviraptor, Diablophis, and Portugalophis* were recently classified as snakes by Caldwell et al. (2015). Previously, they were considered to be anguimorph lizards (Evans, 1994; Evans, 1996; Broschinski, 2000; Caldwell *et al.,* 2015). The character coding of the four-limbed snake *Tetrapodophis* has not been

assessed by researchers other than Martill *et al.* (2015), possibly leaving some doubt that it is a stem snake as well. To determine the effect of the inclusion of *Tetrapodophis* or the fossils classified as stem snakes by Caldwell *et al.* (2015) in our analyses, we performed analyses excluding *Tetrapodophis* or *Tetrapodophis* and the stem snakes from Caldwell *et al.* (2015) using a diversified FBD prior with relationships constrained to match Streicher & Wiens (2016).

Character Evolution

We used the method MultiState as implemented in BayesTraits v2.0 (Pagel *et al*, 2004; http://www.evolution.reading.ac.uk/BayesTraits.html) to reconstruct the evolution of the macrostomatan phenotype and limblessness. For the macrostomatan phenotype, taxa were coded as being either macrostomatan or non-macrostomatan. The fossils *Dinilysia* and *Najash* were coded as non-macrostomatan (Estes *et al.*, 1970; Apesteguía & Zaher, 2006; Zaher *et al.*, 2009; Zaher & Scanferla, 2012) and madtsoiids, simoliophiids, and *Kataria* were coded as possessing the macrostomatan phenotype (Scanlon & Lee, 2000; Tchernov *et al.*, 2000; Rieppel *et al.*, 2002; Zaher & Rieppel, 2002; Wilson *et al.*, 2010; Rieppel, 2012; Scanferla *et al.*, 2013). There is some debate about the ability of madtsoiids to consume large prey (e.g., Wilson *et al.*, 2010), and we also ran one analysis with madtsoiids coded as missing data to ensure that this coding does not strongly bias our results. Loxocemidae and Xenopeltidae are often considered to be intermediate between the macrostomatan and non-macrostomatan phenotype, but because both are known to consume relatively large prey, we coded these taxa as

macrostomatan (Cundall & Greene, 2000). For reconstructions of hind limb states, we coded three states corresponding to well-developed, external hind limbs (seen in *Najash*, *Tetrapodophis*, and Simoliophiids [Haas, 1979; Rage & Escuillié, 2000; Tchernov *et al.*, 2000; Apesteguía & Zaher, 2006; Martill *et al.*, 2015]), reduced hind limbs including pelvic girdle elements or limb remnants as spurs present (as in boids and pythonids [Vitt & Caldwell, 2008]), or limbs completely absent (as in Colubroidea [Vitt & Caldwell, 2008]). We coded *Wonambi* as uncertain for either well-developed or reduced limbs because recently discovered fossil material indicates that this taxon possessed remnants of hind limbs to some degree (i.e., minimally, pelvic girdle elements were present), but it is uncertain if external limbs fitting our coding of well-developed limbs were present (Palci *et al.*, 2014). Due to an absence of fossil material from which hind limb states can be inferred, limb states for many fossil taxa were coded as missing data.

For all analyses, the root was fixed to the ancestral state (non-macrostomatan and well-developed hind limbs) to combat possible pathological effects of likelihood-based reconstructions of ancestral states at the root of phylogenies (Pagel, 1999). The ancestral state reconstruction analyses were run using the Bayesian implementation of MultiState for 10 M generations (burn-in of 1 M generations). We reconstructed both characters using the reversible-jump MCMC option in the MultiState method with exponential distributions on character transition rates pulled from uniform hyperprior distributions (0–3 for limbs and 0–2 for gape) based on preliminary analyses exploring a range of values. We treated the limb states as ordered, and therefore fixed the transition rates from well-developed to absent limbs and from absent to well-developed limbs equal to zero.

Convergence of runs was assessed using Tracer v1.6 to ensure that analyses had reached stationarity and that ESS values for all parameters were above 200. We ensured that the prior means did not appear truncated (i.e., most of the posterior density was not concentrated toward the upper limit imposed by the hyperprior), which would indicate that the hyperprior distribution chosen was too narrow (Pagel & Meade, 2006). We found that increasing the interval of the hyperprior for analyses generally resulted in increasing rates of transitions among states, as well as decreasing posterior probability for the most probable state at a given node, and therefore sought to use the narrowest hyperprior distribution that did not overly restrict the prior. We also compared our results to preliminary analyses run using the maximum likelihood option in MultiState to help guide selection of appropriate hyperpriors that were neither too restrictive nor too vague (Pagel *et al.*, 2004). All analyses were run on a random sample of 2,000 trees from the combined post-burn-in posterior distributions of the six independent runs using the constrained analysis with the diversified FBD prior, as this represents our preferred phylogeny. We also performed these analyses on the uniform clock; constrained, random fossil tip; constrained, diversified FBD without *Tetrapodophis*; and constrained, diversified FBD without *Tetrapodophis* or fossils from Caldwell *et al.* (2015) analyses (supplementary Figs. S1–8), but results were similar across analyses, and so we focus only on the results using our preferred phylogenetic analyses. Before combining the posterior distributions, they were each thinned by retaining every tenth tree. All trees were rescaled to a total tree length of 1 prior to ancestral state reconstructions.

RESULTS

Non-clock Analysis

In our non-clock phylogenetic analysis of the combined morphological and molecular data, we observed relatively low support values for many of the basal relationships in the tree, including a posterior probability of 0.75 for the node containing Serpentes (Fig. 1.1; File S1). However, when extinct taxa are removed from the tree, the relationships among extant taxa are all strongly supported by posterior probabilities of 1.0 (File S2). As such, the low support values found throughout the tree are the result of uncertain placement of fossil taxa. The positions of *Dinilysia, Najash,* and *Tetrapodophis* are particularly poorly supported, although they are strongly supported (posterior probability ≥ 0.95) as more closely related to crown snakes than to the more basal *Eophis, Parviraptor, Diablophis, Portugalophis,* and *Coniophis,* and as being strongly placed outside of the clade containing Alethinophidia and the Simoliohiidae and Madtsoiidae. As in other recent studies, the extinct Simoliophiidae and Madstoiidae are strongly supported as members of Serpentes that are placed outside of Alethinophidia. As in Caldwell et al. (2015), *Eophis, Parviraptor, Diablophis,* and *Portugalophis* are supported as the first-branching stem snakes, here forming a clade with strong support.

Relaxed Clock Analysis

Considering extant taxa alone, the relationships inferred under the uniform, FBD diversified, and FBD random fossil tips tree priors in relaxed clock analyses were all congruent with the non-clock topology and with strong support for all nodes (Files S3–5).

Considering extinct and extant taxa, support values are lower in many areas of the relaxed clock trees, and support values are generally similar across the trees for the non-clock, uniform clock, and FBD random fossil tip clock trees (Files S6–8). The phylogeny inferred using the FBD prior with diversified sampling resulted in even lower support values throughout much of the tree (File S7). This may be an effect of the fact that two of the three madtsoiids lineages were not included in this analysis to better fit the diversified sampling FBD model. It may be more difficult to infer the placement of the single remaining madtsoiid when the other madtsoiid fossils are not present.

Estimated divergence dates differed widely depending on the tree prior used, with the deepest nodes in the phylogeny showing the largest differences (Fig. 1.2). The uniform clock analysis produced dates that are older than the diversified FBD clock analysis for all nodes except for some less than 60 My old. In contrast, the FBD random fossil tip clock analysis recovered ages that were the oldest of all three analyses for the most basal nodes in the tree, including the root and the age of Ophidia, but that were similar to ages estimated using the uniform tree prior for most other nodes and generally older than those estimated using the FBD diversified tree prior. Other than the assumption about sampling of extant lineages, the random fossil tip FBD prior and diversified FBD priors differ in that the latter permits fossil taxa to be sampled ancestors of a clade and the former does not (Zhang *et al.*, 2015). In our analyses using the diversified FBD prior, many of the fossil taxa were inferred to be sampled ancestors in any given generation of the analyses, which is reflected by the very short branch lengths

of several of the terminal fossils (in a given tree from the posterior, sampled ancestors are shown as zero-length branches).

Node-calibrated analyses excluding morphology and all fossil tips (DNA-only analyses of extant taxa) recovered the same topology among extant lineages as the combined analyses. Analyses using the FBD diversified or uniform tree prior resulted in generally similar ages (Fig. 1.2; Files S9–10). These ages were similar to those inferred by the uniform tree prior analysis of the combined dataset including fossil tips. Constrained analyses using the full combined dataset closely matched the inferred topologies and ages of the analysis without these constraints that used the same tree priors, with the obvious exception of small differences in the vicinity of the topology constraints (Figs. 1.2, 1.3; Files S11–12). For the random fossil tip tree prior, our analyses excluding morphology closely match the results with morphology included, with dates for most nodes differing by less than 10 My (Fig. 1.2; File S13). However, for the diversified FBD prior, node ages for many major clades were much younger in the analyses that excluded morphology (Fig. 1.2; File S14).

When we performed constrained analyses using the diversified FBD prior with *Tetrapodophis* excluded, we inferred divergence dates that are highly similar to those inferred when this taxon was included (File S15–16). When we additionally excluded *Eophis, Parviraptor, Diablophis, and Portugalophis,* we found a somewhat different age for Ophidia, as expected given that we removed the oldest ophidians in our dataset, but very similar dates within Serpentes as in the analysis including all of these fossil taxa

(File S17). This demonstrates that our results are robust to the possibility that these taxa are not actually snakes, and that removing some stem lineages may not bias dates when estimated under the FBD prior. We include these results for completeness, but because the exclusion of these taxa does not have a large effect on our results, we do not comment on them further.

Ancestral State Reconstruction

Ancestral state reconstructions of limb loss did not recover strong support for a single state at every node, but are suggestive of multiple losses of robust hind limbs (Fig. 1.4). The ancestor of Ophidia is recovered as possessing well-developed hind limbs with strong support (PP = 0.97). Although there is considerable uncertainty in phylogenetic relationships for several basal nodes, the majority of these nodes strongly favor the presence of limbs, including nodes within Serpentes. The ancestor of Alethinophidia (and all nodes within this clade) and the most recent common ancestor of Typhlopoidea + Leptotyphlopidae were all reconstructed as most likely to have possessed either reduced limbs or completely lost limbs, although support for the most probable state is relatively low at most nodes. We expect that the marginal or weak support obtained for some of the basal nodes within snakes is a result of the fact that clades dominated by limbless or limb-reduced species are separated from the robust-limbed simoliophiids by relatively short branches. Low support values for more nested clades (e.g., Alethinophidia) might be a result of the fact that our analysis included only higher taxa, and so our phylogeny is incompletely sampled with respect to the full number of known species. It is most likely

that there have been three independent losses of fully-developed limbs within snakes. Our analyses indicate that limb loss occurred once in the ancestral lineage of Typhlopoidea + Leptotyphlopidae, once in the lineage leading to Anomalepididae (represented by *Liotyphlops*), and a third time in the lineage leading to Alethinophidia. It is also possible that additional limb reduction took place in Madtsoiidae (represented by *Sanajeh* in Fig. 1.4); however, the ambiguity regarding the state of the hind limbs in *Wonambi* and the missing data for *Sanajeh* and *Yurlunggur* make it impossible to make such inferences with any confidence.

Ancestral state reconstruction of the macrostomatan phenotype resulted in surprisingly early appearance of this trait (Figs. 1.5, S9). Results were highly similar across analyses with madtsoiids (represented by Sanajeh in Figs. 1.5 and S9) considered to be macrostomatan or coded as uncertain, and so we focus only the results from the analysis with these taxa coded as macrostomatan. The macrostomatan phenotype was weakly recovered as the most probable state as early as the most recent common ancestor of Anomalepididae (represented by *Liotyphlops albirostris* in Fig. 1.5), Alethinophidia, Simoliophiidae, and Madtsoiidae (PP = 0.89). The macrostomatan phenotype is first recovered with strong support in the ancestor of Alethinophidia + Simoliophiidae + Madtsoiidae (PP = 1.0), and the macrostomatan phenotype is the most probable state reconstructed for all nodes within this clade, although with variable support. This reconstruction favors a scenario in which the macrostomatan phenotype evolved a single time in the ancestor of Alethinophidia + Simoliophiidae + Madtsoiidae and then was subsequently independently lost in Aniliidae and Uropeltidae + Cylindrophiidae

(represented by *Anilius scytale* and *Cylindrophis ruffus* + *Uropeltis melanogaster* in Fig. 1.5, respectively). The macrostomatan phenotype may have been additionally lost in Anomalepididae, although the support for an origin of the macrostomatan phenotype before the split of this lineage from the rest of Serpentes is somewhat lower.

DISCUSSION

In relaxed clock and non-clock combined morphological and molecular analyses, relationships among extant taxa are largely congruent with previous molecular analyses (e.g., Vidal & Hedges, 2002; Vidal *et al.*, 2007; Wiens *et al.*, 2012; Pyron *et al.*, 2013, Streicher & Wiens, 2016). To generate our preferred phylogeny (Fig. 1.3) we constrained two clades (Henophidia and Bolyeriidae + Pythonidae + Loxocemidae + Xenopeltidae) to be consistent with the topology of Streicher & Wiens (2016), which has the most extensive sampling of independent loci of any study of the relationships among the major clades of snakes to date. These relationships contrast strongly with the relationships inferred by studies that rely on morphological data alone (e.g., Conrad, 2008; Gauthier *et al.*, 2012). In particular, morphology-based studies generally recover the traditionally recognized clades "Macrostomata" and "Scolecophidia", both of which are strongly supported as paraphyletic by our combined and DNA only analyses, as well as previous molecular analyses (e.g., Vidal & Hedges, 2002; Vidal *et al.*, 2007; Wiens *et al.*, 2008; Wiens *et al.*, 2012, Streicher & Wiens, 2016). Fossil taxa are recovered in positions generally congruent with other recent studies. There are no strongly supported conflicts in the placement of any fossil taxa that were included in Hsiang *et al.* (2015) between our

phylogenies and the unconstrained, combined, Bayesian analysis of Hsiang *et al.* (2015). As in Caldwell *et al.* (2015), *Eophis, Portugalophis, Diablophis,* and *Parviraptor* are all recovered as the earliest branching stem snakes. Consistent with Martill *et al.* (2015), *Tetrapodophis* is recovered as a stem snake in all of our analyses, although the support for Serpentes exclusive of several stem snake fossils including *Tetrapodophis* is weak across our phylogenetic analyses.

We find that the approach used for divergence dating can have potentially large effects on estimated ages of clades. Several studies have found that tip dating with a uniform tree prior (previously the only option in MrBayes) or birth-death prior (an option in BEAST that preceded the implementation of the FBD prior) tends to yield dates that are considerably older than those estimated using traditional node-calibration approaches or that have been suggested based on the fossil record alone (Arcila *et al.*, 2015; Beck & Lee, 2014; O'Reilly & Donoghue, 2016; Puttick *et al.*, 2016; Herrera & Dávalos, 2016). We find that this is not the case with our analyses. Our node-calibrated, DNA-only analyses using either the FBD diversified or uniform tree prior produced ages that were similar to those estimated from the tip-dating analysis using the uniform tree prior (Fig. 1.2). Consistent with previous studies that showed that dates inferred using an FBD model (either for node calibration or tip calibration) resulted in younger dates than inferred under other tip-calibrated models and more in line with previous estimates, the diversified FBD prior results in ages that are generally younger than the ages inferred under the uniform tree prior. However, the results of the FBD random fossil tip analysis are not consistent with this pattern. Instead, the FBD random fossil tip analysis is largely

consistent with the tip-dated analysis using the uniform tree prior, with the exception of the deepest nodes in the tree, which are considerably older than those found in the uniform analysis or the FBD diversified analysis. This highlights the importance of selecting appropriate models and priors for divergence dating. Given that the FBD prior provides a more realistic model of the branching process of phylogenetic trees than the uniform prior (Heath *et al.*, 2014; Zhang *et al.*, 2015) and that the diversified sampling assumption matches our sampling more closely than assuming random sampling, we prefer the results of analyses using the diversified FBD prior.

Although we prefer the results using the diversified FBD prior, we consider it unlikely that many of the fossils included in the analyses actually represent sampled ancestors. It is certainly possible that some fossils are sampled ancestors, but for a large proportion of fossils to truly be sampled ancestors would imply high fossil sampling probabilities in conjunction with low extinction rates relative to speciation rates. We are unsure of the exact cause of the high number of inferred sampled ancestors recovered in the analyses, but it is likely an issue caused by the prior placing relatively high weight on fossils as sampled ancestors (Zhang *et al.*, 2015). Zhang *et al.* (2015) identified this same behavior in some analyses using FBD priors in MrBayes and were able to remedy it by using piecewise models in which fossil sampling, speciation, and extinction rates vary across different portions of the tree. We attempted to use a piecewise prior on a dataset that included a small subsample of the molecular data (to shorten run times), but the analyses still inferred many fossils as sampled ancestors (results not shown). Even if most of the fossils are not actually sampled ancestors, it is possible that the zero-length (or

nearly-zero-length in the consensus trees) branches to some fossils may provide a reasonable approximation of species that went extinct during rapid radiation and therefore sit on very short branches of the tree in reality.

Fixing monophyly of the clade containing Pythonidae, Loxocemidae, Xenopeltidae, and Bolyeriidae and the monophyly of this clade plus Boidae and Uropeltidae + Cylindrophiidae had little effect on divergence estimation of nodes deeper in the tree (Figs. 1.2, 1.3), and results in a phylogeny that closely matches the phylogeny of Streicher & Wiens (2016). We found that the inferred dates were similar whether morphology was included to help place fossil tips or if morphology was excluded for the random fossil tip tree prior (Files S12–13). Including fossil tips in the absence of morphology is similar to the original formulation of the FBD model introduced by Heath *et al.* (2014). This suggests that if morphological data are not available in a form amenable to combined morphological and molecular analyses for a given group, including fossil tips as calibrations may yield results that are highly similar to those obtained through analyses of a full combined dataset. Localizing fossil tips to a given clade requires fixing the monophyly of the clades in question, but this is also a requirement for traditional node dating. Therefore, when node calibrations are difficult to specify for a given node, as is often the case (Parham *et al.*, 2012), it may be preferable to include calibrating fossils as a tips instead, even if morphological data is not included. When we excluded morphological data and used the diversified FBD tree prior, which permits sampled ancestors, we found that dates were much younger than when morphology was included (Fig. 1.2; Files S11, S14). This appears to be caused by a

tendency for all fossils to be placed as sampled ancestors in the absence of morphological data. Therefore, the fossils simply sit on branches leading to extant taxa, and do not provide as much calibration information for clades. It may be possible to remedy this issue with priors that place less weight on fossils as ancestors, but we recommend caution if attempting to use the FBD diversified prior for divergence dating when fossils are included as tips in the absence of morphology.

Our preferred phylogeny (constrained, diversified FBD, Fig. 1.3) includes ages for Toxicofera and Ophidia that are older than other studies of squamate divergence dates (e.g., Hedges & Vidal, 2009; Mulcahy *et al.*, 2012; Jones *et al.*, 2013). This is not surprising, given that we have included the recently reclassified *Eophis, Portugalophis, Diablophis,* and *Parviraptor* as calibrating fossils, which are older than many previous estimates of the age of Toxicofera. Our inferred age for Serpentes is within the range of previous estimates based on traditional node-calibrated methods (Burbrink & Pyron, 2008; Vidal *et al.*, 2009; Scanlon & Lee, 2011; Mulcahy *et al.*, 2012; Pyron & Burbrink, 2012; Jones *et al.*, 2013). Our inferred dates are also similar to dates inferred using tip calibration by Hsiang *et al.* (2015) on the consensus tree from their combined data, Bayesian, unconstrained, non-clock analysis, although several nodes are somewhat older in our analyses. Most notably, we recover an age of 120 Ma for Serpentes, compared to ~107 Ma in Hsiang *et al.* (2015). These differences may be due to the additional fossil taxa that we have included, the different tree prior that we used, the fact that we co-estimated phylogeny and divergence dates (Hsiang *et al.* estimated dates on a fixed topology), or some combination of these factors. Hsiang *et al.* also calibrated the

Alethinophidia node, and their choice of calibration for this node may have restricted this and other nodes to younger ages than would otherwise be recovered. We therefore prefer our estimated dates over those of Hsiang *et al.* because they are based on a larger set of calibrating tips, use an improved tree prior, and accommodate more uncertainty associated with estimating clade ages, including uncertainty resulting from topological uncertainty.

Our Bayesian ancestral state reconstructions inferred earlier evolution of the macrostomatan phenotype and later losses of robust limbs than have traditionally been inferred based on extant taxa alone (Figs. 1.4, 1.5). Considering extant snake taxa alone, it would appear obvious that external, well-developed hind limbs were lost in an ancestor of Serpentes. However, our character state reconstruction analyses using fossil and extant snakes most strongly favor a scenario in which robust hind limbs are maintained in the early ancestors of snakes until the ancestor of Alethinophidia + Madtsoiidae + Simoliophiidae. This therefore indicates that robust hind limbs were independently lost in multiple early snake lineages (i.e., Alethinophidia, Anomalepididae, and Typhlopoidea + Leptotyphlopidae). Multiple losses of hind limbs have been previously suggested in studies that inferred the simoliophiids to be nested within crown snakes (Serpentes) as an alternative to a single loss of limbs in the ancestor of Serpentes followed by a re-evolution of limbs in Simoliophiidae (Tchernov *et al.*, 2000; Rieppel *et al.*, 2003), which would constitute a major violation of Dollo's Law. Our analyses are the first to explicitly test and support this hypothesis within a Bayesian statistical framework. These findings suggest that reasonably well-developed hind limbs were maintained for at least 70 M

years (based on the median estimates of the ages of Toxicofera, and the clade containing Simoliophiidae, Madtsoiidae, and Alethinophidia [the youngest snake node strongly supported as possessing well-developed hind limbs]) in the ancestors of modern snakes. Such a finding is consistent with the well-known phenomenon of repeated independent evolution of limb reduction and persistence of reduced limb structures for long periods of time within other major squamate clades (Brandley *et al.*, 2008). Many modern snakes still possess external remnants of hind limbs, demonstrating that limb morphologies apparently intermediate between fully-developed hind limbs and the complete absence of limbs can persist for very long periods of time.

The macrostomatan phenotype is inferred to have evolved a single time within snakes, most probably in the ancestor of Alethinophidia + Madtsoiidae + Simoliophiidae, although there is weak support for an even earlier evolution of this trait (Fig. 1.5). This reconstruction therefore indicates that the macrostomatan phenotype evolved relatively early in snake history, and was subsequently independently lost in Aniliidae and Uropeltidae + Cylindrophiidae, and potentially in the Anomalepididae as well. This contrasts with traditional hypotheses that "scolecophidians", aniliids and uropeltids + cylindrophiids, and "macrostomatans" represent an evolutionary grade progressing from small to large gapes (Cundall & Greene, 2000). The independent loss of the macrostomatan phenotype in these lineages may be associated with a primarily subterranean lifestyle, as all of these lineages exhibit robust skulls and a number of apparent cranial adaptations for burrowing (Rieppel, 1977, Rieppel *et al.*, 2009). This is not surprising, given that whole of suites of characters have evolved convergently in

snakes and other limbless, burrowing squamates which have often caused these divergent lineages to group together in morphology-based analyses (Lee, 1998; Wiens *et al.*, 2006).

Reduction in gape size is thought to be associated with adaptations to fossorial life (Savitsky, 1983), and has been observed in fossorial colubroids, which tend to have shorter lower jaws and quadrates, traits associated with smaller gape, than non-fossorial colubroids (Haines, 1967). Such convergence may also explain the similarity in the skulls of "scolecophidians" that has traditionally caused them to be grouped together based on morphology. In addition to their burrowing habits, "scolecophidians" share dietary specializations of feeding on larvae and pupae of social insects, and their skulls exhibit a non-macrostomatan condition very different from the non-macrostomatan condition of aniliids and uropeltids + cylindrophiids (List, 1966; Kley & Brainerd, 1999; Kley, 2001; Rieppel *et al.*, 2009). Our reconstruction of feeding phenotype for Serpentes and Serpentes exclusive of Typhlopoidea + Leptotyphlopidae were equivocal (Fig. 1.5), but even assuming that the ancestors of these clades did not possess the macrostomatan phenotype, we consider it unlikely that they possessed skulls as specialized for burrowing and feeding on larval arthropods as those of "scolecophidians", and therefore suggest that the "scolecophidian" skull phenotype evolved convergently due to the similar feeding and burrowing habits of Anomalepididae and Typhlopoidea + Leptotyphlopidae. This is consistent with recent evidence showing that the visual system of the most recent common ancestor of extant snakes was likely not as reduced as in modern fossorial snakes (Simões *et al.,* 2015). The strong support for the macrostomatan phenotype evolving before the diversification of Alethinophidia indicates that the

aniliid/uropeltid/cylindrophiid feeding phenotype does not represent an ancestral feeding type, but one that was independently evolved from a feeding system more similar to those of macrostomatan snakes. This does not necessarily mean that the ancestors of alethinophidian snakes possessed feeding systems as specialized for consuming large prey as those of modern boids, pythonids, or colubroids (muscular anatomy may even imply that they were not [Rieppel, 2012]), but does indicate that they were capable of larger gapes than aniliids, uropeltids, or cylindrophiids, and that this phenotype is perhaps maladaptive for burrowing snakes, which may be better served by more robust skulls that can facilitate burrowing. More detailed morphological and anatomical studies will be needed to more clearly understand the pathways by which the ability to consume large prey has been lost.

CONCLUSIONS

We used tip calibration to simultaneously estimate the phylogeny of the major clades of snakes and important fossils, including several that have been recently discovered, and infer divergence dates for the major clades of snakes. We show that for our dataset, the diversified FBD prior results in ages that are more consistent with previous estimates based on node calibration and the fossil record than the older dates inferred under the uniform or FBD random fossil tip priors. When we calibrated DNA-only phylogenies with node calibrations only, these analyses produced ages similar to the uniform or FBD random fossil tip prior analyses. We additionally demonstrate that when fossil tips are included in FBD analyses in the absence of morphology, they can yield

similar dates to analyses of the full combined dataset, although this is dependent on the tree prior used. Using Bayesian ancestral state reconstruction methods, we show strong support for multiple independent losses of robust hind limbs within Serpentes, and a single strongly supported origin of the macrostomatan phenotype with subsequent loss of this phenotype in multiple burrowing lineages of snakes.

REFERENCES

Apesteguía, S. & Zaher, H. (2006) A Cretaceous terrestrial snake with robust hindlimbs and a sacrum. *Nature*, **440**, 1037–1040.

Arcila, D., Pyron, R.A., Tyler, J.C., Ortí, G., & Betancur-R., R. (2015) An evaluation of fossil tip-dating versus node-age calibrations in tetraodontiform fishes (Teleostei: Percomorphaceae). *Molecular Phylogenetics and Evolution*, **82**, **Part A**, 131–145.

Beck, R.M.D. & Lee, M.S.Y. (2014) Ancient dates or accelerated rates? Morphological clocks and the antiquity of placental mammals. *Proceedings of the Royal Society B: Biological Sciences*, **281**, 20141278.

Brandley, M.C., Huelsenbeck, J.P., & Wiens, J.J. (2008) Rates and patterns in the evolution of snake-like body form in squamate reptiles: evidence for repeated re-evolution of lost digits and long-term persistence of intermediate body forms. *Evolution*, **62**, 2042–2064.

Broschinski, A. (2000) The lizards from the Guimarota mine. *Guimarota: A Jurassic Ecosystem.* (ed. by T. Martin and B. Krebs), pp. 59–68. Verlag Dr. Friedrich Pfeil, Munich.

Burbrink, F.T. & Pyron, R.A. (2008) The taming of the skew: estimating proper confidence intervals for divergence dates. *Systematic Biology*, **57**, 317–328.

Caldwell, M.W., Nydam, R.L., Palci, A., & Apesteguía, S. (2015) The oldest known snakes from the Middle Jurassic-Lower Cretaceous provide insights on snake evolution. *Nature Communications*, **6**, 5996.

Conrad, J.L. (2008) Phylogeny and systematics of Squamata (Reptilia) based on morphology. *Bulletin of the American Museum of Natural History*, **310**, 1–182.

Cundall, D. & Greene, H.W. (2000) Feeding in snakes. *Feeding, form, function, and evolution in tetrapod vertebrates* (ed. by K. Schwenk), pp. 293–333. Academic Press, San Diego.

Estes, R., Frazzetta, T.H., & Williams, E.E. (1970) Studies on the fossil snake Dinilysia patagonica Smith Woodward: Part 1. Cranial morphology. *Bulletin of the Museum of Comparative Zoology*, **140**, 25–74.

Evans, S.E. (1994) A new anguimorph lizard from the Jurassic and Lower Cretaceous of England. *Palaeontology*, **37**, 33–49.

Evans, S.E. (1996) Parviraptor (Squamata: Anguimorpha) and other lizards from the Morrison Formation at Fruita, Colorado. *Mus North Arizona Bull*, **60**, 243–248.

Finarelli, J.A. & Flynn, J.J. (2006) Ancestral state reconstruction of body size in the Caniformia (Carnivora, Mammalia): the effects of incorporating data from the fossil record. *Systematic Biology*, **55**, 301–313.

Gauthier, J.A., Kearney, M., Maisano, J.A., Rieppel, O., & Behlke, A.D.B. (2012) Assembling the squamate tree of life: perspectives from the phenotype and the fossil record. *Bulletin of the Peabody Museum of Natural History*, **53**, 3–308.

Haas G. (1979) On a new snakelike reptile from the Lower Cenomanian of Ein Jabrud, near Jerusalem. *Bulletin du Muséum National d'Histoire Naturelle,* **1**, 51–64.

Haines, T.P. (1967) Variations of colubrid skulls, their correlations and their value in taxonomy. *Herpetologica*, **23**, 142–145.

Harrington SM, Reeder TW. (2016) Data from: Phylogenetic inference and divergence dating of snakes using molecules, morphology, and fossils: new insights on convergent evolution of feeding morphology and limb reduction. DryadDigital Repository http://dx.doi.org/10.5061/dryad.cm603.

Heath, T.A., Huelsenbeck, J.P., & Stadler, T. (2014) The fossilized birth–death process for coherent calibration of divergence-time estimates. *Proceedings of the National Academy of Sciences*, **111**, E2957–E2966.

Hedges & Vidal, N. (2009) Lizards, snakes, and amphisbaenians (Squamata). *The Timetree of Life* (ed. by S.B. Hedges and S. Kumar), pp. 383–389. Oxford University Press, New York.

Herrera, J.P. & Dávalos, L.M. (2016) Phylogeny and divergence times of lemurs Inferred with recent and ancient fossils in the tree. *Systematic Biology*, **65**, 772–791.

Hsiang, A.Y., Field, D.J., Webster, T.H., Behlke, A.D., Davis, M.B., Racicot, R.A., & Gauthier, J.A. (2015) The origin of snakes: revealing the ecology, behavior, and evolutionary history of early snakes using genomics, phenomics, and the fossil record. *BMC Evolutionary Biology*, **15**, 87.

Huelsenbeck, J.P., Larget, B., & Alfaro, M.E. (2004) Bayesian phylogenetic model selection using reversible jump Markov chain Monte Carlo. *Molecular Biology and Evolution*, **21**, 1123–1133.

Jones, M.E., Anderson, C.L., Hipsley, C.A., Müller, J., Evans, S.E., & Schoch, R.R. (2013) Integration of molecules and new fossils supports a Triassic origin for Lepidosauria (lizards, snakes, and tuatara). *BMC Evolutionary Biology*, **13**, 208.

Kley, N.J. (2001) Prey transport mechanisms in blindsnakes and the evolution of unilateral feeding systems in snakes. *American Zoologist*, **41**, 1321–1337.

Kley, N.J. & Brainerd, E.L. (1999) Feeding by mandibular raking in a snake. *Nature*, **402**, 369–370.

Ksepka, D.T., Parham, J.F., Allman, J.F., et al. (2015) The Fossil Calibration Database—A new resource for divergence dating. *Systematic Biology*, **64**, 853–859.

Lanfear, R., Calcott, B., Ho, S.Y.W., & Guindon, S. (2012) PartitionFinder: combined selection of partitioning schemes and substitution models for phylogenetic analyses. *Molecular Biology and Evolution*, **29**, 1695–1701.

Lee, M.S.Y. (1998) Convergent evolution and character correlation in burrowing reptiles: towards a resolution of squamate relationships. *Biological Journal of the Linnean Society*, **65**, 369–453.

Lee, M.S.Y. & Caldwell, M.W. (2000) Adriosaurus and the affinities of mosasaurs, dolichosaurs, and snakes. *Journal of Paleontology*, **74**, 915–937.

Lee, M.S.Y., Hugall, A.F., Lawson, R., & Scanlon, J.D. (2007) Phylogeny of snakes (Serpentes): combining morphological and molecular data in likelihood, Bayesian and parsimony analyses. *Systematics and Biodiversity*, **5**, 371–389.

Lepage, T., Bryant, D., Philippe, H., & Lartillot, N. (2007) A general comparison of relaxed molecular clock models. *Molecular Biology and Evolution*, **24**, 2669–2680.

Lewis, P.O. (2001) A likelihood approach to estimating phylogeny from discrete morphological character data. *Systematic biology*, **50**, 913–925.

List, J.C. (1966) Comparative osteology of the snake families Typhlopidae and Leptotyphlopidae. *Illinois Biological Monographs*, **36**, 1–112.

Martill, D.M., Tischlinger, H., & Longrich, N.R. (2015) A four-legged snake from the Early Cretaceous of Gondwana. *Science*, **349**, 416–419.

Miller, M.., Pfeiffer, W., & Schwartz, T. (2010) Creating the CIPRES Science Gateway for inference of large phylogenetic trees. *Gateway Computing Environments Workshop (GCE), 2010*, 1–8.

Mulcahy, D.G., Noonan, B.P., Moss, T., Townsend, T.M., Reeder, T.W., Sites, J.W., & Wiens, J.J. (2012) Estimating divergence dates and evaluating dating methods using phylogenomic and mitochondrial data in squamate reptiles. *Molecular Phylogenetics and Evolution*, **65**, 974–991.

Noonan, B.P. & Chippindale, P.T. (2006) Dispersal and vicariance: the complex evolutionary history of boid snakes. *Molecular Phylogenetics and Evolution*, **40**, 347–358.

O'Reilly, J.E. & Donoghue, P.C.J. (2016) Tips and nodes are complementary not competing approaches to the calibration of molecular clocks. *Biology Letters*, **12**, 20150975.

Pagel, M. (1999) The maximum likelihood approach to reconstructing ancestral character states of discrete characters on phylogenies. *Systematic Biology*, **48**, 612–622.

Pagel, M. & Meade, A. (2006) Bayesian analysis of correlated evolution of discrete characters by reversible-jump Markov chain Monte Carlo. *The American Naturalist*, **167**, 808–825.

Pagel, M., Meade, A., & Barker, D. (2004) Bayesian estimation of ancestral character states on phylogenies. *Systematic Biology*, **53**, 673–684.

Palci, A., Caldwell, M.W., & Albino, A.M. (2013b) Emended diagnosis and phylogenetic relationships of the Upper Cretaceous fossil snake Najash rionegrina Apesteguía and Zaher, 2006. *Journal of Vertebrate Paleontology*, **33**, 131–140.

Palci, A., Caldwell, M.W., & Nydam, R.L. (2013a) Reevaluation of the anatomy of the Cenomanian (Upper Cretaceous) hind-limbed marine fossil snakes Pachyrhachis, Haasiophis, and Eupodophis. *Journal of Vertebrate Paleontology*, **33**, 1328–1342.

Palci, A., Caldwell, M.W., & Scanlon, J.D. (2014) First report of a pelvic girdle in the fossil snake Wonambi naracoortensis Smith, 1976, and a revised diagnosis for the genus. *Journal of Vertebrate Paleontology*, **34**, 965–969.

Parham, J.F., Donoghue, P.C.J., Bell, C.J., et al. (2012) Best practices for justifying fossil calibrations. *Systematic Biology*, **61**, 346–359.

Puttick, M.N., Thomas, G.H., & Benton, M.J. (2016) Dating placentalia: Morphological clocks fail to close the molecular fossil gap. *Evolution*, **70**, 873–886.

Pyron, R.A. (2011) Divergence time estimation using fossils as terminal taxa and the origins of Lissamphibia. *Systematic Biology*, **60**, 466–481.

Pyron, R.A. & Burbrink, F.T. (2012) Extinction, ecological opportunity, and the origins of global snake diversity. *Evolution*, **66**, 163–178.

Pyron, R.A., Burbrink, F.T., & Wiens, J.J. (2013) A phylogeny and revised classification of Squamata, including 4161 species of lizards and snakes. *BMC evolutionary biology*, **13**, 93.

Rage, J.-C. & Escuillié, F. (2000) Un nouveau serpent bipède du Cénomanien (Crétacé). Implications phylétiques. *Comptes Rendus de l'Académie des Sciences - Series IIA - Earth and Planetary Science*, **330**, 513–520.

Rambaut A, Suchard MA, Xie D, Drummond AJ. (2014) Tracer v1.6. Available at: http://beast.bio.ed.ac.uk/Tracer

Reeder, T.W., Townsend, T.M., Mulcahy, D.G., Noonan, B.P., Wood, P.L., Jr., Sites, J.W., Jr., & Wiens, J.J. (2015) Integrated Analyses Resolve Conflicts over Squamate Reptile Phylogeny and Reveal Unexpected Placements for Fossil Taxa. *PLoS ONE*, **10**, e0118199.

Rieppel, O. (1977) Studies on the skull of the Henophidia (Reptilia: Serpentes). *Journal of Zoology*, **181**, 145–173.

Rieppel, O. (2012) "Regressed" macrostomatan snakes. *Fieldiana Life and Earth Sciences*, **5**, 99–103.

Rieppel, O., Kley, N.J., & Maisano, J.A. (2009) Morphology of the skull of the white-nosed blindsnake, Liotyphlops albirostris (Scolecophidia: Anomalepididae). *Journal of Morphology*, **270**, 536–557.

Rieppel, O., Kluge, A.G., & Zaher, H. (2002) Testing the phylogenetic relationships of the Pleistocene snake Wonambi naracoortensis Smith. *Journal of Vertebrate Paleontology*, **22**, 812–829.

Rieppel, O., Zaher, H., Tchernov, E., & Polcyn, M.J. (2003) The anatomy and relationships of Haasiophis terrasanctus, a fossil snake with well-developed hind limbs from the mid-Cretaceous of the Middle East. *Journal of Paleontology*, **77**, 536–558.

Ronquist, F., Klopfstein, S., Vilhelmsen, L., Schulmeister, S., Murray, D.L., & Rasnitsyn, A.P. (2012a) A total-evidence approach to dating with fossils, applied to the early radiation of the Hymenoptera. *Systematic Biology*, **61**, 973–999.

Ronquist, F., Teslenko, M., van der Mark, P., Ayres, D.L., Darling, A., Hohna, S., Larget, B., Liu, L., Suchard, M.A., & Huelsenbeck, J.P. (2012b) MrBayes 3.2: efficient Bayesian phylogenetic inference and model choice across a large model space. *Systematic Biology*, **61**, 539–542.

Sanders, K.L. & Lee, M.S.Y. (2008) Molecular evidence for a rapid late-Miocene radiation of Australasian venomous snakes (Elapidae, Colubroidea). *Molecular Phylogenetics and Evolution*, **46**, 1165–1173.

Savitzky, A.H. (1983) Coadapted character complexes among snakes: fossoriality, piscivory, and durophagy. *American Zoologist*, **23**, 397–409.

Scanferla, A., Zaher, H., Novas, F.E., de Muizon, C., & Céspedes, R. (2013) A new snake skull from the Paleocene of Bolivia sheds light on the evolution of macrostomatans. *PLoS ONE*, **8**, e57583.

Scanlon, J.D. & Lee, M.S.Y. (2000) The Pleistocene serpent Wonambi and the early evolution of snakes. *Nature*, **403**, 416–420.

Scanlon, J.D. & Lee, M.S.Y. (2011) The major clades of living snakes: morphological evolution, molecular phylogeny, and divergence dates. *Reproductive Biology and Phylogeny of Snakes* (ed. by R.D. Aldridge and D. Sever), pp. 55–95. CRC Press, Boca Raton.

Simões, B.F., Sampaio, F.L., Jared, C., Antoniazzi, M.M., Loew, E.R., Bowmaker, J.K., Rodriguez, A., Hart, N.S., Hunt, D.M., Partridge, J.C., & Gower, D.J. (2015) Visual system evolution and the nature of the ancestral snake. *Journal of Evolutionary Biology*, **28**, 1309–1320.

Slater, G.J. (2013) Phylogenetic evidence for a shift in the mode of mammalian body size evolution at the Cretaceous-Palaeogene boundary. *Methods in Ecology and Evolution*, **4**, 734–744.

Slater, G.J., Harmon, L.J., & Alfaro, M.E. (2012) Integrating fossils with molecular phylogenies improves inference of trait evolution. *Evolution*, **66**, 3931–3944.

Streicher, J.W. & Wiens, J.J. (2016) Phylogenomic analyses reveal novel relationships among snake families. *Molecular Phylogenetics and Evolution*, **100**, 160–169.

Tchernov, E., Rieppel, O., Zaher, H., Polcyn, M.J., & Jacobs, L. (2000) A fossil snake with limbs. *Science*, **287**, 2010–2012.

Vidal, N., Delmas, A.-S., & Hedges, S.B. (2007) The higher-level relationships of alethinophidian snakes inferred from seven nuclear and mitochondrial genes. *Biology of the Boas and Pythons* (ed. by R.W. Henderson and R. Powell), pp. 27–33. Eagle Mountain Publishing, Eagle Mountain, Utah.

Vidal, N. & Hedges, S.B. (2002) Higher-level relationships of snakes inferred from four nuclear and mitochondrial genes. *Comptes Rendus Biologies*, **325**, 977–985.

Vidal, N., Rage, J.-C., Couloux, A., & Hedges, S.B. (2009) Snakes (Serpentes). *The timetree of life* (ed. by S.B. Hedges and S. Kumar), pp. 390–397. Oxford University Press, New York.

Vitt, L.J. & Caldwell, J.P. (2008) *Herpetology: An Introductory Biology of Amphibians and Reptiles.* Academic Press, San Diego.

Wiens, J.J., Brandley, M.C., & Reeder, T.W. (2006) Why does a trait evolve multiple times within a clade? Repeated evolution of snakelike body form in squamate reptiles. *Evolution*, **60**, 123–141.

Wiens, J.J., Hutter, C.R., Mulcahy, D.G., Noonan, B.P., Townsend, T.M., Sites, J.W., & Reeder, T.W. (2012) Resolving the phylogeny of lizards and snakes (Squamata) with extensive sampling of genes and species. *Biology Letters*, **8**, 1043–1046.

Wiens, J.J., Kuczynski, C.A., Smith, S.A., Mulcahy, D.G., Sites, J.W., Townsend, T.M., & Reeder, T.W. (2008) Branch lengths, support, and congruence: testing the phylogenomic approach with 20 nuclear loci in snakes. *Systematic Biology*, **57**, 420–431.

Zaher, H., Apesteguía, S., & Scanferla, C.A. (2009) The anatomy of the upper cretaceous snake Najash rionegrina Apesteguía & Zaher, 2006, and the evolution of limblessness in snakes. *Zoological Journal of the Linnean Society*, **156**, 801–826.

Zaher, H. & Rieppel, O. (2002) On the phylogenetic relationships of the Cretaceous snakes with legs, with special reference to Pachyrhachis problematicus (Squamata, Serpentes). *Journal of Vertebrate Paleontology*, **22**, 104–109.

Zaher, H. & Scanferla, C.A. (2012) The skull of the Upper Cretaceous snake Dinilysia patagonica Smith-Woodward, 1901, and its phylogenetic position revisited. *Zoological Journal of the Linnean Society*, **164**, 194–238.

Zhang, C., Stadler, T., Klopfstein, S., Heath, T.A., & Ronquist, F. (2016) Total-Evidence Dating under the Fossilized Birth–Death Process. *Systematic Biology*, **65**, 228–249.

Figure 1.1. Consensus phylogeny based on morphology and DNA including all compatible groups for the major clades of snakes and key fossil taxa from non-clock MrBayes analyses. Circles at nodes denote posterior probabilities (PP): black = PP ≥ 0.95, gray = 0.95 > PP ≥ 0.75, white = 0.75 > PP. Selected families and higher clades are indicated at nodes or at tips in association with vertical bars. Note that Henophidia is not recovered as monophyletic in our unconstrained analyses, but is constrained to be monophyletic for our preferred analysis (see text).

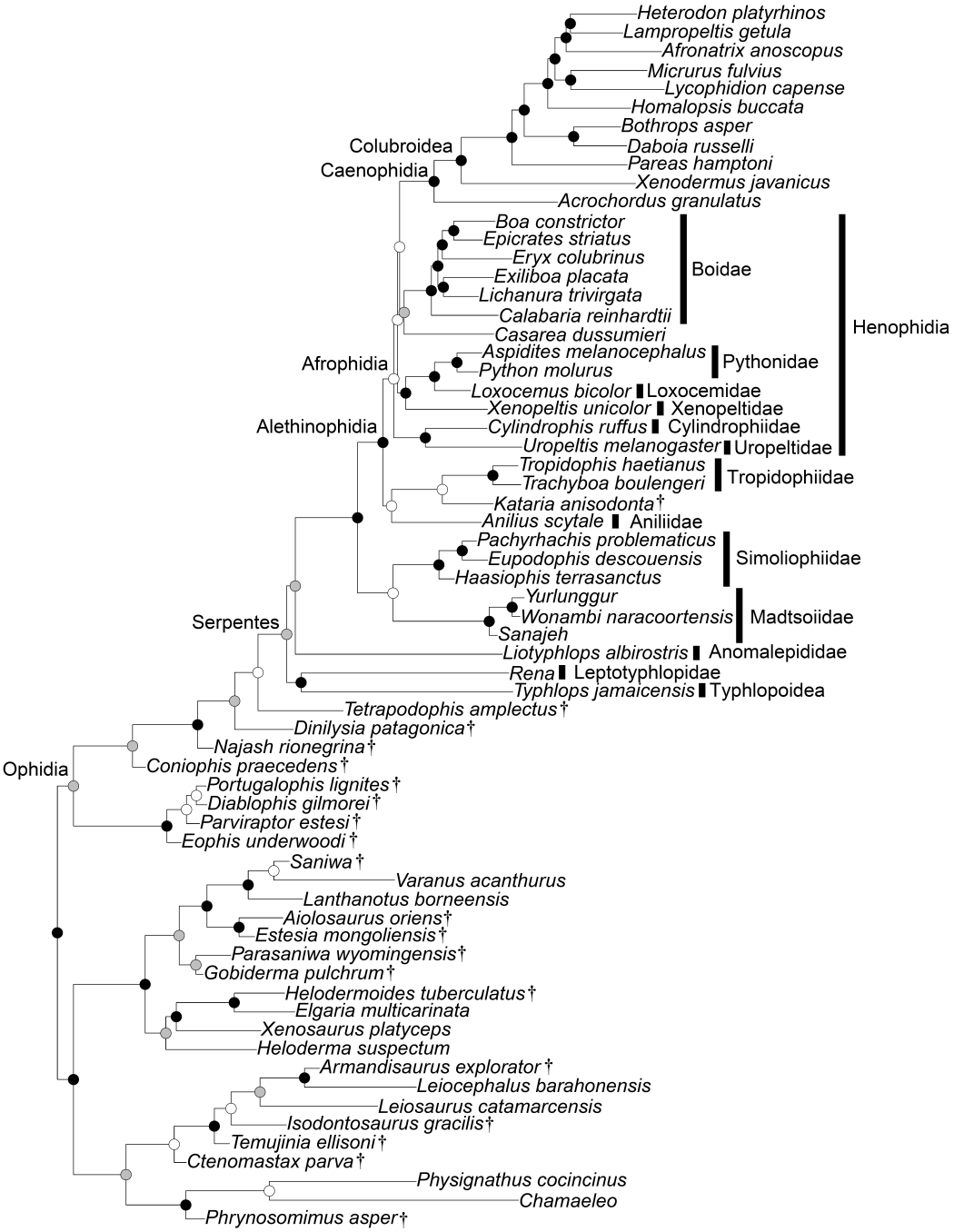
Heterodon platyrhinos
Lampropeltis getula
Afronatrix anoscopus
Micrurus fulvius
Lycophidion capense
Homalopsis buccata
Bothrops asper
Daboia russelli
Pareas hamptoni
Xenodermus javanicus
Acrochordus granulatus
Colubroidea
Caenophidia
Boa constrictor
Epicrates striatus
Eryx colubrinus
Exiliboa placata
Lichanura trivirgata
Calabaria reinhardtii
Boidae
Casarea dussumieri
Henophidia
Aspidites melanocephalus
Python molurus
Pythonidae
Afrophidia
Loxocemus bicolor
Loxocemidae
Xenopeltis unicolor
Xenopeltidae
Alethinophidia
Cylindrophis ruffus
Cylindrophiidae
Uropeltis melanogaster
Uropeltidae
Tropidophis haetianus
Trachyboa boulengeri
Tropidophiidae
Kataria anisodonta†
Anilius scytale
Aniliidae
Pachyrhachis problematicus
Eupodophis descouensis
Haasiophis terrasanctus
Simoliophiidae
Yurlunggur
Wonambi naracoortensis
Sanajeh
Madtsoiidae
Serpentes
Liotyphlops albirostris
Anomalepididae
Rena
Leptotyphlopidae
Typhlops jamaicensis
Typhlopoidea
Tetrapodophis amplectus†
Dinilysia patagonica†
Najash rionegrina†
Coniophis praecedens†
Ophidia
Portugalophis lignites†
Diablophis gilmorei†
Parviraptor estesi†
Eophis underwoodi†
Saniwa†
Varanus acanthurus
Lanthanotus borneensis
Aiolosaurus oriens†
Estesia mongoliensis†
Parasaniwa wyomingensis†
Gobiderma pulchrum†
Helodermoides tuberculatus†
Elgaria multicarinata
Xenosaurus platyceps
Heloderma suspectum
Armandisaurus explorator†
Leiocephalus barahonensis
Leiosaurus catamarcensis
Isodontosaurus gracilis†
Temujinia ellisoni†
Ctenomastax parva†
Physignathus cocincinus
Chamaeleo
Phrynosomimus asper†

Figure 1.2. Top: Representation of our preferred phylogeny (constrained, diversified FBD) with clades collapsed and most fossil taxa removed with key major clades indicated. Bottom: Divergence dates inferred across our different analyses for five major clades shown in the top panel. Bars represent 95% HPD intervals for the age of a clade and points represent the median age. The DNA-only analyses did not include fossil taxa, and so no age could be estimated for Ophidia in these analyses.

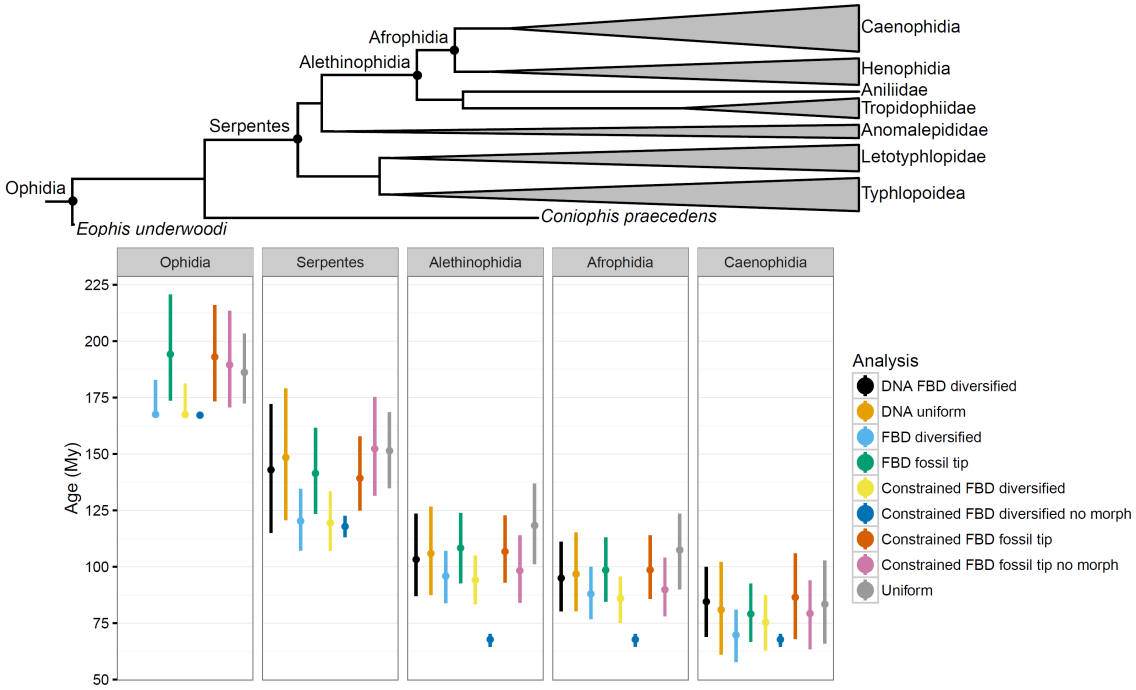

Figure 1.3. Consensus phylogeny including all compatible groups showing divergence dates from the constrained, diversified FBD MrBayes analyses. Circles at nodes denote posterior probabilities (PP): black = PP ≥ 0.95, gray = 0.95 > PP ≥ 0.75, white = 0.75 > PP. Node bars represent the 95% HPD intervals of divergence dates.

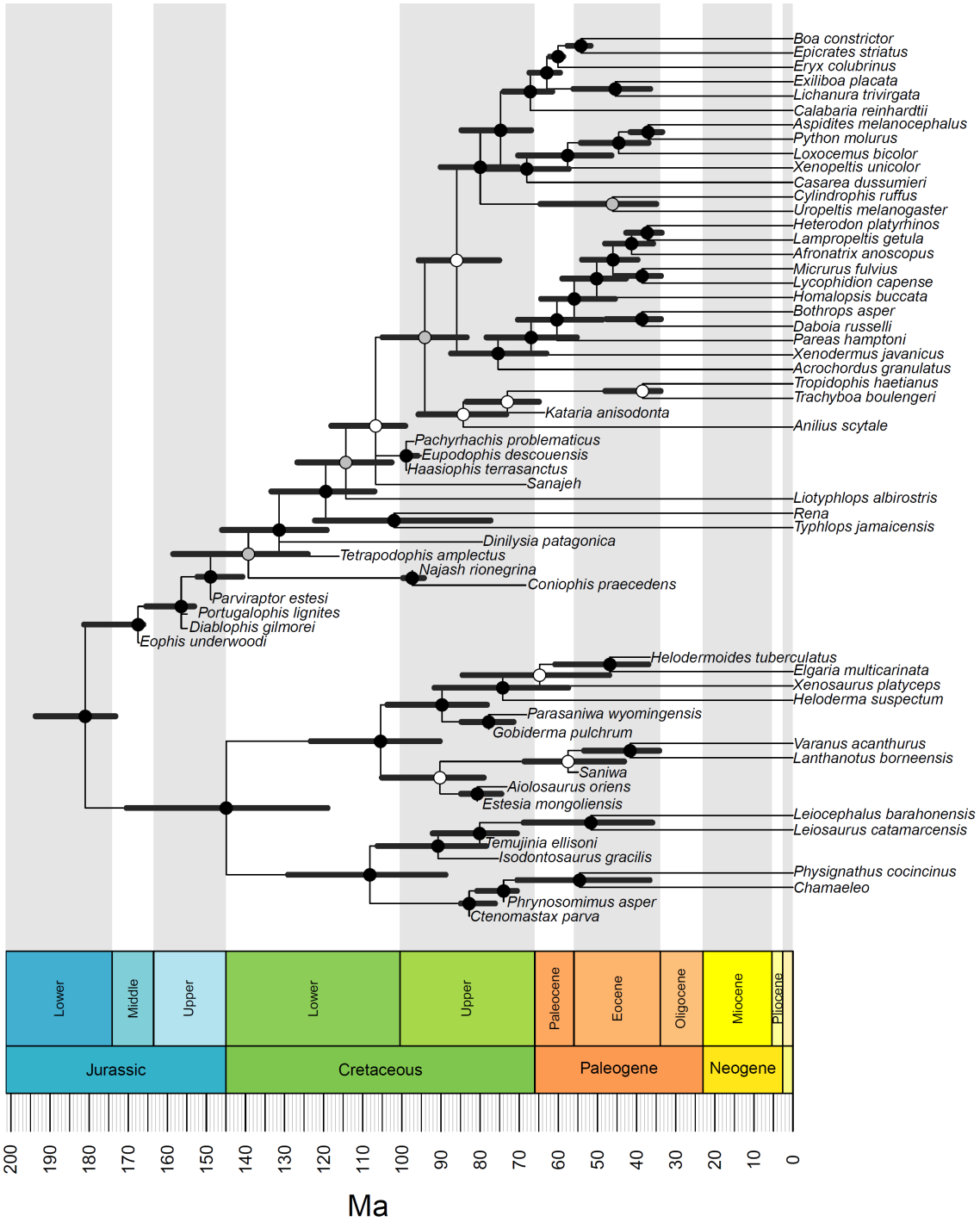

Figure 1.4. Ancestral state reconstructions from MultiState in BayesTraits showing the probability of fully-developed hind limbs (blue), reduced limbs (yellow), and completely lost limbs (red) for each node as well as the states coded for terminal taxa on our preferred phylogeny (constrained, diversified FBD). White areas of pies at internal nodes indicate the posterior probability that a node does not exist (i.e., proportion of pie colored white = 1 – PP for that node), because the certainty with which a node can be assigned any state is bounded by the certainty that the node in question exists. Pies at terminal taxa showing an equal probability of all states represent fossil taxa for which limb data are missing due to incomplete fossil material.

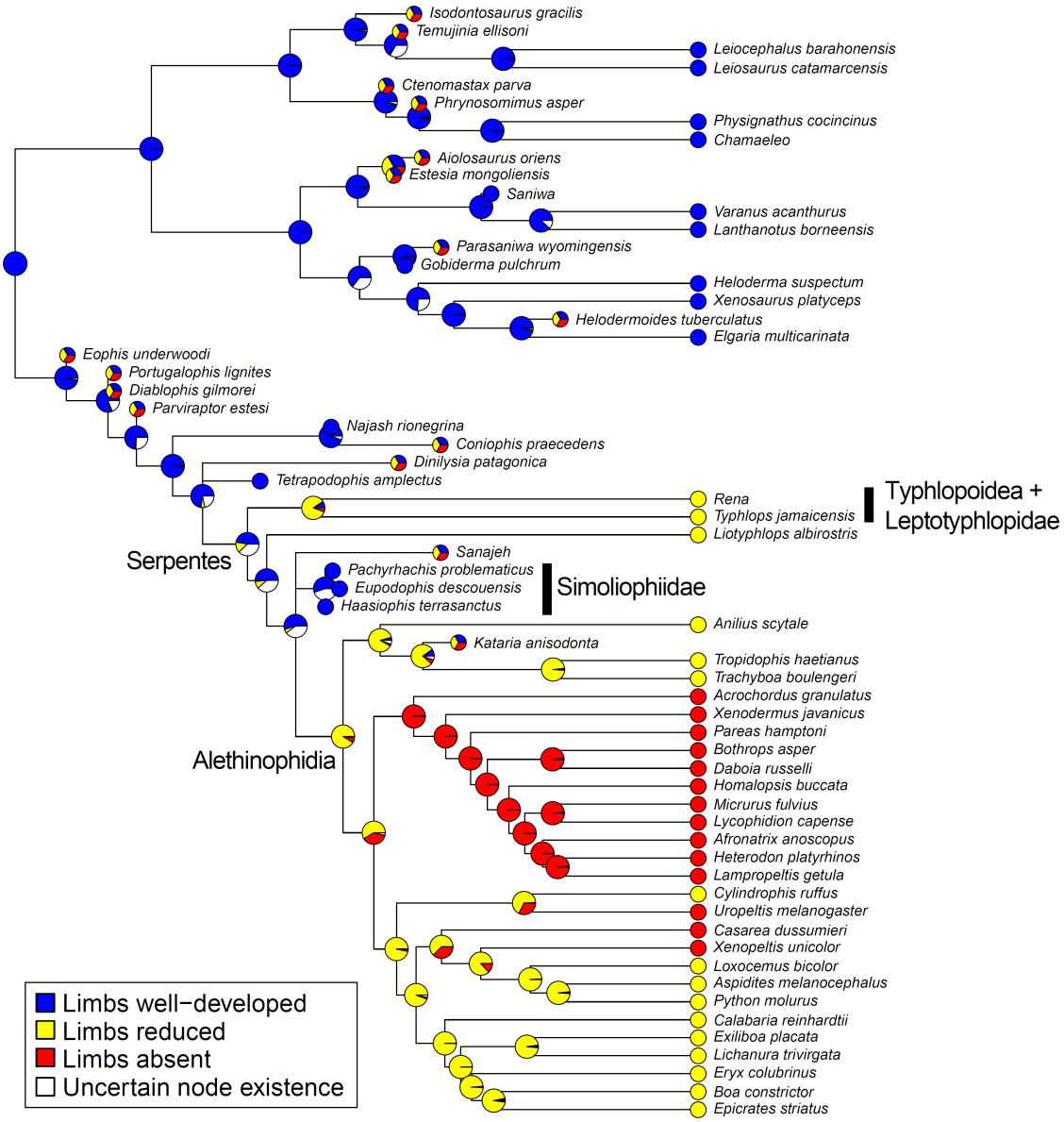

Figure 1.5. Ancestral state reconstructions from MultiState in BayesTraits showing the probability of the non-macrostomatan phenotype (blue) and macrostomatan phenotype (yellow) for each node as well as the states coded for terminal taxa on our preferred phylogeny (constrained, diversified FBD). As in Fig. 4, white areas of pies at internal nodes indicate the posterior probability that a node does not exist.

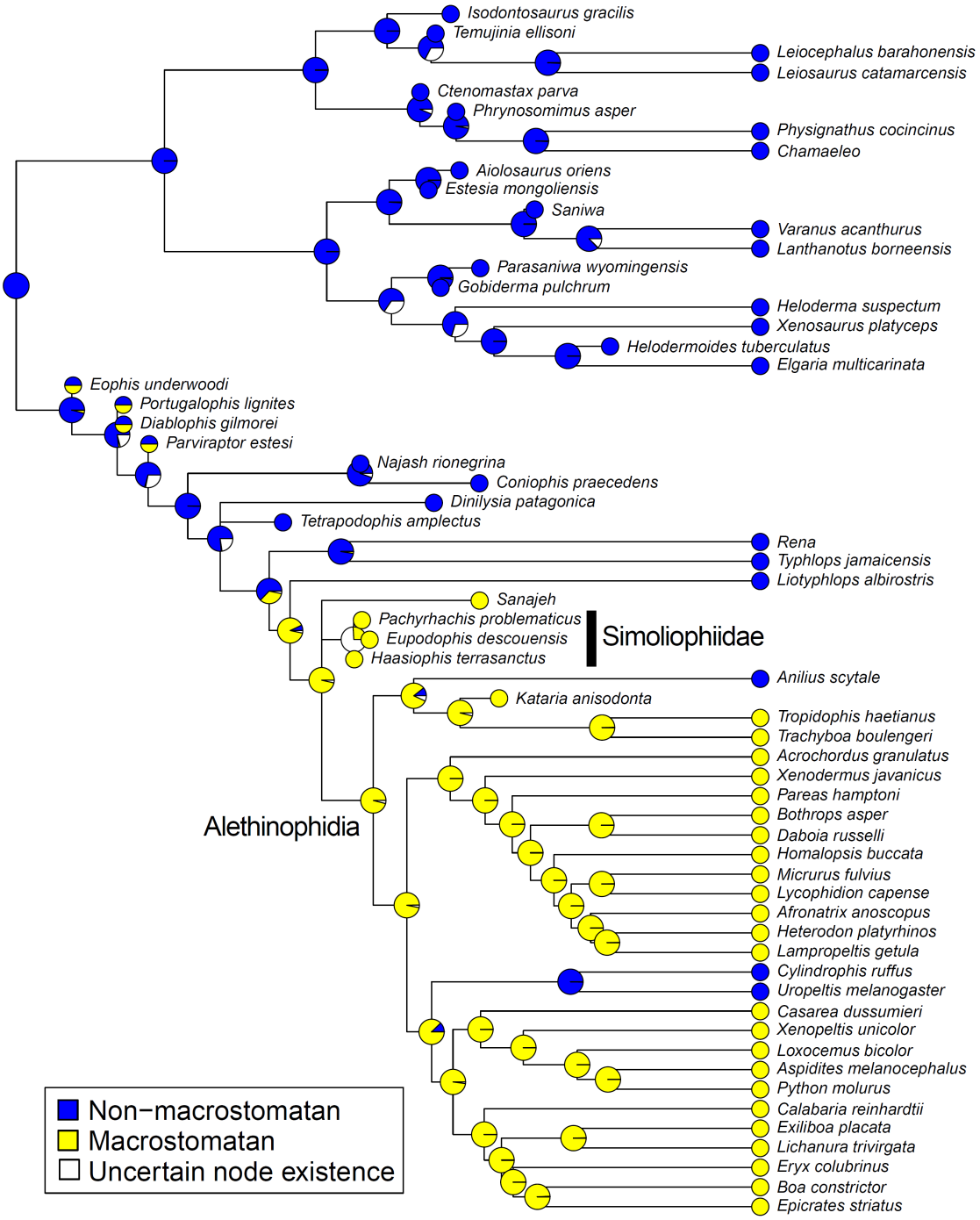

Chapter 2: Rate Heterogeneity across Squamata, Misleading Ancestral State Reconstruction, and the Importance of Proper Null Model Specification

The binary-state speciation and extinction (BiSSE) model has been used in many instances to identify state-dependent diversification and reconstruct ancestral states. However, recent studies have shown that the standard procedure of comparing the fit of the BiSSE model to constant-rate birth-death models often inappropriately favors the BiSSE model when diversification rates vary in a state-independent fashion. The newly-developed HiSSE model enables researchers to identify state-dependent diversification rates while accounting for state-independent diversification at the same time. The HiSSE model also allows researchers to test state-dependent models against appropriate state-independent null models that have the same number of parameters as the state-dependent models being tested. We reanalyze two datasets that originally used BiSSE to reconstruct ancestral states within squamate reptiles and reached surprising conclusions regarding the evolution of toepads within Gekkota and viviparity across Squamata. We used this new method to demonstrate that there are many shifts in diversification rates across squamates. We then fit various HiSSE submodels and null models to the state and phylogenetic data and reconstructed states under these models. We found that there is no single, consistent signal for state-dependent diversification associated with toepads in gekkotans or viviparity across all squamates. Our reconstructions show limited support for the recently proposed hypotheses that toepads evolved multiple times independently in Gekkota and that transitions from viviparity to oviparity are common in Squamata. Our

results highlight the importance of considering an adequate pool of models and null models when estimating diversification rate parameters and reconstructing ancestral states.

INTRODUCTION

It is widely recognized that rates of clade diversification can vary greatly across phylogenies (Sanderson & Donoghue, 1994; Alfaro *et al.*, 2009; Rabosky *et al.*, 2013). How rates of diversification change can be informative about evolutionary processes that produce biodiversity. Initially high rates of diversification slowing through time may suggest past adaptive radiation (Schluter, 2000; Yoder *et al.*, 2010; Etienne & Haegeman, 2012). Significantly different rates of diversification among clades may hint at the development of key innovations that allow lineages to invade new niches and better outcompete rivals (Mitter *et al.*, 1988; Hodges & Arnold, 1995; Lynch, 2009; Magnuson-Ford & Otto, 2012). Many likelihood-based methods now exist to quantify rates of diversification from phylogenies (e.g., Rabosky, 2006; Stadler, 2011), detect changing rates of diversification through time (e.g., Etienne *et al.*, 2012; Morlon *et al.*, 2011; Stadler, 2011), and detect different rates of diversification among clades (e.g., Alfaro *et al.*, 2009; Rabosky *et al.*, 2013).

When there is an *a priori* hypothesis that a particular trait is related to rates of clade diversification, the binary-state speciation and extinction (BiSSE) model (Maddison *et al.*, 2007) and models derived from it (GeoSSE [Goldberg *et al.*, 2011], QuaSSE

[FitzJohn, 2010], MuSSE [FitzJohn *et al.*, 2009], ClaSSE [Goldberg & Igić, 2012], BiSSE-ness [Magnuson-Ford & Otto, 2012]) have been the most commonly used methods (e.g., Goldberg *et al.*, 2010; Pyron & Burbrink, 2014; Pyron, 2014; Sorenson *et al.*, 2014) for evaluating the relationships between trait evolution and clade diversification. BiSSE is a likelihood-based model that allows for branches of a phylogeny to have different speciation and extinction rates for each of two states of a character, and can therefore be used to determine whether a given trait is associated with changes in diversification rates, representing a major step forward in identifying the drivers of biodiversity dynamics (Maddison *et al.*, 2007; Ng & Smith, 2014). The BiSSE model can additionally be used to reconstruct ancestral states of a character while accounting for differences in rates of diversification across states of that trait (Lancaster & Kay, 2013; Pyron & Burbrink, 2014; Silvestro *et al.*, 2014; Weber & Agrawal, 2014). This is important because if diversification rates are state-dependent and models that do not account for state-dependent diversification are used to reconstruct states, ancestral state reconstruction will be biased (Maddison, 2006).

It has recently been shown that BiSSE results may be inaccurately interpreted when null models are improperly specified (Beaulieu & O'Meara, 2016; Rabosky & Goldberg, 2015). As Beaulieu & O'Meara (2016) and Rabosky & Goldberg (2015) point out, the tendency for BiSSE models to fit better than alternative models (models in which rates of diversification are fixed to be equal across states) even in the absence of state-dependent diversification is because BiSSE models are joint models of diversification and trait evolution. If diversification rates vary across a given tree, a BiSSE model may

provide a better fit than a model with equal diversification rates across the entire tree simply because BiSSE models allow diversification rates to vary. Incorrectly modeling diversification rate heterogeneity and favoring state-dependent models when diversification is not actually state-dependent can lead not only to biased parameter estimates, but to incorrect ancestral state reconstructions when states are reconstructed based on biased parameter estimates from BiSSE.

Two recent squamate reptile studies have used BiSSE to reconstruct states within squamates and identified unexpected results that run counter to traditional hypotheses about character evolution. The first was Gamble *et al.* (2012) who used BiSSE to reconstruct ancestral states and investigate the evolution of adhesive toepads in gekkotans (geckos). Gamble *et al.* (2012) found that BiSSE favored multiple independent origins and losses of toepads across several gekkotan clades, in contrast to traditional hypotheses that toepads originated in the ancestor of all gekkotans followed by multiple losses (Underwood, 1954). Pyron & Burbrink (2014) found even more surprising results when using BiSSE to reconstruct the ancestral states of viviparity and oviparity across Squamata, reconstructing the evolution of viviparity near the base of the phylogeny, with the favored reconstruction implying that all instances of oviparity in squamates are the result of reversals from viviparity. This finding is highly contrary to views based on previous reconstructions, and on physiological and developmental evidence. Thus, the findings of Pyron & Burbrink (2014) have recently been highly criticized on methodological and biological grounds (King & Lee, 2015; Griffith *et al.*, 2015; Blackburn, 2015; Shine, 2015; Wright *et al.*, 2015). Pyron & Burbrink (2014) also found

that rates of speciation were higher for viviparous lineages than oviparous lineages, but differences in extinction rates led to net diversification rates that were lower for viviparous lineages, in contrast to previous studies within smaller squamate clades (Lynch, 2009; Lambert & Wiens, 2013).

Most of the responses to Pyron and Burbrink (2014) have argued from physiological and developmental principles that multiple regains of oviparity are unlikely (Shine, 2015; Blackburn, 2015; Griffith *et al.*, 2015). Wright *et al.* (2015) showed that improved tree topologies result in far fewer strongly supported reversals to oviparity than were recovered by Pyron & Burbrink (2014). King & Lee (2015) utilized the splitBiSSE approach, which fits a BiSSE model with independent sets of parameters for different portions of the tree, and found that a splitBiSSE model provided a considerably better fit to the data than the standard BiSSE model which assumes a single set of two speciation, two extinction, and two transition rates across the entire phylogeny. This finding indicates that rates of diversification vary not only by character state, but also across squamate clades. Additionally, King & Lee (2015) performed simulations to demonstrate that character transition rate heterogeneity across a phylogeny can result in inaccurate character reconstructions. They then used methods that account for variation in character transition rates across the phylogeny (CorHMM [Beaulieu *et al.*, 2013] and the random local clock model in BEAST [Drummond & Suchard, 2010]), and found that these analyses resulted in far fewer reversals to oviparity. In particular, the results from their random local clock analysis show only three putative reversals. Although these alternative models most likely provide improved results, they do not account for state-

dependent diversification, which is likely present given the results of the splitBiSSE analyses and previous studies on smaller clades (Lynch, 2009; Lambert & Wiens, 2013).

Here, we focus on re-examining the datasets of Gamble *et al.* (2012) and Pyron & Burbrink (2014) to determine what effect variation in diversification rates across the squamate phylogeny may have on ancestral state reconstruction under the BiSSE model. We first estimated rates of clade diversification across Squamata (using the phylogeny from Pyron & Burbrink [2014]) using the method BAMM (Rabosky, 2014), which estimates diversification rates in the absence of state data but can detect shifts in rates among clades as well as diversification rates that slow through time within clades. We performed these analyses to identify if there are large shifts in diversification rates among squamate clades, which are likely to bias BiSSE analyses that do not account for such rate variation. We additionally performed analyses using the newly-developed HiSSE model (Beaulieu & O'Meara, 2016). This method is based on the BiSSE model, but incorporates "hidden states". Each observed state (e.g., toepad-bearing) may be composed of two hidden states, which have different rates of diversification (e.g., a "toepad-bearing with fast diversification rates" state and a "toepad-bearing with slow diversification rates" state). This method is therefore better able to account for diversification rate heterogeneity that is not linked to states while also identifying state-dependent processes. HiSSE also accounts for different rates of transitions among hidden states, allowing it to accommodate transition rate heterogeneity, which King & Lee (2015) demonstrated was present at moderate to high levels in the viviparity data.

METHODS

BAMM Analyses:

To quantify overall rate heterogeneity across the squamate phylogeny, we used the program BAMM v2.5.0 (Rabosky, 2014), a Bayesian method that simultaneously accounts for rate changes among clades and through time within clades, and analyzed results in the R (R Core Team 2015) package BAMMtools (Rabosky *et al.*, 2014). We performed two replicate BAMM analyses on the full dated phylogeny of 4,161 squamate species from Pyron & Burbrink (2014), which we obtained from the online supporting information. BAMM analyses were run for 30 M generations using a prior of 1 on the expected number of shifts. Although this prior is conservative for a tree of this size (see BAMM documentation at http://bamm-project.org/), both analyses converged rapidly on highly similar likelihood values and numbers of rate shifts. The best shift configurations (i.e., single configuration of rate shifts across the tree that has the highest posterior probability) and maximum shift credibility configurations (roughly analogous to maximum clade credibility trees but for shift configurations; see BAMM documentation for further details) are also highly similar across both analyses. Given that good convergence was achieved, we used this prior to remain conservative in our estimates of the number of shifts across the phylogeny, despite the fact that higher values could potentially be justified. Priors on the initial values of speciation and extinction rates, and the prior on the speciation rate shift parameter were set to values determined by the function "setBAMMpriors" in BAMMtools. Incomplete taxon sampling was accounted

for by specifying the sampling fractions of species in the phylogeny for each family within Squamata. The total numbers of species currently recognized in each family were determined from the Reptile Database (Uetz & Hošek 2014) as of October 15th, 2014. Moore *et al.* (2016) have raised concerns that the posterior estimates of the number of rate shifts in BAMM may be unduly influenced by the prior. We plotted the prior and posterior to demonstrate the posterior strongly differs from the prior in our BAMM analyses (Fig. S1).

State-dependent diversification and ancestral state reconstructions:

To assess how rate variation and diversification rate parameter estimation might affect ancestral state reconstructions, we fit and reconstructed states under several subsets of the full HiSSE model for each dataset using the R package HiSSE (Beaulieu & O'Meara, 2016). For the purposes of the current discussion, we use the term "full HiSSE model" to refer to a HiSSE model in which two hidden states are contained within each observed state (i.e., states 0A, 0B, 1A, 1B), turnover and extinction fractions vary across all four hidden states, and there are eight character transition rates among hidden states, with dual character transitions that involve a change in the observed and hidden states (e.g., state 0A to 1B) disallowed. Although dual transitions can be included in the model, they are not readily interpretable and inclusion of these rates is not recommended in the HiSSE vignette associated with the package, and so we exclude these transitions from all models. We fit HiSSE models to the Gamble *et al.* (2012) and Pyron & Burbrink (2014) datasets, as well as several taxon subsets of the Pyron & Burbrink (2014) dataset. These

subsets included Scincoidea, Anguimorpha, and Serpentes, all major clades that were inferred to be ancestrally viviparous by Pyron & Burbrink (2014), implying many reversals to oviparity from viviparity within each of these major clades. We also fit models to younger clades that showed strong support for reversals to oviparity in Pyron & Burbrink (2014), including Liolaemidae, Phrynosomatidae, and Viperidae.

To each dataset, we fit a total of 16 models of trait evolution/diversification. These models are described in Table 2.1. Most of the models that we fit are state-dependent subsets of the full HiSSE model, with various constraints on transition rates among states. Other models include models in which hidden states were excluded, producing BiSSE-like models. Two models fixed diversification rates to be equal across states (i.e., diversification is modeled by a simple birth-death process across the entire phylogeny), one including hidden states and one excluding them. The remaining models tested are null models constructed to have the same number of diversification rate parameters as the full HiSSE or BiSSE-like models, but with diversification rates independent of the states. Use of these specific null models, rather than null models in which diversification rates are equal across states, alleviates concerns that state-dependent models will provide a better fit to data with state-independent diversification heterogeneity simply because they contain additional diversification parameters (Beaulieu & O'Meara, 2016; Rabosky & Goldberg, 2015).

We implemented two classes of null models, with several variants of each permitting different numbers of distinct transition rates among states. Null-two models

refer to null models in which speciation and extinction each have two rates across the phylogeny. However, unlike the standard HiSSE model, these rates differ only across the hidden states and so are state-independent. As such, null-two models are useful for comparison to BiSSE-like models that feature two distinct sets of diversification rate parameters. In contrast, full HiSSE models and variants with constrained state transition rates contain a total of four distinct sets of diversification rate parameters (one for each of the two hidden states within each of two observed states). Null-four models therefore contain a total of four states within each observed state, with the hidden states each fixed equal across the observed states (e.g., parameters for state 0a = states 1a), totaling four diversification rates that are independent of the observed states.

The null-four model potentially implements up to 56 distinct transition rates, because of the four hidden states per observed state, for a total of eight hidden states. The current implementation of HiSSE allows users to specify a single rate for all transitions or a transition rate matrix with three distinct rates: one rate from observed state 0 to 1, one reverse rate for 1 to 0, and one rate for transitions among hidden states within an observed state. We had concerns that if there is a strong signal for transition rate heterogeneity in the data, a full HiSSE model (with eight transition rates) might outperform a null-four model with only three transition rates even if there is no signal for state-dependent diversification. Therefore, we modified the hisse.null4 function to allow for a total of nine transition rates (included as a supplemental file on the Dryad Digital Repository: http://dx.doi.org/10.5061/dryad.c494p). This transition rate matrix is based on assuming that the four hidden states of the standard HiSSE model (which we will here

refer to as higher-level hidden states) are further subdivided into two lower-level hidden states each for the null-four model, such that state 0A is split into state 0a and 0b and state 0B is split into states 0c and 0d. Therefore, we allowed a single transition rate for transitions among hidden lower-level states that belong to a single higher-level hidden state, and separate rates for transitions among higher-level hidden states (corresponding to the same eight rates present in the full HiSSE model). If there is significant transition rate heterogeneity but no state-dependence, this model should outperform the full HiSSE model, even if the full HiSSE model might outperform the null-four model with only three transition rates. The HiSSE package allows users to plot model-averaged ancestral states and inferred diversification rates, with inferred values from each model weighted by that model's Akaike weight. This allows uncertainty in model selection to be incorporated into the visualization of ancestral states and diversification rates across the tree, and we report ancestral state reconstructions that have been model-averaged across all tested models for each dataset examined.

For all analyses, we accounted for incomplete taxon sampling by specifying the proportion of taxa in each state that are present in the entire tree. For the analyses of the Pyron & Burbrink (2014) full dataset, we used the sampling fraction used in the original analysis. Gamble *et al.* (2012) used a phylogeny with unresolved clades as tips and specified the sampling fraction for each tip in their BiSSE analyses. Because HiSSE does not currently support unresolved clades as tips, we only performed analyses on the full maximum likelihood phylogeny of Gamble *et al.* (2012), with the proportion of sampling across the tree calculated from the number of taxa sampled and not sampled within each

unresolved clade in the original analysis. Following Gamble *et al.* (2012), we scaled the phylogeny to an arbitrary root height of 100. We initially performed an analysis on the gekkotan dataset to fit the BiSSE model using the Diversitree package to ensure that our differences in accounting for incomplete sampling are not primarily responsible for any differing results.

In addition to the analyses that we performed on the full Pyron & Burbrink (2014) datasets, we reconstructed viviparity using the approaches described above on subsets of taxa. We did this because of the large number of shifts identified by BAMM and to test if additional hidden states may be needed to accurately reconstruct the ancestral states of viviparity and oviparity across Squamata. For each subtree that we analyzed, we calculated the sampling fraction of species by dividing the number of species in the phylogeny with a given state by the number of species in the full dataset from Pyron & Burbrink (2014) for that clade. For the clade Liolaemidae, only 56% of the species recognized in the Reptile Database (Uetz & Hošek, 2014) were present in the parity dataset. To account for this, we ran two sets of analyses for this group. The first calculated the sampling fraction like our other analyses, as the fraction of species in each state in the liolaemid part of the phylogeny relative to the total number of liolaemid species in each state in the parity dataset. The second analysis multiplied these fractions by the number of liolaemid species in the parity dataset divided by the number of liolaemid species in the Reptile Database (i.e., 56%), assuming that the ratio of oviparous to viviparous species will remain similar as more species are coded. Both analyses resulted in nearly identical ancestral state reconstructions despite slightly different

rankings of model fits, and we focus on the results of the second set of analyses, as this likely represents a better approximation of the actual sampling fractions. We present the results of the first analysis using the uncorrected sampling fractions in supplementary fig. S2 and table S1. All supplementary information, including figures, tables, and scripts used to perform analyses can be found on Dryad (http://dx.doi.org/10.5061/dryad.c494p).

RESULTS:

BAMM Analyses:

BAMM analyses using a prior on the expected number of rate shifts of one resulted in good convergence as determined by ESS values for the likelihood and number of rate shifts (assessed using R package coda [Plummer *et al.*, 2006]). The best shift configurations and maximum shift credibility (MSC) configuration of rate shifts were similar across both BAMM runs on the squamate phylogeny. The number of shifts recovered in the top 95% of the posterior distribution ranges from 14–25 in both runs, suggesting a very strong signal in the data for the presence of multiple rate shifts. Given the strong evidence of convergence between runs, we present only the results from the first run (Fig. 2.1).

Gecko toepads:

Analyzing the Gamble *et al*. (2012) dataset using a global sampling fraction in the Diversitree implementation of the BiSSE model rather than sampling fractions for unresolved clades inferred ancestral states that were identical to those of the original

study (Fig. S6). Under the BiSSE-like HiSSE model, speciation and extinction parameters were very similar to those reconstructed under the Diversitree BiSSE models, as expected (Table S2). However, the different implementations inferred different character transition rates. As a result, when states were reconstructed under the BiSSE-like HiSSE model, results were highly incongruent with those of Gamble *et al.* (2012). In contrast to the multiple gains and losses of toepads identified by the BiSSE models, the BiSSE-like HiSSE model identified the root state of Gekkota as possessing toepads, followed exclusively by losses of toepads in several gekkotan subclades (Fig. S7). We found that the irreversible null-two model with six transition rates provided the best fit to the data (Table 2.2), suggesting state-independent clade diversification. We found that the fits of several additional models were only slightly worse than this best-fit model. This suggests that there may be considerable uncertainty in the best model. The ancestral state reconstruction model averaged across all tested models showed considerable uncertainty near the base of the tree (Fig. 2.2, S8). Although we find a slightly higher probability for the root and early nodes within Gekkota lacking toepads, we find no instances of decisive support for multiple gains of toepads, in contrast with the results of Gamble *et al.* (2012).

Squamate viviparity:

For the full squamate parity dataset, the null-four model with nine transition rates among states provided a considerably better fit than all other models (Table 2.2). This indicates that across the entire squamate tree, there is no single, consistent signal for parity-dependent diversification, and diversification rates and character state transition

rates differ considerably across the phylogeny. Model-averaged ancestral state reconstructions favored viviparity for many basal nodes of the tree, although frequently with about 75% probability or less (Fig. 2.3; for tip labels, see Fig. S9). Several major clades were inferred as ancestrally viviparous with strong support, including alethinophidian snakes, Anguimorpha, and Scincoidea. Each of these clades then features several reversals from viviparity back to oviparity, and in some cases even strongly supported subsequent transitions back to viviparity (e.g., viviparous elapids), implying a sequence of transitions from oviparity to viviparity, back to oviparity, and finally to viviparity once more. Given that the most parameter-rich model tested provided the best fit to the data, we could not rule out the possibility that more complex models might provide an even better fit if we had been able to test models that allow more diversification rate heterogeneity (e.g., by having three hidden states per observed state). To explore this possibility, we fit models to smaller clades, including all of the major clades that are reconstructed as ancestrally viviparous with many reversals to oviparity. Smaller clades contain less diversification rate heterogeneity than Squamata as a whole, and so if even the full HiSSE model and null-four model with nine transition rates are under-parameterized for the full dataset, this issue should be lessened for subsets of the full tree.

Scincoidea viviparity:

A large portion of transitions between oviparity and viviparity within Squamata occur within Scincoidea, which includes Scincidae, Cordylidae, Gerrhosauridae, and

Xantusiidae. We found that for this major clade, the null-four model with nine transitions rates provided a better fit than all other models tested, suggesting that even within this clade, there is a large amount of diversification and transition rate heterogeneity (Table 2.2). State-independent diversification rate heterogeneity either masks the signal of state-dependent diversification, or there is no signal for state-dependent diversification in the data. Model-averaged reconstructed states for Scincoidea strongly support the root and all backbone nodes as oviparous, and do not support any reversals from viviparity to oviparity, strongly contrasting with the results of the reconstruction for all Squamata (Table 2.3; Fig. S10).

Serpentes viviparity:

Serpentes (snakes) is another major clade that contains a large number of transitions between oviparity and viviparity. For Serpentes, the full HiSSE model provided the best fit to the tree and parity data (Table 2.2). This indicates that there is signal for state-dependent diversification, as well as state-independent diversification and transition rate heterogeneity among hidden states. Model-averaged ancestral state reconstructions for Serpentes show reasonably strong support for viviparity at the root (90%), with Alethinophidian snakes being recovered with very high probability as having been ancestrally viviparous (100%). We also performed analyses on the clade Viperidae alone, which contains the most transitions between viviparity and oviparity within Serpentes.

The best fit HiSSE model for Viperidae clade was an irreversible null-two model with six transition rates (Table 2.2), indicating the presence of state-independent diversification rate variation and transition rate heterogeneity with no transitions from viviparity to oviparity, but no signal for state-dependent diversification, in contrast to the findings of Lynch (2009), who used BiSSE to detect parity-dependent diversification in Viperidae. Model-averaged reconstructed states strongly support oviparity as the ancestral state for the root node and major backbone nodes (Table 2.3; Fig. S12). Nearly all nodes that subtend clades containing any oviparous species are strongly supported (> 95%) as oviparous, with the exception of the nodes within New World pitvipers that contain *Lachesis.* These nodes still favor oviparity, but support is somewhat weaker, ranging from 84–86% in favor of oviparity. These results strongly contrast with our reconstruction for all Serpentes.

Anguimorpha viviparity:

Anguimorpha is the third major squamate clade that was reconstructed as ancestrally oviparous in the analysis of all Squamata. When we fit models to this group alone, we found that the relatively simple null-two model with three transition rates provided the best fit (Table 2.2). This indicates that there is little transition rate heterogeneity among hidden states, and that there is some diversification rate heterogeneity, but no state-dependence. As in the analyses of the snake subtree, model-averaged ancestral state reconstruction showed a high degree of uncertainty for basal nodes within Anguimorpha (Table 2.3; Fig. S13). Although reversals may be slightly

favored for some nodes, no oviparous species has any ancestor that is reconstructed as viviparous with greater than 73% probability.

Phrynosomatidae viviparity:

As another clade that exhibited reversals from viviparity to oviparity in analyses of the full dataset, we fit models to the iguanian Phrynosomatidae. A simple BiSSE-like model provided the best fit to these data (Table 2.2), similar to the findings of Lambert & Wiens (2013), although they found that an irreversible model with equal extinction rates fit better than a full BiSSE model. Model-averaged ancestral state reconstructions show that there is a high degree of uncertainty for all nodes that are ancestral to a combination of oviparous and viviparous species (Table 2.3; Fig. S14). Many of these nodes somewhat favor early evolution of viviparity; however, the maximal support is 77%, leaving considerable uncertainty.

Liolaemidae viviparity:

Liolaemidae is another iguanian family that features many transitions between oviparity and viviparity, and for which reversals from viviparity to oviparity were reconstructed in the analyses of the full squamate dataset. When we fit models to Liolaemidae, we found that a HiSSE model with equal transition rate among all hidden states was favored (Table 2.2). This model only slightly outperformed the null-four model with equal rates and the HiSSE model with three transition rates. Ancestral state reconstructions again showed considerable uncertainty near the root of the phylogeny, but most backbone nodes were strongly supported as oviparous (Table 2.3; Fig. S15). Two

species were somewhat strongly supported as reversals to oviparity from viviparous ancestors, *Liolaemus chiliensis* and *L. calchaqui*. The ancestors of these species were reconstructed as most probably viviparous with 83% and 90% support, respectively.

DISCUSSION

Rate variation across Squamata

Significant diversification rate heterogeneity exists among many of the major squamate clades, with both of our BAMM runs including shift configurations with 14–25 shifts in the 95% credible set. Some of the shifts shown in the MSC configuration (Fig. 2.1) occur near the bases of clades with large numbers of viviparous species or that are exclusively viviparous, including New World natricine snakes, sea snakes in Elapidae, *Liolaemus,* and a subset of *Sceloporus* (Phrynosomatidae). The shift at the base of Gekkota could be related to the presence of toepads as a key innovation for this group. Although our HiSSE analyses argue against an effect of toepads on diversification rates within Gekkota, our HiSSE analyses do not compare the diversification of gekkotans to other squamate clades that completely lack toepads. Evolution of toepads in early gekkotan lineages could have resulted in a burst of diversification relative to other major clades of squamates even if the presence or absence of toepads within Gekkota does not result in detectable differences among gekkotan species. The shift at the base of iguanian Dactyloidae could also plausibly be related to toepads as a key innovation that has allowed this lineage to radiate so successfully.

It is also possible that each of these major shifts is the result of other traits or dispersal into new areas opening up new ecological opportunity (Simpson, 1953; Schluter, 2000; Yoder *et al.*, 2010). The shift in the ancestor of *Lerista* and *Ctenotus* was previously identified by Rabosky *et al.* (2007) and hypothesized to be a potential result of colonization of the arid zones of Australia and traits that allowed this colonization. One of the most notable shifts occurs near the base of Colubroidea, the hyper-diverse radiation that contains the vast majority of extant snakes. This shift has been previously identified in analyses focused on diversification rate variation among snakes (Pyron & Burbrink, 2012). As suggested by Pyron & Burbrink (2012), the success of Colubroidea may be partially linked to the presence of venom and the invasion of new habitats. The rate increases in these groups could have been driven by increased ecological opportunity available to these lineages following the invasion of new habitats. A thorough exploration of such drivers is beyond the scope of the current study, and identification of such drivers can be difficult in principle, particularly when idiosyncratic conditions or innovations drive the diversification of a single clade (Maddison & FitzJohn, 2015).

Gekkotan toepads

The null-two model with six transition rates provided the best fit to the gekkotan toepad data, indicating a lack of strong evidence to support hypotheses that the presence of toepads is linked to diversification rates within Gekkota (Table 2.2). The improved performance of the null-two model with six transition rates over the HiSSE model with all diversification rates fixed to be equal indicated that diversification rate heterogeneity

is present across the tree, but is simply unlinked to the presence or absence of toepads. Although no rate shifts are shown in our MSC configuration of shifts from BAMM, the branch leading to gekkotans exclusive of the Australasian Diplodactyloidea has a relatively high marginal odds ratio in support of a shift occurring on this branch, indicating that there is at least some evidence for a shift along a branch leading to a large number of gekkotan species. The six-rate null-two model is an irreversible model in which toepads are already present at the root of Gekkota and can only be subsequently lost, with no independent gains.

Although the best-fit model is irreversible, other models that permit independent gains of toepads fit the data nearly as well (e.g., the full HiSSE model and the nine-rate null-four model). When we performed model-averaged ancestral state reconstruction across all models, we therefore found somewhat equivocal results with high amounts of uncertainty for the most basal nodes in the tree (Fig. 2.2). Given the large amounts of uncertainty, there is no strong support for multiple independent gains of toepads in gekkotans. The marginally better fit provided by the irreversible six-rate null-two model instead provides some evidence to support the traditional hypothesis that toepads arose once in gekkotans, followed by independent losses in several lineages. These findings also fit well with recent discoveries of stem gekkotan fossils possessing toepads, suggesting that toepads arose very early in the diversification of Gekkota (Arnold & Poinar, 2008; Daza *et al.,* 2016)

Squamate viviparity

We found that our modified nine-rate null-four model provided a considerably better fit to the full squamate dataset than all other HiSSE models tested (Table 2.2). This indicates that there is a strong signal for state-independent diversification, consistent with the results of BAMM analyses, and that state-dependent differences in diversification rates are either not present or, more likely, do not produce a consistent signal across the phylogeny due to the amount of heterogeneity among clades. The better fit of the nine-rate null-four model than the equal-rate or three-rate null-four models also suggests that there is heterogeneity in transition rates among hidden states, consistent with the findings of King & Lee (2015).

Model-averaged ancestral state reconstructions across all Squamata inferred the most basal nodes as most likely to have been viviparous (Fig. 2.3, S9), similar to the findings of Pyron & Burbrink (2014), although with somewhat lower support. The higher probabilities of viviparity than oviparity for these basal nodes seems to be driven by reconstruction of three major clades as ancestrally viviparous: Scincoidea, Anguimorpha, and Serpentes. Given that the nine-rate null-four is the most parameter-rich HiSSE-based model that we tested, we had concerns about the possibility that although this model provided the best fit to the data, it could potentially provide a poor absolute fit. These concerns were largely motivated by the fact that BAMM inferred the presence of at least 14 rate shifts and that even the null-four model can only accommodate four distinct sets of diversification rate parameters. To investigate this possibility further, we fit HiSSE

models to the three subtrees (Scincoidea, Anguimorpha, and Serpentes) that potentially drive the support for early evolution of viviparity within Squamata, as well as other smaller clades that feature a large number of reversals from viviparity to oviparity in analyses of the entire squamate dataset.

Model-averaged ancestral states reconstructions for Scincoidea and Anguimorpha resulted in greatly reduced support for early evolution of viviparity followed by multiple reversals within each of these clades (Figs. S10, S13). Although there is considerable uncertainty for many of the backbone nodes within Anguimorpha, ancestral state reconstructions for this clade and Scincoidea recovered no strong support for any reversals, with no ancestor of any oviparous species reconstructed as viviparous with more than 73% probability. In contrast, analyses of Serpentes alone retained a strong signal for early evolution of viviparity within this clade, followed by multiple reversions to oviparity. However, when we fit HiSSE models to the snake subclade Viperidae we found that this pattern was reversed. Viperidae contains the oviparous genus *Lachesis,* which is nested within an otherwise viviparous clade of New World vipers and has often been suggested to be one of the strongest candidates for a reversal from viviparity to oviparity (Fenwick *et al.,* 2012).

Serpentes is the largest squamate subclade that we analyzed, and our results on Viperidae suggest that, as for all Squamata, all of the HiSSE models may be inadequate to describe the full amount of rate diversification and character transition rate heterogeneity present in Serpentes. The best-fit model for Viperidae contains six

transition rates and two state-independent diversification rates, out of a total of eight transition rates and two state-dependent and two state-independent diversification rates in the best-fit model for all Serpentes. Given that Viperidae makes up a fairly small portion of all Serpentes, it seems unlikely that it would actually account for all of the state-independent diversification rate heterogeneity and six of eight character transition rates identified in the best-fit HiSSE model for Serpentes. Several of the other early-diverging lineages that include a large proportion of viviparous species contain relatively few species and may therefore be prone to over-fitting models or difficulty in identifying transition rates among characters, and so we did not further atomize the phylogeny to fit models to additional clades within Serpentes. Instead, we suggest that models may need to be developed that account for more hidden states than currently allowed in HiSSE in order to accurately reconstruct states and infer patterns of state-dependent and state-independent diversification within large clades such as Serpentes and Squamata.

Reconstructions for Phrynosomatidae, which showed several reversals in the full Squamata analysis, show considerable uncertainty at the majority of nodes (Fig. S14), failing to lend strong support to multiple reversals within this clade. We find that a BiSSE-like model provides the best fit to the phrynosomatid data, consistent with the findings of Lambert & Wiens (2013). Analyses on the final remaining clade to demonstrate reversals, Liolaemidae, showed strong support for reversals from viviparity to oviparity (Fig. S15). Ancestors of the oviparous species *Liolaemus chiliensis* receive up to 83% support and ancestors of *L. calchaqui* receive up to 90% support as having been viviparous. However, we also note that the phylogenetic placement of *L. calchaqui*

is likely incorrect. Camargo *et al*. (2012) used 20 nuclear loci to examine the group containing *L. calchaqui* and inferred *L. calchaqui* to be sister to the group of viviparous species within which it is nested in the phylogeny from Pyron & Burbrink (2014). Placing *L. calchaqui* outside of this group would almost certainly reduce the support for a reversal to oviparity in this species, and we therefore do not consider it to be a strong candidate for a reversal. Using a different phylogeny of Liolaemidae, Pincheira-Donoso *et al.* (2013) found that irreversible models of trait evolution (including BiSSE models) provided a better fit than reversible models, supporting our conclusion that *L. calchaqui* is unlikely to represent a reversal to oviparity.

General conclusions regarding HiSSE models:

Across all of the datasets we tested, we found that the BiSSE-like model provided the best fit only for analyses of Phrynosomatidae. All other datasets were fit best by one of the null models (state-independent diversification), or by one of the HiSSE models including hidden states. The strong evidence in favor of models that include hidden states and/or null models that include diversification rate heterogeneity suggests that patterns of diversification and state-dependence are highly complex and variable across Squamata. This provides further evidence that attempting to fit overly simplistic models to such complex data can lead to erroneous conclusions (Rabosky & Goldberg 2015; King & Lee 2015; Beaulieu & O'Meara, 2016). Null models allowing for state-independent variation in diversification provided the best fit to many of the datasets that we tested (Table 2.2). For all of these datasets, except the Gekkota toepad dataset, the BiSSE-like model

outperformed the BiSSE-like model with equal rates of diversification across the entire tree (i.e., a simple birth-death model of diversification). In analyses using the BiSSE model in Diversitree, BiSSE models with state-dependent diversification have always been tested against models with no diversification rate variation to determine if diversification is related to the trait under investigation (e.g., Lynch & Wagner, 2010, Gamble *et al.*, 2012; Fenwick *et al.*, 2012; Pyron & Burbrink 2014). Using this approach, nearly all of the datasets that were best fit by null models would have incorrectly been inferred to demonstrate state-dependent diversification (again, except Gekkota for which the BiSSE-like and BiSSE-like with equal diversification rates models fit equally well). This underscores the importance of including realistic null models that include similar numbers of parameters as the alternative model.

In addition to state-independent diversification rate heterogeneity, HiSSE-based models are capable of accounting for character state transition rate heterogeneity by incorporating distinct transition rates among hidden states. If transition rates are variable across a phylogeny, failure to account for this can also lead to biased estimates of ancestral states (Beaulieu *et al.*, 2013). Transition rate heterogeneity was previously demonstrated to be problematic for ancestral state reconstructions of viviparity in Squamata (King & Lee, 2015). As expected, we found that across most of our reconstructions, models with unequal transition rates among hidden states were favored over models with constrained transition rates, indicating that accounting for both types of rate heterogeneity is highly important. By accounting for heterogeneity in both character

state transition and diversification rates, HiSSE-based models offer a promising method to control for two major potential sources of bias when inferring ancestral states.

By fitting a broader set of models and performing model-averaged ancestral state reconstructions across all models, we inferred different character histories for gekkotan toepads and squamate viviparity than did Gamble *et al.* (2012) and Pyron & Burbrink (2014). Both of these previous studies used Diversitree to reconstruct ancestral states after fitting a BiSSE model and found strong support for multiple gains of toepads and early evolution of viviparity followed by multiple reversals to oviparity, respectively. In contrast, we find that the best-fit model to the gekkotan toepad data was an irreversible model that forces toepads to be present in the last common ancestor of all Gekkota and only permits losses of toepads. For squamate viviparity, our model-averaged reconstructions across all Squamata show weaker support for viviparity as the ancestral state of Squamata than the BiSSE reconstruction of Pyron & Burbrink (2014), but still support many reversals from viviparity to oviparity in several clades. Reconstructions on these individual clades showed limited support for reversals in most clades, with the most probable reversals occurring within Serpentes, but given results in Viperidae, we strongly suspect that all available HiSSE models provide an inadequate fit to Serpentes. Other reversals are supported within Liolaemidae, although the species reconstructed as most likely to have undergone a reversal, *Liolaemus calchaqui* (90% support for having had a viviparous ancestor), is likely phylogenetically misplaced (Camargo *et al.*, 2012). Phylogenetic uncertainty has been demonstrated to have a potentially large effect on ancestral state reconstructions and inferences from BiSSE (Wright *et al.*, 2015). Although

our ancestral state reconstructions for squamate viviparity and gekkotan toepads are ambiguous and highly uncertain at many nodes, we find no compelling support that argues against the long-held hypotheses that gekkotan toepads arose a single time, followed only by losses, and that reversals from viviparity to oviparity in squamates are extremely unlikely and are likely to have occurred very few times in the history of Squamata, if any (Underwood, 1954; King & Lee, 2015; Griffith *et al.*, 2015; Blackburn, 2015; Shine, 2015; Wright *et al.*, 2015).

Conclusions:

Large clades are likely to exhibit heterogeneous diversification and trait evolution processes. Using BAMM, we have demonstrated that there are many shifts in diversification rates across Squamata. The BiSSE model has previously been used to reconstruct ancestral states of toepads within Gekkota and of parity mode across Squamata, but is unable to account for state-independent variation in diversification rates. By fitting HiSSE models and appropriate null models that include diversification rate variation but not state-dependence, we show that there is no clear and consistent signal for state-dependent diversification related to toepads in Gekkota or to parity mode across Squamata. Only one dataset was fit best by a BiSSE-like model, and many were fit best by null models that included diversification rate heterogeneity, despite the fact that the BiSSE-like model outperformed a pure birth-death model in nearly all cases. Our ancestral state reconstructions using HiSSE show limited support for multiple gains of toepads in gekkotans or multiple reversions from viviparity to oviparity in squamates.

On the basis of our findings, we recommend that researchers investigating state-dependent diversification patterns use methods that accommodate state-independent diversification when possible (e.g., HiSSE) and, even more importantly, compare state-dependent models to appropriate null models whenever possible. This means comparing state-dependent models to models that are state-independent but include comparable numbers of diversification and character transition rate parameters. Although HiSSE introduces several additional models and null models, researchers should remain aware that these still do not represent the full set of possible models, and all may still be an inadequate fit to a dataset. We believe that this is the case for the full Squamata and Serpentes datasets, for which the best-fit models are the null-four nine-rate HiSSE model and full HiSSE model, respectively, and we urge researchers to be especially wary of results, including ancestral state reconstructions, when the most complex available models provide the best fit to the data at hand.

REFERENCES

Alfaro, M.E., Santini, F., Brock, C., Alamillo, H., Dornburg, A., Rabosky, D.L., Carnevale, G., & Harmon, L.J. (2009) Nine exceptional radiations plus high turnover explain species diversity in jawed vertebrates. *Proceedings of the National Academy of Sciences*, **106**, 13410–13414.

Arnold, E.N. & Poinar, G. (2008) A 100 million year old gecko with sophisticated adhesive toe pads, preserved in amber from Myanmar. *Zootaxa*, **1847**, 62–68.

Beaulieu, J.M. & O'Meara, B.C. (2016) Detecting Hidden Diversification Shifts in Models of Trait-Dependent Speciation and Extinction. *Systematic Biology*, **65**, 583–601.

Beaulieu, J.M., O'Meara, B.C., & Donoghue, M.J. (2013) Identifying hidden rate changes in the evolution of a binary morphological character: The evolution of plant habit in campanulid angiosperms. *Systematic Biology*, **62**, 725–737.

Blackburn, D.G. (2015) Evolution of viviparity in squamate reptiles: Reversibility reconsidered. *Journal of Experimental Zoology Part B: Molecular and Developmental Evolution*, **324**, 473–486.

Camargo, A., Avila, L.J., Morando, M., & Sites, J.W. (2012) Accuracy and precision of species trees: Effects of locus, individual, and base pair sampling on inference of species trees in lizards of the Liolaemus darwinii group (Squamata, Liolaemidae). *Systematic Biology*, **61**, 272–288.

Daza, J.D., Stanley, E.L., Wagner, P., Bauer, A.M., & Grimaldi, D.A. (2016) Mid-Cretaceous amber fossils illuminate the past diversity of tropical lizards. *Science Advances*, **2**, e1501080.

Drummond, A.J. & Suchard, M.A. (2010) Bayesian random local clocks, or one rate to rule them all. *BMC Biology*, **8**, 114.

Etienne, R.S. & Haegeman, B. (2012) A conceptual and statistical framework for adaptive radiations with a key role for diversity dependence. *The American Naturalist*, **180**, E75–E89.

Etienne, R.S., Haegeman, B., Stadler, T., Aze, T., Pearson, P.N., Purvis, A., & Phillimore, A.B. (2012) Diversity-dependence brings molecular phylogenies closer to agreement with the fossil record. *Proceedings of the Royal Society B: Biological Sciences*, **279**, 1300–1309.

Fenwick, A.M., Greene, H.W., & Parkinson, C.L. (2012) The serpent and the egg: unidirectional evolution of reproductive mode in vipers? *Journal of Zoological Systematics and Evolutionary Research*, **50**, 59–66.

FitzJohn, R.G. (2010) Quantitative traits and diversification. *Systematic Biology*, **59**, 619–633.

FitzJohn, R.G., Maddison, W.P., & Otto, S.P. (2009) Estimating trait-dependent speciation and extinction rates from incompletely resolved phylogenies. *Systematic Biology*, **58**, 595–611.

Gamble, T., Greenbaum, E., Jackman, T.R., Russell, A.P., & Bauer, A.M. (2012) Repeated origin and loss of adhesive toepads in geckos. *PLoS ONE*, **7**, e39429.

Goldberg, E.E. & Igić, B. (2012) Tempo and mode in plant breeding system evolution. *Evolution*, **66**, 3701–3709.

Goldberg, E.E., Kohn, J.R., Lande, R., Robertson, K.A., Smith, S.A., & Igić, B. (2010) Species selection maintains self-incompatibility. *Science*, **330**, 493–495.

Goldberg, E.E., Lancaster, L.T., & Ree, R.H. (2011) Phylogenetic inference of reciprocal effects between geographic range evolution and diversification. *Systematic Biology*, **60**, 451–465.

Griffith, O.W., Blackburn, D.G., Brandley, M.C., Van Dyke, J.U., Whittington, C.M., & Thompson, M.B. (2015) Ancestral state reconstructions require biological evidence to test evolutionary hypotheses: A case study examining the evolution of reproductive mode in squamate reptiles. *Journal of Experimental Zoology Part B: Molecular and Developmental Evolution*, **324**, 493–503.

Hodges, S.A. & Arnold, M.L. (1995) Spurring plant diversification: are floral nectar spurs a key innovation? *Proceedings of the Royal Society of London. Series B: Biological Sciences*, **262**, 343–348.

King, B. & Lee, M.S.Y. (2015) Ancestral state reconstruction, rate heterogeneity, and the evolution of reptile viviparity. *Systematic Biology*, **64**, 532–544.

Lambert, S.M. & Wiens, J.J. (2013) Evolution of viviparity: a phylogenetic test of the cold-climate hypothesis in phrynosomatid lizards. *Evolution*, **67**, 2614–2630.

Lancaster, L.T. & Kay, K.M. (2013) Origin and diversification of the California flora: re-examining classic hypotheses with molecular phylogenies. *Evolution*, **67**, 1041–1054.

Lynch, V.J. (2009) Live-birth in vipers (Viperidae) is a key innovation and adaptation to global cooling during the Cenozoic. *Evolution*, **63**, 2457–2465.

Lynch, V.J. & Wagner, G.P. (2010) Did egg-laying boas break Dollo's law? Phylogenetic evidence for reversal to oviparity in sand boas (Eryx: Boidae). *Evolution*, **64**, 207–216.

Maddison, W.P. (2006) Confounding asymmetries in evolutionary diversification and character change. *Evolution*, **60**, 1743–1746.

Maddison, W.P. & FitzJohn, R.G. (2015) The unsolved challenge to phylogenetic correlation tests for categorical characters. *Systematic Biology*, **64**, 127–136.

Maddison, W.P., Midford, P.E., & Otto, S.P. (2007) Estimating a binary character's effect on speciation and extinction. *Systematic Biology*, **56**, 701–710.

Magnuson-Ford, K. & Otto, S.P. (2012) Linking the investigations of character evolution and species diversification. *The American Naturalist*, **180**, 225–245.

Mitter, C., Farrell, B., & Wiegmann, B. (1988) The phylogenetic study of adaptive zones: has phytophagy promoted insect diversification? *The American Naturalist*, **132**, 107–128.

Moore, B.R., Höhna, S., May, M.R., Rannala, B., & Huelsenbeck, J.P. (2016) Critically evaluating the theory and performance of Bayesian analysis of macroevolutionary mixtures. *Proceedings of the National Academy of Sciences*, **113**, 9569–9574.

Morlon, H., Parsons, T.L., & Plotkin, J.B. (2011) Reconciling molecular phylogenies with the fossil record. *Proceedings of the National Academy of Sciences*, **108**, 16327–16332.

Ng, J. & Smith, S.D. (2014) How traits shape trees: new approaches for detecting character state-dependent lineage diversification. *Journal of Evolutionary Biology*, **27**, 2035–2045.

Pincheira-Donoso, D., Bauer, A.M., Meiri, S., & Uetz, P. (2013) Global taxonomic diversity of living reptiles. *PloS one*, **8**, e59741.

Plummer, M., Best, N., Cowles, K. & Vines, K. (2006) coda: Output analysis and diagnostics for MCMC. *R. News* **6**, 7–11.

Pyron, R.A. (2014) Temperate extinction in squamate reptiles and the roots of latitudinal diversity gradients. *Global Ecology and Biogeography*, **23**, 1126–1134.

Pyron, R.A. & Burbrink, F.T. (2012) Extinction, ecological opportunity, and the origins of global snake diversity. *Evolution*, **66**, 163–178.

Pyron, R.A. & Burbrink, F.T. (2014) Early origin of viviparity and multiple reversions to oviparity in squamate reptiles. *Ecology Letters*, **17**, 13–21.

R Core Team (2015) R: A language and environment for statistical computing. R Foundation for Statistical Computing. Vienna, Austria. https://www.R-project.org.

Rabosky, D.L. (2006) Likelihood methods for detecting temporal shifts in diversification rates. *Evolution*, **60**, 1152–1164.

Rabosky, D.L. (2014) Automatic detection of key innovations, rate shifts, and diversity-dependence on phylogenetic trees. *PLoS ONE*, **9**, e89543.

Rabosky, D.L., Donnellan, S.C., Talaba, A.L., & Lovette, I.J. (2007) Exceptional among-lineage variation in diversification rates during the radiation of Australia's most diverse vertebrate clade. *Proceedings of the Royal Society of London B: Biological Sciences*, **274**, 2915–2923.

Rabosky, D.L. & Goldberg, E.E. (2015) Model inadequacy and mistaken inferences of trait-dependent speciation. *Systematic Biology*, **64**, 340–355.

Rabosky, D.L., Grundler, M., Anderson, C., Title, P., Shi, J.J., Brown, J.W., Huang, H., & Larson, J.G. (2014) BAMMtools: an R package for the analysis of evolutionary dynamics on phylogenetic trees. *Methods in Ecology and Evolution*, **5**, 701–707.

Rabosky, D.L., Santini, F., Eastman, J., Smith, S.A., Sidlauskas, B., Chang, J., & Alfaro, M.E. (2013) Rates of speciation and morphological evolution are correlated across the largest vertebrate radiation. *Nature Communications*, **4**, 1958.

Sanderson, M.J. & Donoghue, M.J. (1994) Shifts in diversification rate with the origin of angiosperms. *Science*, **264**, 1590–1593.

Schluter, D. (2000) *The ecology of adaptive radiation.* Oxford University Press, Oxford.

Shine, R. (2015) The evolution of oviparity in squamate reptiles: An adaptationist perspective. *Journal of Experimental Zoology Part B: Molecular and Developmental Evolution*, **324**, 487–492.

Silvestro, D., Zizka, G., & Schulte, K. (2014) Disentangling the effects of key innovations on the diversification of Bromelioideae (Bromeliaceae). *Evolution*, **68**, 163–175.

Simpson, G.G. (1953) *The major features of evolution.* Columbia University Press, New York.

Sorenson, L., Santini, F., & Alfaro, M.E. (2014) The effect of habitat on modern shark diversification. *Journal of Evolutionary Biology*, **27**, 1536–1548.

Stadler, T. (2011) Mammalian phylogeny reveals recent diversification rate shifts. *Proceedings of the National Academy of Sciences*, **108**, 6187–6192.

Uetz, P. & Hošek, J. (2014) The reptile database. http://www.reptile-database.org (accessed 15 October 2014).

Underwood, G. (1954) On the classification and evolution of geckos. *Proceedings of the Zoological Society of London*, **124**, 469–492.

Weber, M.G. & Agrawal, A.A. (2014) Defense mutualisms enhance plant diversification. *Proceedings of the National Academy of Sciences*, **111**, 16442–16447.

Wright, A.M., Lyons, K.M., Brandley, M.C., & Hillis, D.M. (2015) Which came first: The lizard or the egg? Robustness in phylogenetic reconstruction of ancestral states. *Journal of Experimental Zoology Part B: Molecular and Developmental Evolution*, **324**, 504–516.

Yoder, J.B., Clancey, E., Des Roches, S., Eastman, J.M., Gentry, L., Godsoe, W., Hagey, T.J., Jochimsen, D., Oswald, B.P., Robertson, J., Sarver, B. a. J., Schenk, J.J., Spear, S.F., & Harmon, L.J. (2010) Ecological opportunity and the origin of adaptive radiations. *Journal of Evolutionary Biology*, **23**, 1581–1596.

Table 2.1. Descriptions of HiSSE models that were fit to each dataset.

Model	Hidden states	state-dependent	reversible	# distinct diversification rates	# distinct transition rates
BiSSE-like irreversible	no	yes	no	2	1
BiSSE-like	no	yes	yes	2	2
Null-two three-rate	yes	no	yes	2	3
null-two 6-rate irreversible	yes	no	no	2	6
null-two 8-rate	yes	no	yes	2	8
HiSSE equal-rate irreversible	yes	yes	no	4	1
HiSSE equal-rate	yes	yes	yes	4	1
HiSSE irreversible two-rate	yes	yes	no	4	2
HiSSE three-rate	yes	yes	yes	4	3
HiSSE irreversible	yes	yes	no	4	6
Full HiSSE	yes	yes	yes	4	8
HiSSE equal diversifcation (birth-death)	yes	no	yes	1	8
Null-four equal-rate	yes	no	yes	4	1
Null-four three-rate	yes	no	yes	4	3
Null-four nine-rate	yes	no	yes	4	9
BiSSE-like equal diversification (birth-death)	no	no	yes	1	2

Table 2.2. AICc scores for each HiSSE model for each dataset with the best fit model shown in bold.

Models	Gekkota	Squamata	Scincoidea	Serpentes	Viperidae	Anguimorpha	Phrynoso-matidae	Liolaemidae
BiSSE-like irrev	2243.8	33305.4	5218.8	10028.7	1478.5	874.6	885.0	830.9
BiSSE-like	2245.9	33158.5	5220.8	9964.2	1473.2	863.7	**861.1**	826.9
Null-two three-rate	2241.8	32566.4	5131.0	9769.8	1472.9	**849.5**	873.0	817.1
null-two 6-rate irrev	**2228.5**	32164.8	5034.9	9623.5	**1461.3**	849.8	864.9	822.2
null-two 8-rate	2248.8	32045.0	5039.1	9565.7	1464.3	854.8	882.0	818.5
HiSSE equal-rate irrev	2244.4	32751.3	5155.4	9812.5	1476.5	857.6	884.6	824.0
HiSSE equal-rate	2251.1	32658.0	5164.7	9763.0	1481.0	853.8	882.0	**815.3**
HiSSE irrev two-rate	2239.4	32750.4	5147.5	10010.5	1477.8	858.8	890.8	821.4
HiSSE three-rate	2246.7	32532.3	5131.2	9760.1	1473.2	856.8	870.9	816.4
HiSSE irrev	2234.8	32157.2	5063.1	9663.0	1467.7	858.6	869.9	820.8
Full HiSSE	2230.1	32341.1	5043.0	**9560.7**	1473.8	855.8	879.4	823.9
HiSSE equal div	2243.0	33055.4	5221.3	9946.8	1491.1	882.6	881.9	822.6
Null-four equal-rate	2250.4	32589.2	5152.8	9725.3	1480.1	849.6	885.1	816.0
Null-four three-rate	2240.9	32406.6	5094.1	9660.1	1474.0	849.8	879.1	820.3
Null-four nine-rate	2231.6	**31973.9**	**5014.8**	9564.2	1474.8	858.1	883.2	820.4
BiSSE-like equal div	2245.9	33176.0	5226.3	9969.6	1480.1	869.7	872.3	832.3

Table 2.3. Probability of viviparity as the root state and maximum viviparous probability for any node that has oviparous descendants across datasets from HiSSE ancestral state reconstructions model-averaged across all models examined.

	Probability root viviparous	Highest probability of viviparity for node with oviparous descendants
Squamata	0.74	1
Scincoidea	0	0
Serpentes	0.90	1
Anguimorpha	0.67	0.73
Viperidae	0	0.19
Phrynosomatidae	0.72	0.73
Liolaemidae	0.41	0.90

* Analyses on all Squamata were performed with the outgroup *Sphenodon* included in analyses, but the reported root state is for the root of Squamata

Figure 2.1. Maximum shift credibility tree from BAMM showing diversification rate shifts across Squamata. Rates shown are net diversification rates.

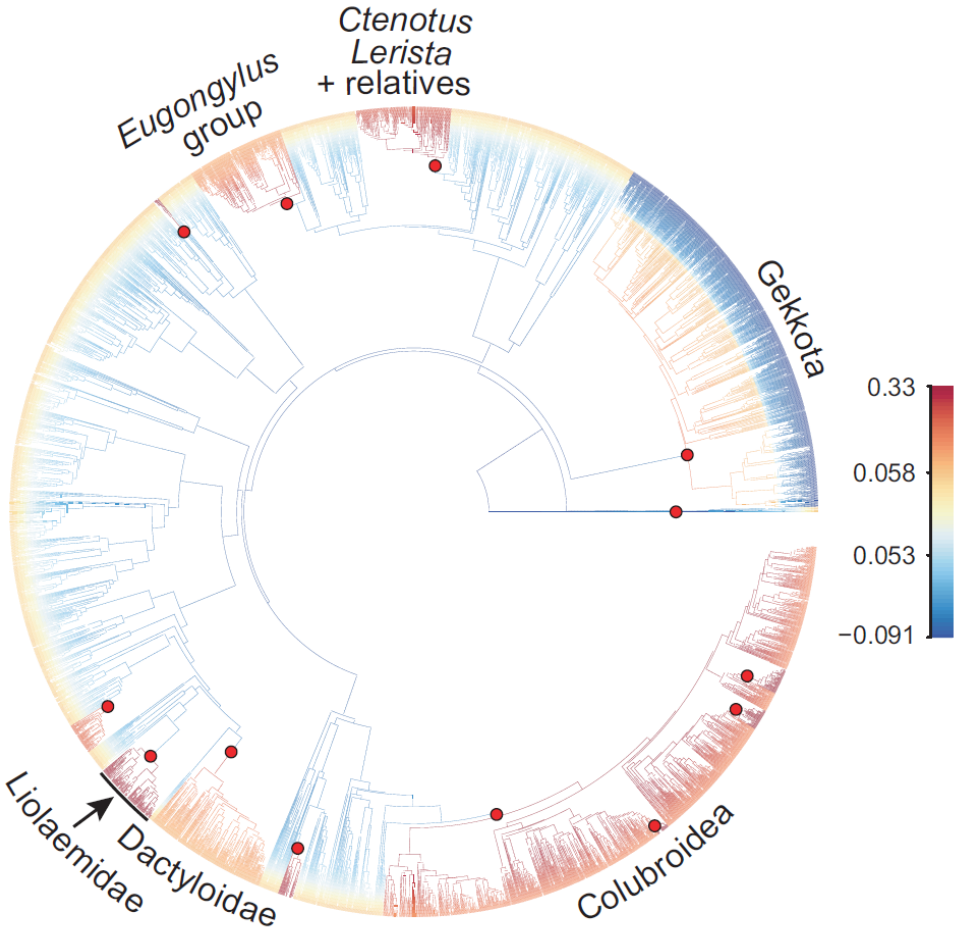

Figure 2.2. Ancestral state reconstruction of gekkotan toepads from HiSSE model-averaged across all tested models. Colored circles at tips and nodes indicate the states of species and probability that ancestors were toepad-bearing (white) or padless (black). Branches are colored by model-averaged diversification rates.

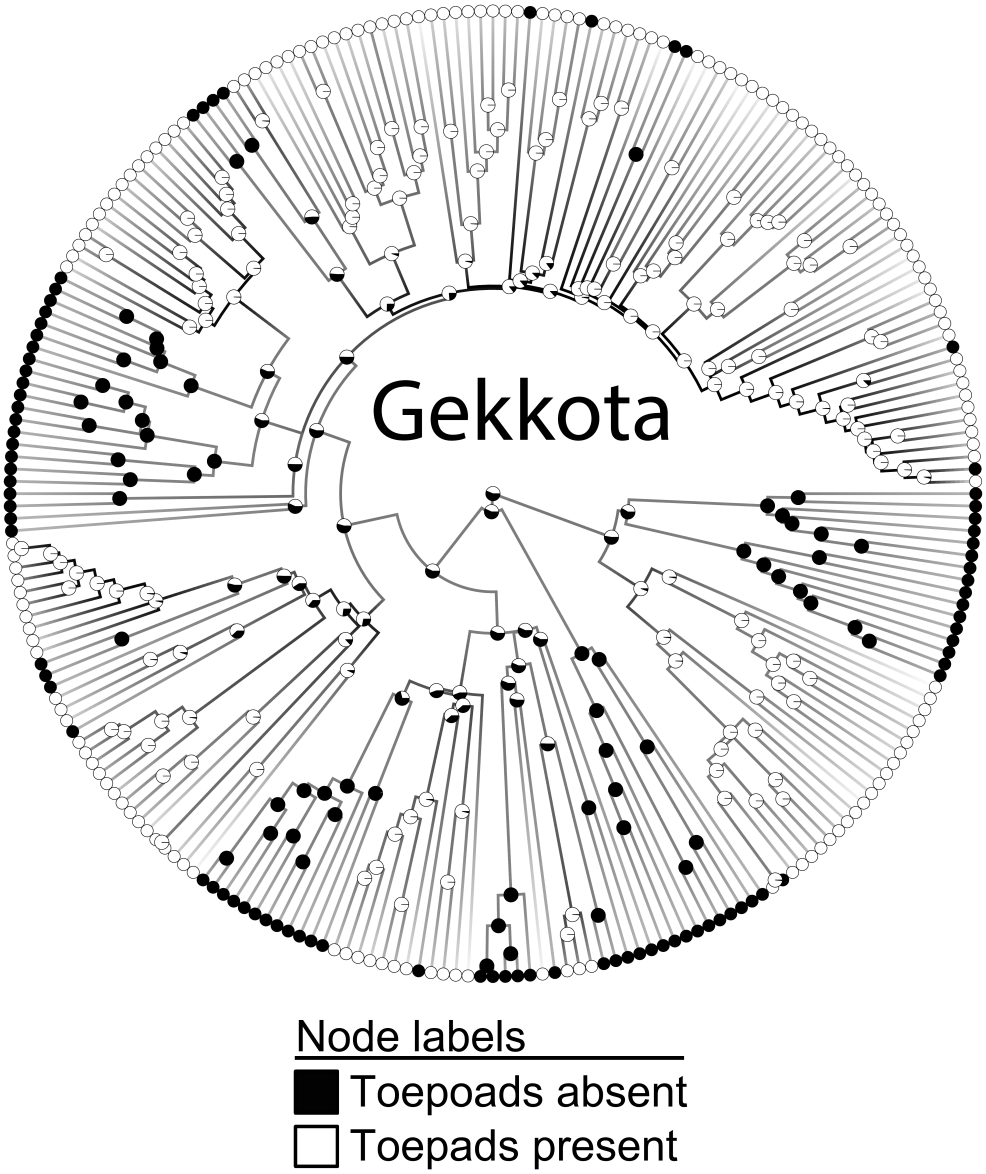

Figure 2.3. Ancestral state reconstruction of viviparity for basal nodes within Squamata from HiSSE model-averaged across all tested models. Colored circles at nodes indicate the states of species and probability that ancestors were oviparous (black) or viviparous (white). Branches are colored by model-averaged diversification rates.

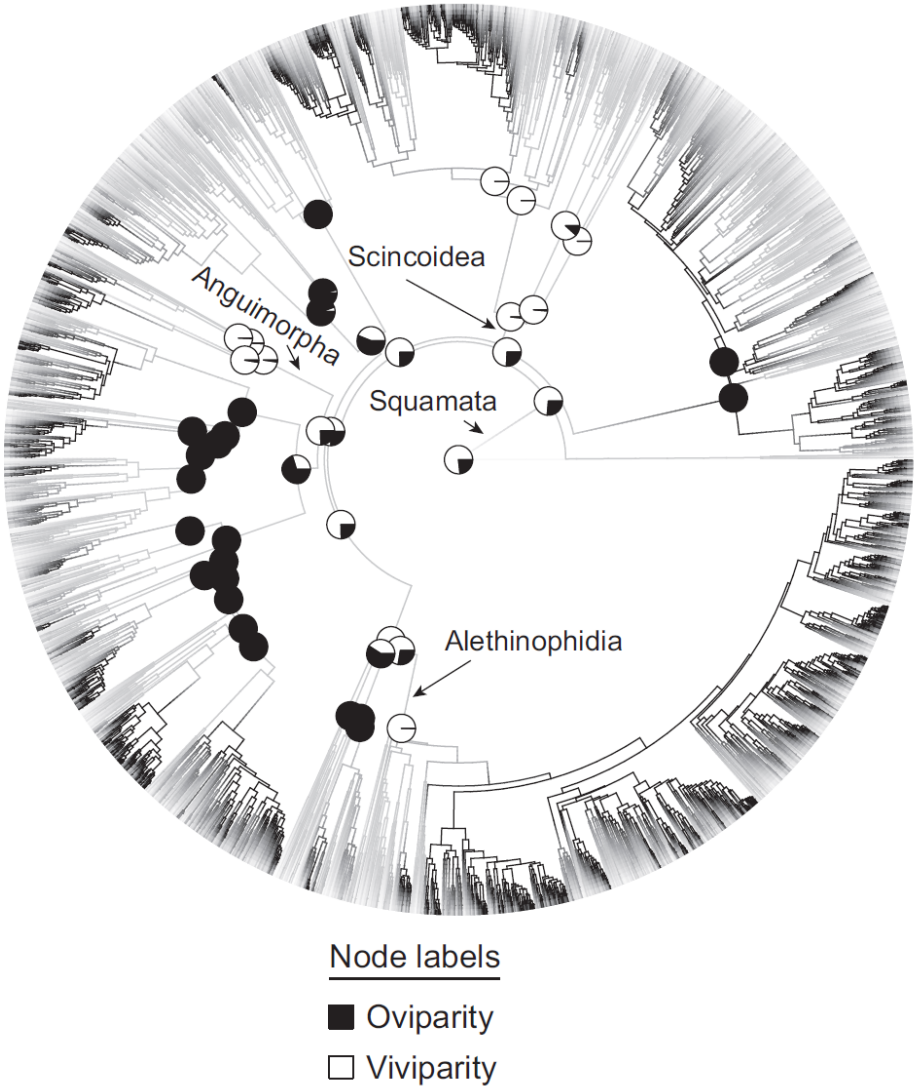

Chapter 3: Pleistocene climatic fluctuations drive isolation and secondary contact in the red diamond rattlesnake (*Crotalus ruber*) in Baja California

ABSTRACT

Aim: Many studies have investigated the phylogeographic history of species on the Baja California Peninsula, and they often show one or more genetic breaks that are spatially concordant among many taxa. These phylogeographic breaks are commonly attributed to vicariance as a result of geological or climatic changes, followed by secondary contact when barriers are no longer present. We use restriction-site associated DNA sequence data and a phylogeographic model selection approach to explicitly test the secondary contact hypothesis in the red diamond rattlesnake, *Crotalus ruber*.

Location: Baja California and Southern California.

Methods: We used phylogenetic and population clustering approaches to identify population structure. We then used coalescent methods to simultaneously estimate population parameters and test the fit of phylogeographic models to the data. We used ecological niche models to infer suitable habitat for *C. ruber* at the Last Glacial Maximum (LGM).

Results: *C. ruber* is composed of distinct northern and southern populations with a boundary near the town of Loreto in Baja California Sur. A model of isolation followed by secondary contact provides the best fit to the data, with both divergence and contact occurring in the Pleistocene. We also identify a genomic signature of northern range expansion in the northern population, consistent with LGM niche models showing that

the northern-most portion of the range of *C. ruber* was not suitable habitat during the LGM.

Main conclusions: We provide the first explicitly model-based test of the secondary contact model in Baja California and show that populations of *C. ruber* were isolated before coming back into contact near Loreto, a region that shows phylogeographic breaks for other taxa. Given the timing of divergence and contact, we suggest that climatic fluctuations have driven the observed phylogeographic structure observed in *C. ruber* and that they may have driven similar patterns in other taxa.

Baja California has been the focus of many phylogenetic and phylogeographic studies due to its unique geologic history and high endemism (Savage, 1960; Riddle *et al.*, 2000a; Grismer, 2002; Zink, 2002; Lindell *et al.*, 2008; Dolby *et al.*, 2015). Many of the taxa that have been examined have shown spatially concordant phylogenetic or phylogeographic breaks at one, two, or three key regions in Baja California: the mid-peninsula, near the town of Loreto, and at the Isthmus of La Paz (Fig. 1; Riddle *et al.*, 2000a). These breaks have been found in diverse sets of taxa, including, but not limited to, spiders (Crews and Hedin, 2006), reptiles (Upton and Murphy, 1997; Lindell *et al.*, 2005, 2008), birds (Zink *et al.*, 2001), cacti (Nason *et al.*, 2002), and mammals (Riddle *et al.*, 2000b; Whorley *et al.*, 2004). A common explanation for the mid-peninsular and La Paz splits, which are more common than the Loreto break, are seaways proposed to have crossed the peninsula and since receded (Murphy, 1983; Aguirre *et al.*, 1999). However, this hypothesis has been weakened by a general lack of direct geological evidence and the finding that mid-peninsular divergences indicate at least two episodes of divergence (Crews & Hedin, 2006; Leaché *et al.*, 2007; Dolby *et al.*, 2015). No strong evidence has been presented to suggest that a seaway crossed the peninsula in the vicinity of Loreto, leaving the drivers of spatially concordant phylogenetic and phylogeographic breaks unclear at all of these regions.

The phylogeographic patterns observed could be produced by at least two different processes: 1) isolation with ongoing migration between diverging populations (the IM model), 2) vicariance followed by secondary contact (the secondary contact model), as well as more complex scenarios. Despite the absence of strong evidence for

barriers to dispersal, the secondary contact model has often been invoked to explain patterns of genetic structure (e.g., Crews & Hedin, 2006; Lindell *et al.*, 2008). However, tools to statistically compare IM and secondary contact models have only recently become available (e.g., Beaumont, 2010; Excoffier *et al.*, 2013; Jackson *et al.*, 2017), and these models have not yet been explicitly tested in Baja California taxa.

Here, we sought to examine the phylogeography of mainland populations of *Crotalus ruber* (the red diamond rattlesnake), a large rattlesnake that ranges throughout Baja California and into southern California (Fig. 1), using genomic data and explicit testing of alternative phylogeographic models. We also investigated the effect that past climatic fluctuations may have had on populations of *C. ruber* using an ecological niche modeling approach to determine if geographic shifts in suitable habitat could explain phylogeographic patterns. Mainland populations of *C. ruber* were previously recognized as two subspecies on the basis of morphological characters including scale counts and coloration, with *C. r. ruber* in the north and *C. r. lucasensis* in the south, and with the boundary between these subspecies occurring somewhere in the vicinity of Loreto (Van Denburgh, 1920; Klauber, 1949). The subspecies were subsequently synonymized due to the presence of individuals with intermediate phenotypes at the boundary near Loreto (Klauber, 1949; Grismer *et al.*, 1994). Despite the presence of morphological variation between northern and southern populations of *C. ruber,* a previous study that included individuals sampled from southern California, northernmost Baja California, and one sample from southernmost Baja California Sur showed very low mitochondrial DNA (mtDNA) divergence across the peninsula (0.3%, Douglas *et al.*, 2006). Similarly,

Murphy *et al.* (1995) found very low mtDNA divergence between individuals sampled from Cedros Island, Baja California and from Riverside, CA. Although *C. ruber* shows low mtDNA divergence across the peninsula, many other squamate reptiles (lizards and snakes) show strong phylogenetic or phylogeographic mtDNA and/or nuclear breaks (e.g., Upton & Murphy, 1997; Lindell, 2005, 2008; Leaché & McGuire, 2006; Mulcahy 2008; Meik *et al.*, 2015). We used a restriction site-associated DNA sequencing (RADseq) approach to determine if the increased power of a large genome-wide dataset would be able to identify phylogeographic breaks even in the face of the low observed mtDNA divergence. We used these data to evaluate two primary hypotheses: 1) *C. ruber* will show a phylogeographic break at one or more of the mid-peninsula, Loreto, or La Paz regions, as found in other taxa; and 2) observed phylogeographic breaks will be the result of isolation followed by secondary contact, rather than isolation with migration or strict isolation.

MATERIALS AND METHODS

Sequencing and bioinformatics processing:

We sequenced 35 individuals of *Crotalus ruber* from across the range of the species (sampling localities shown in Fig. 1) and one individual each from the outgroup taxa *C. atrox, C. horridus, C. cerastes, C. scutulatus* and *C. molossus*. Samples used in this study were obtained from specimens in the collections of the Universidad Autónoma de Baja California in Ensenada, Centro de Investigaciones Biológicas del Noroseste, Universidad Nacional Autónoma de México, San Diego Natural History Museum, and

San Diego State University collections (Appendix S1). In the text, we refer to all samples by field collection numbers, and refer readers to Appendix S1 for the corresponding specimen numbers. We followed the double digest RADseq protocol of Peterson *et al.* (2012) with modifications following Gottscho *et al.* (2017), with the exception that we used the enzymes SbfI and Sau3AI as in Schield *et al.* (2015). We sequenced the final libraries (100 bp single-end reads) on one half flow-cell lane of an Illumina HiSeq 2500 at the University of California, Riverside Institute of Integrative Genome Biology. We used the PyRAD 3.0.5 pipeline (Eaton 2014) for data processing using a clustering threshold of 0.85 and requiring at least 10x coverage with 10 or fewer Ns. We included outgroups in phylogenetic analyses for rooting purposes but not population clustering and demographic analyses; thus, different outgroup taxa were excluded or included in different PyRAD runs, resulting in datasets with differing numbers of taxa that were used for different analyses. We also used different thresholds for the number of individuals that must have data for a given locus for that locus to be retained in the dataset due to differences in the ability of analyses to accommodate missing data. One individual that recovered low quality sequence was removed from all datasets during PyRAD processing (SD 506). The presence or absence of outgroups and minimum number of individuals that a locus was required to be present in are shown in Table S1.

Concatenated phylogenetic analysis

We estimated the relationships among individuals on datasets including all outgroup taxa using RAxML 8.2.4 (Stamatakis, 2006, 2014) on the CIPRES Science Gateway (Miller *et al.*, 2010). We acknowledge that phylogenetic analyses that force a

bifurcating tree such as RAxML are not the most appropriate for intraspecific data, but they provide a useful heuristic to see how individuals cluster, even if gene flow likely makes many of the inferred relationships uninformative. To test that excluding missing data did not have a large effect on our analyses (see Huang & Knowles, 2016), we ran RAxML on two datasets differing only in the number of individuals required to retain each locus in PyRAD processing, using thresholds of either 10 or 20 individuals. We did not partition our data and performed rapid bootstrapping (using automatic stopping under the autoMRE criterion) and a search for the best tree under the GTRCAT model with final optimization of trees using GTR+Γ. We also inferred the relationships among ingroup individuals using the program SplitsTree 4.14.2 (Huson & Bryant, 2006), which infers phylogenetic networks, and therefore does not force a strict bifurcating topology. We used the Jukes Cantor model (Jukes and Cantor, 1969) when calculating distances and used the NeighborNet algorithm for constructing the network.

Population clustering and isolation by distance

We used the model-based Bayesian clustering method Structure 2.3.4 (Pritchard *et al.*, 2000) and its maximum likelihood analog Admixture 1.23 (Alexander *et al.*, 2009) to assign individuals to populations and detect admixed individuals. We ran Structure with correlated allele frequencies for 300k post-burn-in generations with 300k generations of burn-in. For Structure, the optimal number of populations (K) was determined by running Structure with K=1–5 for 15 replicates each and using the Evanno method (Evanno *et al.*, 2005) in Structure Harvester 0.6.94 (Earl & vonHoldt, 2012). The optimal number of populations in Admixture was determined

using the cross-validation approach (Alexander & Lange, 2011), testing K=1–5, as in STRUCTURE. We also explored population structure using the non-model-based methods spatial principal components analysis (sPCA) and discriminant analysis of principal components (DAPC) in the R package 'Adegenet' 2.0.1 (Jombart, 2008; Jombart & Ahmed, 2011) in R 3.3.2 (R Core Team 2016). We used k-means clustering and the Bayesian information criterion (BIC) to determine the optimum number of clusters for DAPC, and retained all principal components. R code for performing these analyses is deposited on Dryad. To test the effect of dataset completeness on population clustering, we performed ADMIXTURE analyses using two datasets of differing completeness that required a locus to be present in either 26 or 17 individuals to be retained. All population clustering analyses were highly concordant, and so for all subsequent analyses that required assigning individuals to populations *a priori,* we based these assignments on the most probable population assignment from ADMIXTURE using the more complete dataset.

To ensure that our population clustering analyses were not erroneously interpreting isolation by distance as population structure, we ran a Mantel test on genetic and geographic distances among individuals using the mantel.randtest function in the 'Adegenet' package. Significance of the Mantel test was assessed using 99,999 permutations. We plotted genetic and geographic distances to visualize if isolation by distance exists as a continuous cline or is the result of patches of distant, divergent individuals. Plots were coloured by point density as measured by 2-dimensional kernel density estimation using the kde2d function in the R package 'MASS' 7.3-47 (Venables & Ripley, 2002). We also ran a Mantel test and plotted genetic against geographic

distance for the northern population to test if patterns of isolation by distance within this population are consistent with a northern population expansion suggested by other analyses.

Coalescent phylogenetic analysis and population modelling

We utilized three coalescent-based approaches to estimate divergence times and migration rates between populations of *C. ruber* identified by our population clustering analyses. For all of these analyses, we assigned individuals to populations based on the results from STRUCTURE and ADMIXTURE (which are highly concordant with each other and other analyses), with admixed individuals assigned to whichever population makes up the majority of their ancestry.

We used the program FASTSIMCOAL2 2.5.2.21 (FSC2; Excoffier *et al.*, 2013) to perform phylogeographic model selection and estimate the parameters of each model. FSC2 is a coalescent-based method that takes site frequency spectra as input and uses a simulation approach to approximate the likelihood of any arbitrarily complex phylogeographic model that can be specified and estimate the demographic parameters specified in each model. We generated joint site frequency spectra from each of ten downsampled SNP datasets using code developed by Jordan Satler (https://github.com/jordansatler/SNPtoAFS) following Thomé and Carstens (2016) to account for the effects of missing data using a missing data threshold of 50%. We compared a set of nine phylogeographic models, summarized in Fig. 2. For each model, we calculated the Akaike information criterion (AIC) from the approximated likelihood and number of parameters in order to rank models. For folded SFS, FSC2 requires that

the mutation rate is specified. We assumed a genome-wide mutation rate of $2.2x10^{-9}$ mutations/site/year based on similar rates calculated across a large pool of mammalian loci (Kumar and Subramanian 2002) and a few lizard loci (Gottscho *et al.*, 2014). We used a generation time of 3.3 years/generation based on the estimated generation time of the sister species of *C. ruber, C. atrox* (Castoe *et al.*, 2007). Combining these, we get a mutation rate of $7.26x10^{-9}$ mutations/site/generation. We acknowledge that use of a mutation rate from a more closely related taxon would be preferable, but we do not expect our main conclusions to change unless the true mutation rate is very different from what we have used, and we address this in our discussion section. We ran 100 replicate FSC2 analyses under each model on each of the 10 downsampled datasets to ensure that we found the optimum likelihood. Each individual FSC2 run included 100,000 simulations for estimation of the composite likelihood and 10 ECM cycles for parameter optimization. For each downsampled dataset, we retained only the FSC2 run that obtained the highest likelihood. We report parameter estimates and AIC scores as averages across the 10 downsampled datasets.

As an alternative method to estimate demographic parameters, we used the program G-PHOCS 1.2.2 (Gronau *et al.*, 2011) to estimate divergence time, population size, and migration rates between populations of *C. ruber* under an IM model. We ran two replicate G-PHOCS runs using automatic fine-tuning for a total of 300k generations each, sampling every 50 generations, and discarding the first 10% of samples as burn-in. We allowed asymmetric migration between the northern and southern populations and set the two populations to coalesce into a single ancestral population in the past. We set

α=1.0 and β=10,000 for the gamma distribution used for priors on τ and Θ parameters, and α=0.002 and β= 0.00001 for the gamma distribution used for priors on migration rates. We checked for convergence between runs using TRACER 1.6 (Rambaut *et al.*, 2014). To convert divergence times we used the same mutation rate that we used for FSC2 analyses. To convert migration rates output by G-PHOCS and FSC2 into more easily interpretable number of individual migrants/generation, we multiplied migration rates by $\Theta/2$ to yield $2N_em$.

Finally, as a sanity check on the divergence times estimated from FSC2 and G-PHOCS, we used the method SNAPP 1.2.5 (Bryant *et al.*, 2012) implemented in BEAST 2.3.1 (Bouckaert *et al.*, 2014), which models a bifurcating tree topology in the absence of gene flow, to estimate the divergence time between populations. SNAPP analyses included one individual of *C. atrox* as an outgroup, such that divergence times initially estimated in substitutions/site could be roughly converted to absolute time on the basis of assuming a split between *C. ruber* and *C. atrox* approximately 3 Ma based on previous fossil-calibrated phylogenies (Reyes-Velasco *et al.*, 2013; Blair & Sánchez-Ramírez, 2016). SNAPP does not currently support node calibrations, and so we estimated the divergence between *C. ruber* populations as the ratio of the height of the node uniting *C. ruber* populations and the height of the node uniting *C. ruber* and *C. atrox* multiplied by the assumed 3 Ma divergence between *C. atrox* and *C. ruber.* This is an admittedly coarse procedure, but we are only seeking to determine broad similarity between estimates from FSC2, G-PHOCS, and SNAPP. Because this procedure does not rely on the mutation rate assumed for FSC2 and G-PHOCS analyses, it helps provides

independent validation of the dates produced using this rate. Although the estimated divergence is likely to be inaccurate if there is gene flow among populations, radically different divergence times from SNAPP and demographic modelling approaches could indicate problems with our assumed mutation rate. Two replicate SNAPP analyses were run for a total of 300k generations with 10% of generations discarded as burn-in. Convergence was assessed using TRACER and trees from both runs were combined and summarized using the LOGCOMBINER and TREEANNOTATOR programs distributed with BEAST2, respectively.

Niche modelling

We used MAXENT 3.3.3k (Phillips *et al.*, 2006) to estimate current and Last Glacial Maximum (LGM) niches for *C. ruber* to determine if phylogeographic patterns could be related to changes in suitable habitat caused by Pleistocene climatic fluctuations. Global Positioning System (GPS) coordinates were obtained from the VertNet database. Localities outside the range of *C. ruber* were removed and localities were down-sampled so that only localities at least ~20 km apart were included to alleviate issues associated with highly uneven sampling across the range of *C. ruber,* retaining a total of 101 locality points (southern California is sampled far more densely than most of Baja California). We used a total of 11 climatic variables from the BioClim dataset (Bio 2, 3, 5,7–9, 15–19; Hijmans *et al.*, 2005) after removing variables that are highly correlated ($-0.8 \geq r \geq 0.8$). We used two models of LGM climate, the Community Climate System Model (CCSM4) and the Model for Interdisciplinary Research on Climate (MIROC), to estimate the distribution of *C. ruber* at the LGM. To limit over-prediction in areas well outside the

range of *C. ruber,* we clipped all environmental layers to a 300 km buffer around the minimum convex polygon containing all occurrence points used for niche modelling. MAXENT analyses were run using default setting and models were evaluated using the area under the curve (AUC) statistic.

RESULTS

Sequence data

From our Illumina sequencing, we obtained a total of approximately 20 M reads across all samples (including outgroups). After PYRAD processing, the number of loci retained ranged from 998 for the dataset including *C. atrox* as an outgroup and requiring each locus to be present in at least 31 individuals to 2,878 for the dataset including all outgroup taxa and requiring each locus to be present in at least 20 individuals. The number of parsimony informative sites per dataset ranged from 717 (with 629 unlinked SNPs) when all outgroups were excluded and loci were required to be present in at least 30 individuals to 3,834 (with 2,634 unlinked SNPs) for the dataset including all outgroup taxa requiring each locus to be present in at least 20 individuals.

Concatenated phylogenetic analysis

Results from RAXML analyses on the two data matrices that we tested were highly similar, with the exception that support was lower for many nodes in the analysis of the more incomplete dataset (Fig. 3, S1). We therefore focus only on the RAXML results using the more complete dataset. The relationships among individuals inferred by RAXML revealed a basal split between a northern and southern clade (Fig. 3). Most of

the individuals are strongly supported as members of the northern or southern clade, with the exception of the southern-most individuals of the northern clade. The genetic break between the northern and southern clades of individuals is geographically located near the town of Loreto in Baja California Sur. Within the northern clade, the northern-most individuals are the most highly nested, with more southern individuals in the clade recovered as less nested and branching earlier, consistent with a pattern of northern range expansion. Results from SPLITSTREE are largely concordant with RAXML results and also show groupings of northern and southern individuals, corresponding to individuals north and south of Loreto, respectively (Fig. S2). Several individuals that are near Loreto are also placed in intermediate positions on the phylogenetic network, suggesting that these individuals are genetically admixed between the northern and southern groups.

Population clustering and isolation by distance

STRUCTURE and ADMIXTURE both indicate that a two-population model provides the best fit to the data (Fig. S3, table S2). Population assignments of individuals by STRUCTURE and ADMIXTURE are nearly identical, as are the results of ADMIXTURE analyses using datasets of differing completeness, so we discuss only the results from Admixture, with the results from STRUCTURE and ADMIXTURE with the more incomplete dataset shown in Figs. S4 and S5, respectively. Admixture identified northern and southern populations of *C. ruber,* with a boundary between these populations at Loreto (Fig. 3), concordant with the groupings identified by RAXML and SPLITSTREE. As suggested by SPLITSTREE, the individuals nearest the population boundary are recovered as admixed. Admixture of southern ancestry in northern individuals is detectable much

farther from the population boundary than is northern ancestry in southern individuals. We examined the results of Admixture analyses under a three-population model to determine if any other common biogeographic/phylogeographic breaks may be present, and found that this analysis recovered the admixed individuals identified in the two population model as a distinct population that admixes with individuals to the north and south (Fig. S6). Given these results and the lower cross-validation error in Admixture and higher ΔK score in Structure for the two-population model, we do not discuss other K values further.

sPCA and DAPC support the results of concatenated phylogenetic analyses and STRUCTURE and ADMIXTURE (Fig. 4, S7). sPCA shows strong differentiation along PC1 into two distinct clusters of individuals corresponding to northern and southern populations. Intermediate individuals again correspond to the individuals within each population that are closest to the boundary between the populations at Loreto. DAPC supports partitioning of individuals into two populations, similarly to Admixture and Structure (Fig. S7). The Mantel test we performed indicated the presence of significant isolation by distance across the range of *C. ruber* ($p = 0.00001$). However, plotting geographic and genetic distances shows that is not the result of a single cline, but of two distant populations that are genetically distinct (Fig. 5), consistent with the identification of two geographically and genetically distinct populations identified by clustering methods. Significant isolation by distance was also detected within the northern population when southern individuals were excluded from the analysis ($p = 0.00001$). Plotting genetic and geographic distances within the northern population showed a single

cloud of points consistent with a continuous genetic cline resulting from range expansion (Fig. S8).

Coalescent phylogenetic analysis and population modelling

We used FSC2 to select among the phylogeographic models shown in Fig. 2. Rankings of these models by AIC scores are shown in Table 1. The best fit model is model 6, which is a secondary contact model and has an AIC weight more than twice that of any other single model. Several other models provided reasonably good fits to the data, as evidenced by AIC weights ranging from 0.19 to 0.07. These included an IM model, a secondary contact model with expansion of the northern population, an IM model with migration from south to north only, and an IM model with expansion of the northern population (models 2, 9, 3, and 5 in Fig. 2, respectively).

Across all five of the best-fit FSC2 models, the northern population is approximately half as large as the southern population (Table 2). Migration rates between populations are estimated to be highly asymmetric, with a much higher rate for migration from south to north (0.77–1.36 individuals/generation across models) than the opposite (0.26–0.67 individuals/generation across models). Divergence between populations was estimated to have occurred approximately 450–510 ka, with models incorporating secondary contact estimating contact around 80 ka.

The estimated effective population size of the northern population estimated from FSC2 is similar to the estimate from G-PHOCS (Table 2; see Table S3 for uncertainty around estimated values). However, across all of the best models tested in FSC2, higher population sizes were recovered for the southern population and lower population sizes

were recovered for the ancestral population as compared to G-PHOCS estimates. FSC2 also estimates considerably older divergence times for the northern and southern populations than G-PHOCS (~450–510 ka compared to ~280 ka, respectively). The two best-fit IM models with bidirectional migration yielded migration rates somewhat similar to the estimated rates from G-PHOCS, but with higher rates from south to north. Migration rates for other models are considerably different from G-PHOCS estimates, with both secondary contact models recovering more than twice as many migrants/generation moving in each direction.

SNAPP analyses recovered the divergence between the northern and southern *C. ruber* populations as 0.19 times that of the root height of the tree (Fig. S9). Assuming a divergence of 3 Ma between *C. atrox* and *C. ruber* (Reyes-Velasco *et al.*, 2013; Blair & Sánchez-Ramírez, 2016), we converted this to an approximate divergence between the northern and southern *C. ruber* populations of 570 ka.

Niche modeling

The high AUC value of 0.907 suggests that the niche model generated from present-day climatic conditions captures the current distribution of *C. ruber* well. LGM projections are similar whether using MIROC or CCSM climatic reconstructions (Fig. 5, S10). LGM projections suggest that a reasonably large portion of the Baja California Peninsula was suitable habitat for *C. ruber*. However, the northernmost portion of the current range of *C. ruber* is estimated to have been unsuitable habitat.

DISCUSSION

All of our phylogenetic and population clustering analyses concordantly identify two populations within *C. ruber,* a northern and southern population with a boundary near Loreto. In the vicinity of Loreto, there is a large zone of admixture that extends a linear distance of approximately 350 km between the northernmost and southernmost admixed individuals present in our dataset (Fig. 3). This admixed zone extends farther to the north of Loreto than to the south, consistent with the higher migration rates estimated in this direction between populations from G-PhoCS and FSC2. The population break is concordant with the historical subspecific taxonomy of *C. ruber,* including the zone of admixture, indicating that the genetic differentiation of the populations matches previously observed morphological differentiation among traditional subspecies (Van Denburgh, 1920; Klauber, 1949). This phylogeographic break has also been observed in zebra-tailed lizards (*Callisaurus draconoides;* Lindell *et al.*, 2005). However, *C. draconoides* also shows breaks at the mid-peninsula and Isthmus of La Paz, leaving *C. ruber* as unique among squamate reptiles in showing the Loreto break alone.

The estimated divergence times for the northern and southern populations of *C. ruber* can provide some insight into possible processes that have resulted in population divergence centered at Loreto. Divergence dates estimated by SNAPP and the best-fit models in FSC2 are all roughly congruent in the range of ~450–570 ka. These dates are somewhat older than the divergence time estimated by G-PhoCS (280 ka). The discrepancy between divergence times estimated by FSC2 and G-PhoCS may be partially attributable to some combination of the different data types used in each analyses (FSC2

takes site frequency spectra as input and G-PhoCS takes full sequence data and integrates over gene trees) and the higher ancestral population sizes estimated by G-PhoCS (Oswald *et al.*, 2017), but the overall cause of these discrepancies is unclear. Due to the congruence between divergence time estimates from SNAPP and FSC2, we prefer parameter estimates from FSC2 over those from G-PhoCS. Given that G-PhoCS includes migration, it would be expected that the divergence date would be similar to or older than the estimate from SNAPP, because the failure to account for ongoing migration should cause SNAPP to be biased towards younger rather than older divergence times (Leaché *et al.*, 2014). Although the mutation rate that we have used to convert estimates into absolute time is based on taxa not particularly closely related to *C. ruber,* the general congruence in divergence times between SNAPP and FSC2 increases our confidence in the estimated dates. Furthermore, all dates estimated from FSC2 and G-PhoCS would have to be off by a factor of more than 5 to fall outside of the Pleistocene, which would require the true mutation rate to be very different from the rate we have used.

Population divergence and secondary contact in the Pleistocene suggests the possibility that climatic cycles have played a role in past isolation of *C. ruber,* as has been suggested for several other desert southwest taxa (e.g., Riddle *et al.*, 2000a; Schield *et al.*, 2015; Jezkova *et al.*, 2016). There are no obvious current barriers to dispersal by *C. ruber* in the vicinity of Loreto, strongly suggesting that temporary, rather than ongoing, barriers to dispersal have resulted in the observed differentiation between northern and southern populations. No known or proposed geographic barriers, such as seaways, were present during the Pleistocene, further suggesting that climatic fluctuations may have led

to initial population isolation. Unfortunately, we are unable to estimate climatic suitability of areas near Loreto at the timing of divergence due to a lack of climatic data available for this time period. Our niche models suggest that areas near Loreto were suitable habitat for *C. ruber* at the LGM, but climatic conditions at the LGM may not be analogous to conditions during other glacial cycles.

FSC2 analyses indicate that a model of isolation followed by secondary contact provides the best fit to the data. This model provides a better fit than IM, secondary contact with an expanding northern population, IM with northward migration only, and IM with an expanding northern population models, but these models all had reasonably high AIC weights (0.19–0.07; Table 1). All of these models contain high levels of migration between populations and two of them include secondary contact, with the combined AIC weight of these two secondary models totaling 0.6, lending support to the hypothesis that these populations were temporarily isolated by climatic conditions and have subsequently come back into contact and resumed exchanging genes. If Pleistocene climate cycles have produced the patterns of genetic structure observed in *C. ruber,* then it is plausible that older divergences in other taxa might also have been caused by climatic fluctuations rather than historically proposed seaways.

The difference between the migration rates estimated under IM models and secondary contact models highlights the importance of proper model specification for parameter estimation (Thomé & Carstens, 2016). The number of migrants from north to south was just over twice as high when estimated under secondary contact models as when estimated under IM models, and the number of migrants moving from south to

north was also higher under secondary contact than bidirectional IM models. Such differences in estimated migration rates could be critical for researchers seeking to estimate rates of migration to support or reject species delimitation hypotheses (e.g., Gottscho *et al.*, 2017), as use of a mis-specified model could result in biased estimates of migration that could lead to erroneous conclusions about species limits.

A northern range expansion of the northern population of *C. ruber* is suggested by the pattern of more northern individuals being successively nested in the RAxML results (Fig. 3), the much smaller population size of the northern population relative to the southern population, despite occupying a much larger geographic range, the strong signal of isolation by distance within this population, and that two of the five best-fit models evaluated with FSC2 included expansion of the northern population (Hewitt 1996; Excoffier *et al.*, 2009). FSC2 models that include expansion of the northern population estimate the pre-expansion effective population size to have been ~24–27k individuals, compared to ~40–45k individuals at present (across all five best models), representing a considerable increase. A northern population expansion is consistent with our niche models, which show that a large portion of the current distribution of the northern population was not climatically suitable during the LGM. The northern population of *C. ruber* may therefore have been forced to retreat to southern climatic refugia, only to expand to the north once climatic conditions in these regions became suitable once again. Although a pattern of Pleistocene/post-Pleistocene northern range expansion has only been demonstrated for small number of taxa in the region (e.g., Nason *et al.*, 2002; Whorley *et al.*, 2004), many peninsular taxa have similar distributions. In particular,

many lizards and snakes have similar distributions to *C. ruber* (Grismer, 2002), and likely similar climatic requirements, suggesting that it is likely that other Baja California reptiles may be found to have experienced range contractions and northern expansions. For instance, the mitochondrial phylogenies of *C. draconoides* (Lindell *et al.*, 2005) and *U. nigricaudus* (Lindell *et al.*, 2008) both show a general pattern in which more northern individuals tend to be highly nested, suggesting the possibility that these taxa have also experienced northern range expansions in response to changing climates.

CONCLUSIONS

Genomic data strongly support the presence of two populations within mainland *C. ruber* that correspond to historically recognized subspecies with an extensive zone of admixture where the populations contact in a zone of morphological intermediates. Using demographic modeling approaches and phylogeographic model selection, we have shown that migration between populations is extensive, and migration rates are higher from south to north than from north to south. We demonstrate that the population structure within *C. ruber* can be explained by a model of isolation followed by secondary contact during the Pleistocene. There is also evidence for a recent range expansion in the northern population of *C. ruber.* Climatic fluctuations during the Pleistocene are the most plausible driver of the observed phylogeographic patterns in *C. ruber,* given that there are no known geographic barriers in the Pleistocene. We suggest that climatic fluctuations may have produced similar genetic structure in additional species. Finally, we reiterate previous findings that accurate estimation of demographic parameters, such as migration rates, is contingent on proper model selection.

Literature cited:

Aguirre, G., Morafka, D.J., & Murphy, R.W. (1999) The peninsular archipelago of Baja California: a thousand kilometers of tree lizard genetics. *Herpetologica*, **55**, 369–381.

Alexander, D.H. & Lange, K. (2011) Enhancements to the ADMIXTURE algorithm for individual ancestry estimation. *BMC Bioinformatics*, **12**, 246.

Alexander, D.H., Novembre, J., & Lange, K. (2009) Fast model-based estimation of ancestry in unrelated individuals. *Genome Research*, **19**, 1655–1664.

Beaumont, M.A. (2010) Approximate Bayesian computation in evolution and ecology. *Annual Review of Ecology, Evolution, and Systematics*, **41**, 379–406.

Blair, C. & Sánchez-Ramírez, S. (2016) Diversity-dependent cladogenesis throughout western Mexico: Evolutionary biogeography of rattlesnakes (Viperidae: Crotalinae: *Crotalus* and *Sistrurus*). *Molecular Phylogenetics and Evolution*, **97**, 145–154.

Bouckaert, R., Heled, J., Kühnert, D., Vaughan, T., Wu, C.-H., Xie, D., Suchard, M.A., Rambaut, A., & Drummond, A.J. (2014) BEAST 2: a software platform for Bayesian evolutionary analysis. *PLOS Computational Biology*, **10**, e1003537.

Bryant, D., Bouckaert, R., Felsenstein, J., Rosenberg, N.A., & RoyChoudhury, A. (2012) Inferring species trees directly from biallelic genetic markers: bypassing gene trees in a full coalescent analysis. *Molecular Biology and Evolution*, **29**, 1917–1932.

Castoe, T.A., Spencer, C.L., & Parkinson, C.L. (2007) Phylogeographic structure and historical demography of the western diamondback rattlesnake (*Crotalus atrox*): A perspective on North American desert biogeography. *Molecular Phylogenetics and Evolution*, **42**, 193–212.

Crews, S.C. & Hedin, M. (2006) Studies of morphological and molecular phylogenetic divergence in spiders (Araneae: *Homalonychus*) from the American southwest, including divergence along the Baja California Peninsula. *Molecular Phylogenetics and Evolution*, **38**, 470–487.

Dolby, G.A., Bennett, S.E., Lira-Noriega, A., Wilder, B.T., & Munguía-Vega, A. (2015) Assessing the geological and climatic forcing of biodiversity and evolution surrounding the Gulf of California. *Journal of the Southwest*, **57**, 391–455.

Douglas, M.E., Douglas, M.R., Schuett, G.W., & Porras, L.W. (2006) Evolution of rattlesnakes (Viperidae; *Crotalus*) in the warm deserts of western North America shaped by Neogene vicariance and Quaternary climate change. *Molecular Ecology*, **15**, 3353–3374.

Earl, D.A. & vonHoldt, B.M. (2012) STRUCTURE HARVESTER: a website and program for visualizing STRUCTURE output and implementing the Evanno method. *Conservation Genetics Resources*, **4**, 359–361.

Eaton, D.A.R. (2014) PyRAD: assembly of de novo RADseq loci for phylogenetic analyses. *Bioinformatics*, **30**, 1844–1849.

Evanno, G., Regnaut, S., & Goudet, J. (2005) Detecting the number of clusters of individuals using the software structure: a simulation study. *Molecular Ecology*, **14**, 2611–2620.

Excoffier, L., Dupanloup, I., Huerta-Sánchez, E., Sousa, V.C., & Foll, M. (2013) Robust demographic inference from genomic and SNP data. *PLoS Genetics*, **9**, e1003905.

Excoffier, L., Foll, M., & Petit, R.J. (2009) Genetic consequences of range expansions. *Annual Review of Ecology, Evolution, and Systematics*, **40**, 481–501.

Gottscho, A.D., Marks, S.B., & Jennings, W.B. (2014) Speciation, population structure, and demographic history of the Mojave Fringe-toed Lizard (*Uma scoparia*), a species of conservation concern. *Ecology and Evolution*, **4**, 2546–2562.

Gottscho, A.D., Wood, D.A., Vandergast, A.G., Lemos-Espinal, J., Gatesy, J., & Reeder, T.W. (2017) Lineage diversification of fringe-toed lizards (Phrynosomatidae: *Uma notata* complex) in the Colorado Desert: Delimiting species in the presence of gene flow. *Molecular Phylogenetics and Evolution*, **106**, 103–117.

Grismer, L.L. (2002) *Amphibians and reptiles of Baja California, including its Pacific islands, and the islands in the Sea of Cortez.* University of California Press, Berkeley.

Grismer, L.L., McGuire, J.A., & Hollingsworth, B.D. (1994) A report on the herpetofauna of the Vizcaino Peninsula, Baja California, Mexico, with a discussion of its biogeographic and taxonomic implications. *Bulletin of the Southern California Academy of Sciences*, **93**, 45–80.

Gronau, I., Hubisz, M.J., Gulko, B., Danko, C.G., & Siepel, A. (2011) Bayesian inference of ancient human demography from individual genome sequences. *Nature Genetics*, **43**, 1031–1034.

Hewitt, G.M. (1996) Some genetic consequences of ice ages, and their role in divergence and speciation. *Biological Journal of the Linnean Society*, **58**, 247–276.

Hijmans, R.J., Cameron, S.E., Parra, J.L., Jones, P.G., & Jarvis, A. (2005) Very high resolution interpolated climate surfaces for global land areas. *International Journal of Climatology*, **25**, 1965–1978.

Huang, H. & Knowles, L.L. (2016) Unforeseen consequences of excluding missing data from next-generation sequences: simulation study of RAD sequences. *Systematic Biology*, **65**, 357–365.

Huson, D.H. & Bryant, D. (2006) Application of phylogenetic networks in evolutionary studies. *Molecular Biology and Evolution*, **23**, 254–267.

Jackson, N.D., Morales, A.E., Carstens, B.C., & O'Meara, B.C. (2017) PHRAPL: Phylogeographic inference using approximate likelihoods. *Systematic Biology*, DOI: https://doi.org/10.1093/sysbio/syx001.

Jezkova, T., Jaeger, J.R., Oláh-Hemmings, V., Jones, K.B., Lara-Resendiz, R.A., Mulcahy, D.G., & Riddle, B.R. (2016) Range and niche shifts in response to past climate change in the desert horned lizard *Phrynosoma platyrhinos*. *Ecography*, **39**, 437–448.

Jombart, T. (2008) adegenet: a R package for the multivariate analysis of genetic markers. *Bioinformatics*, **24**, 1403–1405.

Jombart, T. & Ahmed, I. (2011) adegenet 1.3-1: new tools for the analysis of genome-wide SNP data. *Bioinformatics*, **27**, 3070–3071.

Jukes, T.H. & Cantor, C.R. (1969) Evolution of protein molecules. *Mammalian protein metabolism* (ed. by H. Munro), pp. 21–132. Academic Press, New York.

Klauber, L.M. (1949) The relationship of *Crotalus ruber* and *Crotalus lucasensis*. *Transactions of the San Diego Society of Natural History*, **11**, 57–60.

Kumar, S. & Subramanian, S. (2002) Mutation rates in mammalian genomes. *Proceedings of the National Academy of Sciences*, **99**, 803–808.

Leaché, A.D., Crews, S.C., & Hickerson, M.J. (2007) Two waves of diversification in mammals and reptiles of Baja California revealed by hierarchical Bayesian analysis. *Biology Letters*, **3**, 646–650.

Leaché, A.D., Harris, R.B., Rannala, B., & Yang, Z. (2014) The influence of gene flow on species tree estimation: a simulation study. *Systematic Biology*, **63**, 17–30.

Leaché, A.D. & McGuire, J.A. (2006) Phylogenetic relationships of horned lizards (*Phrynosoma*) based on nuclear and mitochondrial data: evidence for a misleading mitochondrial gene tree. *Molecular Phylogenetics and Evolution*, **39**, 628–644.

Lindell, J., Méndez-de la Cruz, F.R., & Murphy, R.W. (2005) Deep genealogical history without population differentiation: discordance between mtDNA and allozyme divergence in the zebra-tailed lizard (*Callisaurus draconoides*). *Molecular Phylogenetics and Evolution*, **36**, 682–694.

Lindell, J., Méndez-De La Cruz, F.R., & Murphy, R.W. (2008) Deep biogeographical history and cytonuclear discordance in the black-tailed brush lizard (*Urosaurus nigricaudus*) of Baja California. *Biological Journal of the Linnean Society*, **94**, 89–104.

Meik, J.M., Streicher, J.W., Lawing, A.M., Flores-Villela, O., & Fujita, M.K. (2015) Limitations of climatic data for inferring species boundaries: insights from speckled rattlesnakes. *PLoS ONE*, **10**, e0131435.

Miller, M.., Pfeiffer, W., & Schwartz, T. (2010) Creating the CIPRES Science Gateway for inference of large phylogenetic trees. *Gateway Computing Environments Workshop (GCE), 2010*, 1–8.

Mulcahy, D.G. (2008) Phylogeography and species boundaries of the western North American Nightsnake (*Hypsiglena torquata*): revisiting the subspecies concept. *Molecular Phylogenetics and Evolution*, **46**, 1095–1115.

Murphy, R.W. (1983) Paleobiogeography and genetic differentiation of the Baja California herpetofauna. *Occasional Papers of the California Academy of Sciences*, **137**, 1–48.

Murphy, R.W., Kovac, V., Allen, G.S., Fishbein, A., Mandrak, N.E., & Haddrath, O. (1995) mtDNA gene sequence, allozyme, and morphological uniformity among red diamond rattlesnakes, *Crotalus ruber* and *Crotalus exsul*. *Canadian Journal of Zoology*, **73**, 270–281.

Nason, J.D., Hamrick, J.L., & Fleming, T.H. (2002) Historical vicariance and postglacial colonization effects on the evolution of genetic structure in *Lophocereus*, a Sonoran Desert columnar cactus. *Evolution*, **56**, 2214–2226.

Oswald, J.A., Overcast, I., Mauck, W.M., Andersen, M.J., & Smith, B.T. (2017) Isolation with asymmetric gene flow during the nonsynchronous divergence of dry forest birds. *Molecular Ecology*, **26**, 1386–1400.

Peterson, B.K., Weber, J.N., Kay, E.H., Fisher, H.S., & Hoekstra, H.E. (2012) Double digest RADseq: an inexpensive method for de novo SNP discovery and genotyping in model and non-model species. *PLOS ONE*, **7**, e37135.

Phillips, S.J., Anderson, R.P., & Schapire, R.E. (2006) Maximum entropy modeling of species geographic distributions. *Ecological Modelling*, **190**, 231–259.

Pritchard, J.K., Stephens, M., & Donnelly, P. (2000) Inference of population structure using multilocus genotype data. *Genetics*, **155**, 945–959.

R Core Team 2016. R: A language and environment for statistical computing. R Foundation for Statistical Computing. Vienna, Austria. https://www.R-project.org.

Rambaut A., Suchard M.A., Xie D., Drummond A.J. 2014. Tracer v1.6. Available from http://beast.bio.ed.ac.uk/Tracer

Reyes-Velasco, J., Meik, J.M., Smith, E.N., & Castoe, T.A. (2013) Phylogenetic relationships of the enigmatic longtailed rattlesnakes (*Crotalus ericsmithi*, *C. lannomi*, and *C. stejnegeri*). *Molecular Phylogenetics and Evolution*, **69**, 524–534.

Riddle, B.R., Hafner, D.J., Alexander, L.F., & Jaeger, J.R. (2000a) Cryptic vicariance in the historical assembly of a Baja California Peninsular Desert biota. *Proceedings of the National Academy of Sciences*, **97**, 14438–14443.

Riddle, B.R., Hafner, D.J., & Alexander, L.F. (2000b) Phylogeography and systematics of the *Peromyscus eremicus* species group and the historical biogeography of North American warm regional deserts. *Molecular Phylogenetics and Evolution*, **17**, 145–160.

Savage, J.M. (1960) Evolution of a peninsular herpetofauna. *Systematic Biology*, **9**, 184–212.

Schield, D.R., Card, D.C., Adams, R.H., Jezkova, T., Reyes-Velasco, J., Proctor, F.N., Spencer, C.L., Herrmann, H.-W., Mackessy, S.P., & Castoe, T.A. (2015) Incipient speciation with biased gene flow between two lineages of the Western Diamondback Rattlesnake (*Crotalus atrox*). *Molecular Phylogenetics and Evolution*, **83**, 213–223.

Stamatakis, A. (2006) RAxML-VI-HPC: maximum likelihood-based phylogenetic analyses with thousands of taxa and mixed models. *Bioinformatics*, **22**, 2688–2690.

Stamatakis, A. (2014) RAxML version 8: a tool for phylogenetic analysis and post-analysis of large phylogenies. *Bioinformatics*, **30**, 1312–1313.

Thomé, M.T.C. & Carstens, B.C. (2016) Phylogeographic model selection leads to insight into the evolutionary history of four-eyed frogs. *Proceedings of the National Academy of Sciences*, **113**, 8010–8017.

Upton, D.E. & Murphy, R.W. (1997) Phylogeny of the side-blotched Lizards (Phrynosomatidae: *Uta*) based on mtDNA sequences: support for a midpeninsular seaway in Baja California. *Molecular Phylogenetics and Evolution*, **8**, 104–113.

Van Denburgh, J. (1920) Description of a new species of rattlesnake (*Crotalus lucasensis*) from Lower California. *Proceedings of the California Academy of Sciences*, **10**, 29–30.

Venables, W.N. & Ripley, B.D. (2002) *Modern Applied Statistics with S.* Springer, New York.

Whorley, J.R., Alvarez-Castañeda, S.T., & Kenagy, G.J. (2004) Genetic structure of desert ground squirrels over a 20-degree-latitude transect from Oregon through the Baja California peninsula. *Molecular Ecology*, **13**, 2709–2720.

Zink, R.M. (2002) Methods in comparative phylogeography, and their application to studying evolution in the North American aridlands. *Integrative and Comparative Biology*, **42**, 953–959.

Zink, R.M., Kessen, A.E., Line, T.V., & Blackwell-Rago, R.C. (2001) Comparative phylogeography of some aridland bird species. *The Condor*, **103**, 1–10.

Supplemental figures, files, and Dryad information will be available in the online version of the published manuscript.

Table 3.1. Average AIC, ΔAIC, and AIC weights across 10 replicate subsampled datasets for models fit in FSC2.

Model[1]	avg. AIC	ΔAIC	AICw
SecCon	3545.7	0	0.44
IM	3547.3	1.6	0.19
Sec Con N exp	3547.7	2.0	0.16
IM S to N mig	3548.1	2.4	0.13
IM N exp	3549.3	3.5	0.07
IM N to S mig	3569.6	23.9	$2.8*10^{-6}$
Sec Con N to S	3570.7	25.0	$1.6*10^{-6}$
No M	3570.9	25.2	$1.5*10^{-6}$
Sec Con S to N	3574.8	29.0	$2.1*10^{-7}$

[1]Abbreviations of models are: secondary contact (Sec Con), isolation migration (IM), secondary contact with expansion of the northern population size (Sec Con N Exp), IM with migration from the southern population into the northern population only (IM S to N), IM with expansion of the northern population size (IM N Exp), IM with migration from the northern population into the southern population only (IM N to S), secondary contact with migration from the northern population into the southern population only (Sec Con N to S), no migration (No M), and secondary contact with migration from the southern population into the northern population only (Sec Con S to N).

Table 3.2. Parameter estimates from G-PhoCS and FastSimCoal2.

	N North	N South	N ancestral	N north preExp	Tdiv	Tcont	2Nm N→ S	2Nm S→ N
G-PhoCS IM	38,223	79,201	63,361		283,182		0.21	0.49
FSC2 Sec Con	45,870	93,555	36,211		467,417	86,291	0.59	1.28
FSC2 IM	42,765	92,798	37,641		494,006		0.27	0.77
FSC2 Sec Con N Exp	45,356	93,684	37,126	27,274	462,786	82,880	0.67	1.36
FSC2 IM S to N	39,501	97,612	44,214		446,922			0.88
FSC2 IM N Exp	43,274	91,672	36,478	23,842	508,330		0.26	0.78

The first row shows the parameters estimated in G-PhoCS, while remaining rows show parameter estimates from models fit in FSC2 ordered by AIC score (Table 1). FSC2 models follow abbreviations in Table 3.1. Estimated parameters are the population sizes of the current, ancestral, and pre-expansion northern populations, divergence time, timing of secondary contact, and migration rates in numbers of individuals between populations.

Figure 3.1. Map showing the Baja California Peninsula with positions of the mid-peninsula, Loreto, and La Paz breaks found across many taxa shown. The range of *C. ruber* is outlined in black. Black circles show sampling localities of sequenced individuals.

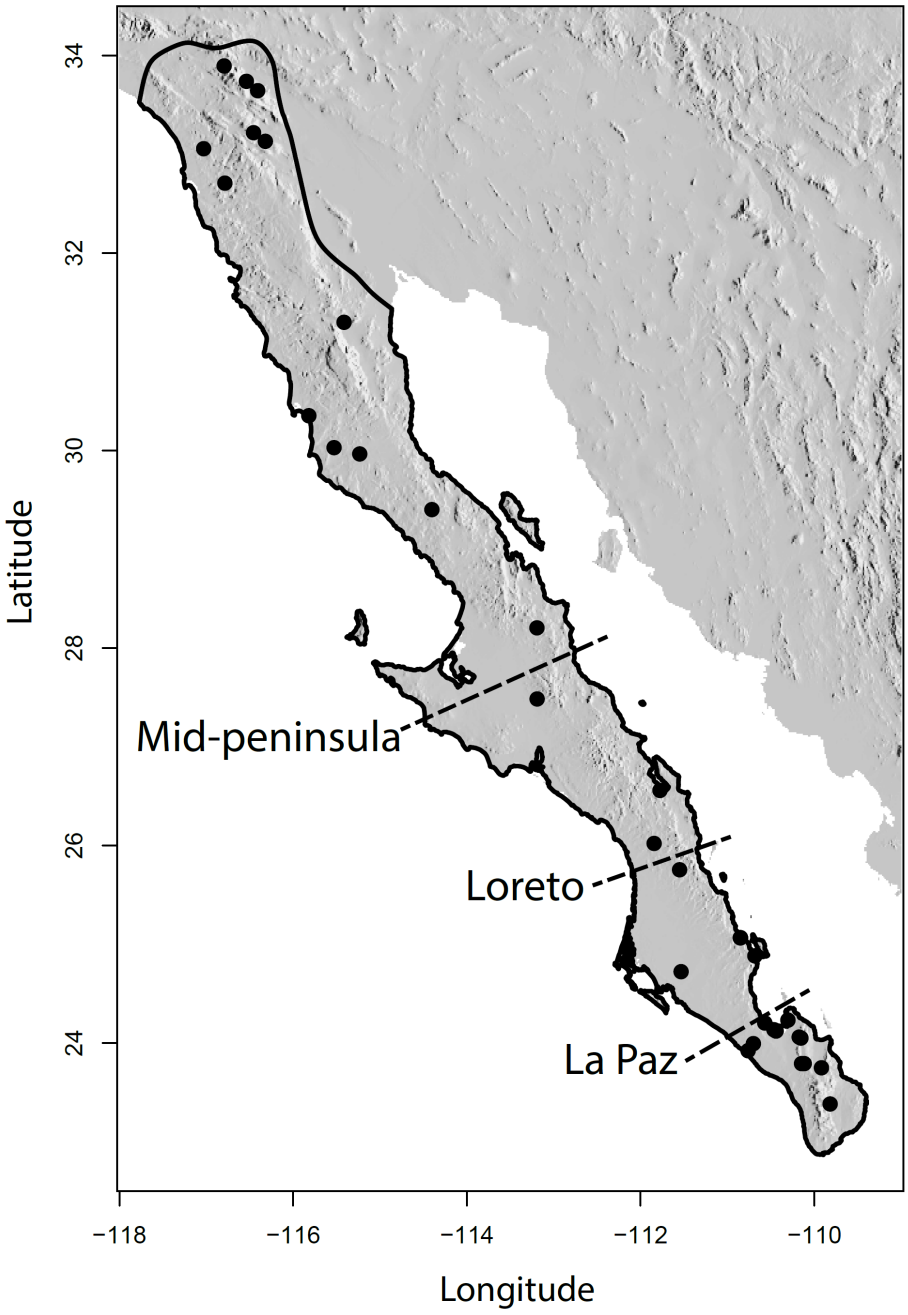

Figure 3.2. Schematic representations of the nine phylogeographic models fit in FSC2. Estimated parameters include population sizes of the southern, northern, and ancestral populations (Θs, Θn, and Θanc, respectively), timing of divergence and secondary contact (Tdiv and Tcont respectively), migration rates from the northern into southern and southern into northern populations (m_{ns} and m_{sn}, respectively), and the size of the northern population before the start of population expansion (Θn pre exp). Vertical black bars represent a period of isolation of lineages before migration initiates at secondary contact.

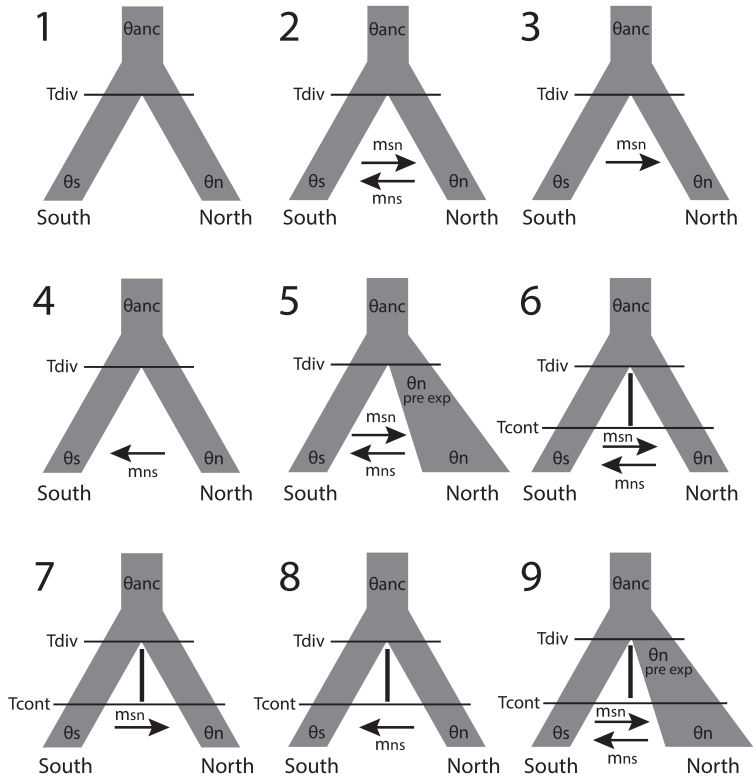

Figure 3.3. Map of the Baja California peninsula showing the results of RAxML (analysis with 20 individuals/locus threshold) and Admixture (analysis with 26 individuals/locus threshold) mapped to sampling localities. Black circles at nodes represent nodes with bootstrap support > 70%. Colored circles at the tips of the phylogeny and lines connecting to sampling localities represent strong support for membership in the northern (orange) or southern (blue) clades, whereas the individual with a white circle and black line indicates that this individual was not strongly supported as a member of either clade. Pies at sampling localities show the proportion of ancestry from each of two populations as estimated in Admixture. These populations align very closely with the northern and southern clades identified using RAxML and so the same color scheme is used.

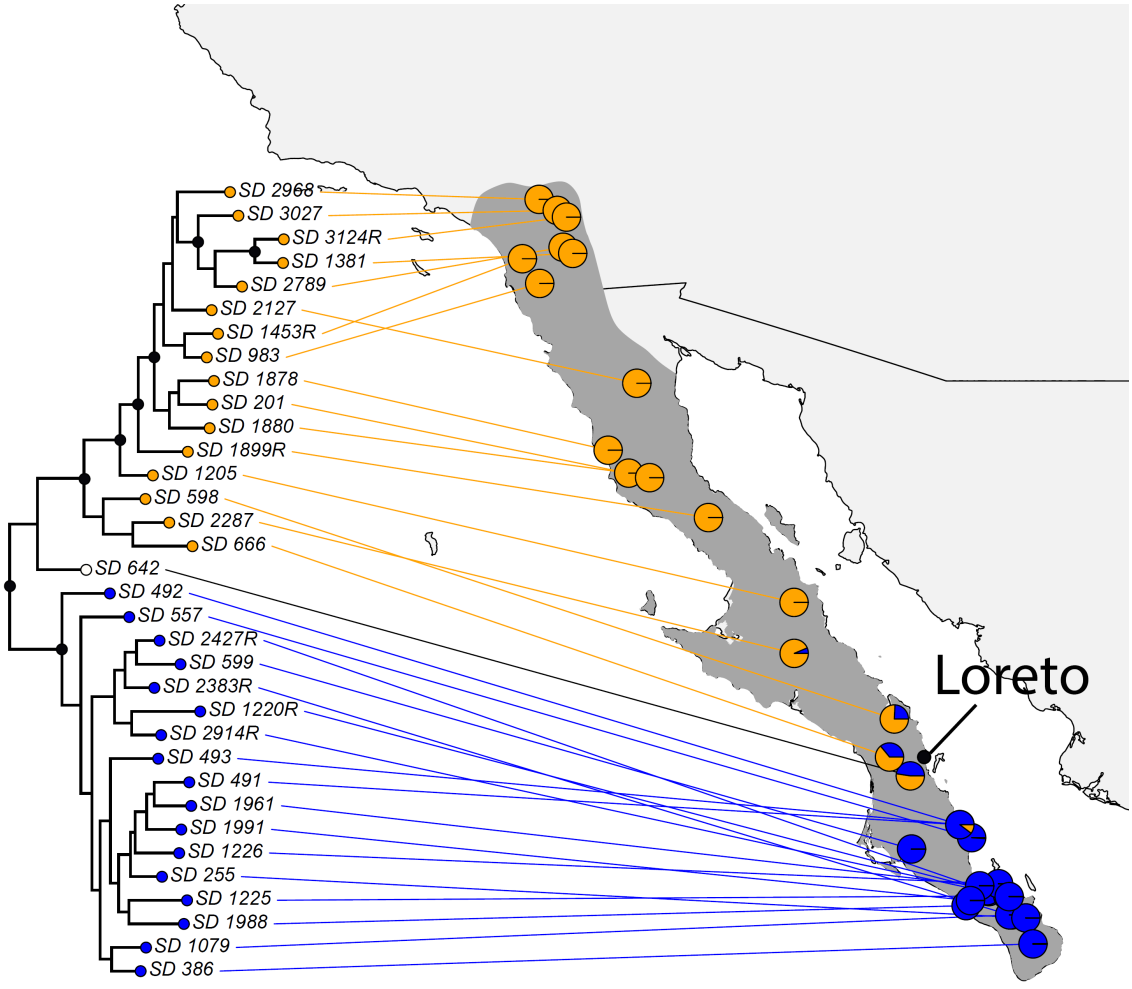

Figure 3.4. Interpolated map of individual lagged PC 1 scores from spatial PCA of *C. ruber* individuals. Black circles represent sampled individuals plotted spatially.

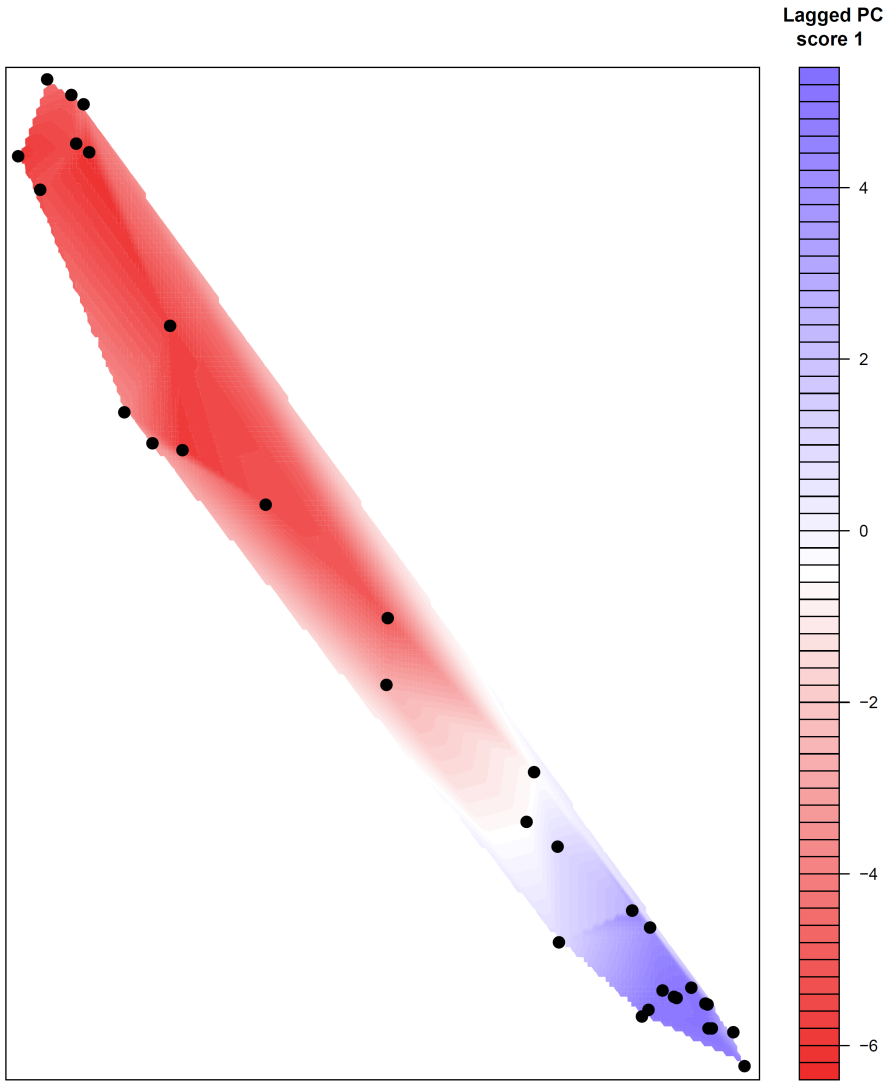

Figure 3.5. Plot of genetic distances against geographic distances among individuals. Warmer colors indicate higher densities of points.

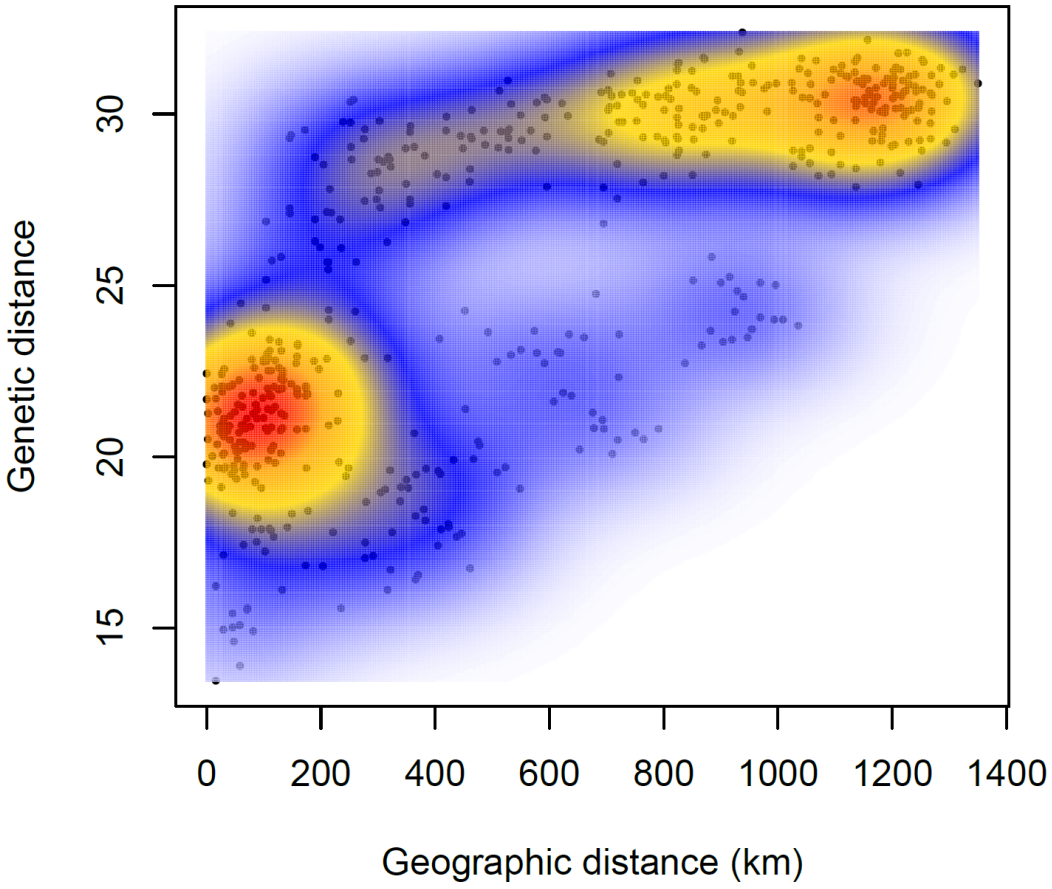

Figure 3.6. Maxent projections of suitable habitat for *C. ruber* at present (top) and during the last glacial maximum (bottom) using the CCSM4 model.

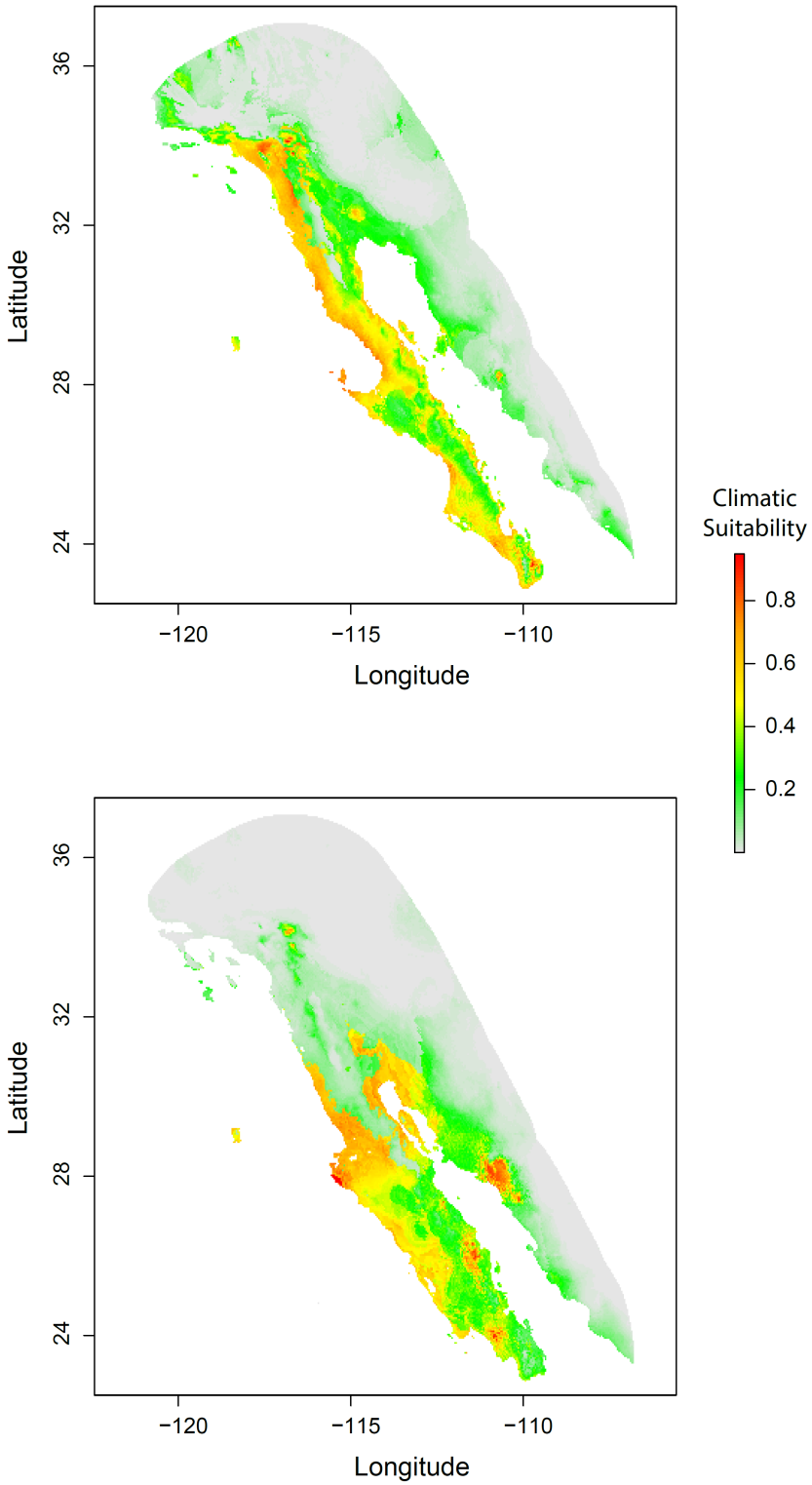

CONCLUSIONS

Throughout this dissertation, I have explored themes related to the morphological evolution and diversification of snakes. In my first chapter, I used a tip dating approach to infer the phylogenetic placement of important snake fossils and infer the divergence dates among the major clades of snakes. I used this phylogeny to reconstruct gape size and show that large gapes evolved early in snake evolution and were subsequently lost independently in multiple lineages. I also showed that well-developed limbs persisted into the crown snake radiation, and were independently reduced and lost in multiple snake lineages. In my second chapter, I showed that use of the HiSSE model can result in very different inferences of state-dependent diversification and reconstructed states than are obtained under a simpler BiSSE model. I showed that evidence for reversals from viviparity back to oviparity is limited, even in the pit viper genus *Lachesis,* which is nested within a clade of entirely viviparous snakes. In my final chapter, I have shown that population structure within *C. ruber* has been produced by historical isolation followed by secondary contact. This indicates these populations were isolated by a temporary barrier in the past that has since ceased to impede gene flow, possibly the result of Pleistocene climatic fluctuations. Given that many Baja California taxa have similar distributions, it is likely that several other taxa will show similar patterns of historical isolation and secondary contact driving genetic structure. Together, these chapters provide insight into how snakes have evolved some of their most recognizable traits, how traits may influence speciation and how we can model this effectively, and how population divergence is driven to ultimately result in new species or not.